Multiscale simulation of polymers under shear

Vom Fachbereich Chemie

der Technischen Universität Darmstadt

zur Erlangung des akademischen Grades eines

Doctor rerum naturalium (Dr. rer.nat)

genehmigte

Dissertation

vorgelegt von

Dipl.-Ing. Xiaoyu Chen

aus Nanjing, China

Berichterstatter:	Professor Dr. Florian Müller-Plathe
Mitberichterstatter:	Professor Dr. Michael Reggelin
Tag der Einreichung:	30. 06. 2008
Tag der mündlichen Prüfung:	07. 07. 2008

Darmstadt 2008

D17

Summary

This PhD thesis deals with the investigation of polymer-melt viscosity from coarse-grained simulations and with the development of a backmapping method from coarse-grained nonequilibrium systems. These studies involve both atomistic and coarse-grained (CG) descriptions. Besides these theoretical studies, efforts are also pursued on programming a code, which is designed for molecular dynamics simulations of coarse-grained polymer systems.

Chapter 1 gives a short overview of polymer properties which can be investigated by means of coarse-grained simulations as well as the algorithms for viscosity calculations via molecular dynamics.

Chapter 2 focuses on the study of the viscosity and the structural alteration of a coarse-grained model of polystyrene under steady shear flow via the reverse nonequilibrium molecular dynamics (RNEMD) method. The applicability of the RNEMD algorithm in predicting the viscosity of polymers is investigated. The viscometric functions predicted by the RNEMD are compared to previous studies of similar models where conventional nonequilibrium molecular dynamics (NEMD) methods have been used. The performance of the dynamics of the CG model, which has been developed taking only structural information into account, is investigated. For the shortest polymer chain, the zero-shear viscosity is compared to recent experimental results. The material functions (namely the first and second normal stress difference) are discussed. Structural alteration (the average chain dimension, shear-induced alignment) under a steady shear flow is also quantitatively characterized.

In Chapter 3, the problems in backmapping coarse-grained polymer models, on which a nonequilibrium shear flow has been imposed, are discussed. Backmapping is the procedure, by which the atomistic description is re-inserted into a coarse-grained configuration. Some strategies and a new backmapping protocol are proposed. In this

method, the deformed conformations are maintained globally during backmapping by applying position restraints. The local optimization of the atomistic structure is performed in the presence of these restraints. The artefact of segment isolation introduced by position restraints is minimized by applying different restraint patterns iteratively. The procedure is demonstrated on the test case of atactic polystyrene under a steady shear flow.

Chapter 4 reports in detail the implementation of the RNMED algorithm and the dissipative particle dynamics (DPD) methodology used as a thermostat into a numerical-potential molecular dynamics program (Ibisco). The program is partially redesigned in order to meet the requirements of these new algorithms. The developed code provides a reliable tool for investigating the rheological behaviour of CG models.

Finally, Chapter 5 outlines some perspectives of future research.

Zusammenfassung

Diese Doktorarbeit beschäftigt sich mit der Untersuchung von Scherviskosität mittels Simulationen von "Coarse-Grained" (CG) vergröberten Modellen und der Entwicklung einer Methode zur Wiedereinführung von atomistischen Details in Nicht-Gleichgewichts-CG-Systemen. Diese Arbeit umfasst sowohl vollständig atomistische als auch CG Beschreibungen von polymeren Systemen. Zusätzlich zu diesen beiden theoretischen Studien wurde ein Computercode zur molekulardynamischen Simulation von CG Systemen geschrieben

Kapitel 1 verschafft einen kurzen Überblick über jene Eigenschaften von Polymeren, die durch CG Simulationen untersucht werden können, und zeigt einige der konventionellen Algorithmen zur Bestimmung von Scherviskositäten mittels molekulardynamischen Simulationen auf.

Kapitel 2 konzentriert sich auf die Untersuchung der Scherviskosität und der Strukturänderungen in einem CG Modellsystem von Polystyrol unter konstantem Scherfluss, welcher durch "Reverse nonequilibrium molecular dynamics" (RNEMD) Algorithmus induziert wurde. Die Anwendbarkeit der RNEMD Methode auf die Scherviskosität von Polymeren wurde hierbei getestet, und die durch RNEMD vorhergesagten viskometrischen Funktionen wurden mit bereits durch konventionelle Nichtgleichgewichtssimulationen (NEMD) errechneten Literaturwerten verglichen. Ebenso wurde die Effizienz des CG Models, welches ausschliesslich Strukturdaten verwendet, untersucht. Für die kürzeste Polymerkette wird die Nullscherviskosität mit aktuellen experimentellen Daten verglichen. Die Materialfunktionen (explizit die erste und die zweite Normaldruckdifferenz) werden genauso diskutiert, wie die Strukturveränderung (durchschnittliches Kettenvolumen und scherinduziertes Ausrichten) unter konstantem Scherfluss.

Kapitel 3 behandelt die Probleme der Wiedereinführung atomistischer Details in CG Polymerkonfigurationen, die einem Nichtgleichgewichts-Scherfluss unterworfen wurden. Das entsprechende Verfahren heisst "Reverse Mapping". Hier werden einige Strategien zur Wiedereinführung aufgezeigt und ein neues Reverse Mapping Protokoll vorgeschlagen. In dieser Methode werden die deformierten Polymerkonformationen während des Reverse Mapping Prozesses durch Anwendung äusserer Kräfte beibehalten. Die dadurch eingeführten Artefakte der Isolierung einzelner Segmente wird minimiert, indem verschiedene Fixierungsmuster iterativ angewendet werden. Das Verfahren wird anhand von ataktischem Polystyrol unter konstantem Scherfluss demonstriert.

Kapitel 4 behandelt detailliert die Impementierung des RNEMD Algorithmus und die Implementierung der "Dissipative Particle Dynamics" (DPD) Methode in ein mit numerischen Potentialen arbeitendes Molekulardynamik-Programm (IBIsco). Das Programm wurde teilweise überarbeitet, um die richtigen Voraussetzungen für obige Algorithmen zu schaffen. Der hierbei entwickelte Code ist ein verlässliches Instrument zur Untersuchung von rheologischem Verhalten von CG Modellen.

Kapitel 5 zeigt schliesslich einige Perspektiven und Ansätze für zukünftige Forschungsarbeiten auf diesem Gebiet auf.

Contents

List of figures

List of tables

1. Introduction

1.1. Motivation

Viscosity is an important characteristic for all materials, especially polymers. Among several viscosity calculation algorithms, the reverse nonequilibrium molecular dynamics (RNEMD) shows its fundamental and technical advantages over previous equilibrium and non-equilibrium techniques. Although RNEMD has successfully predicted the viscosity of simple liquid whose relaxation time is very short, it encounters the typical limitations dictated by inherent time scales when it is implemented on viscosity prediction of polymeric systems. As shear flow in polymer melt involves slow process on the mesoscopic scale, question rises that the feasibility and applicability of this method with fully atomistic model, the huge number of degree of freedom in fully atomistic approach narrows down the applicable range only to very short chain. One way to circumvent this problem is to reduce the number of degrees of freedom in the cost of losing some irrelevant details of molecular structure, so called coarse-grained (CG) model. Following this consideration, an attempt of extending RNEMD methodology to polymeric system has been carried out, the applicability of RNEMD to the prediction of the polymer viscosity is investigated.

Coarse-grained simulations prevail on reproducing the structural and thermodynamical properties. A coarse-graining scheme for reproducing the dynamic and transport properties is not still well-established. It is not clear that the existing CG model can produce reliable melt viscosity. In this study, the rheological behaviour of an existing CG model, which has been successfully tested against structural properties, is explored. This study provides an understanding on the dynamical performance of a structure-optimized CG model.

The relaxation of long chains at the atomistic level is computationally unfeasible. An important purpose of coarse-grained model is generating the well-equilibrated polymer structure. A good CG method also allows the reverse process, i.e. going back to the atomistic description, this process is called reverse-mapping or

backmapping. Currently, the backmapping technique is pursued on equilibrium system. However, dynamic properties, in particular melt viscosities under shear or elongational flow which are of great interest to the polymer manufacturing and processing, only can be investigated under nonequilibrium conditions. The present study intends to develop a backmapping method from coarse-grained nonequilibrium systems.

1.2. Polymer properties from coarse-grained simulations

Polymers exhibit physical properties in a broad range of length and time scales. Many efforts have been made in studying polymer properties through a hierarchical approach.[1,2] Computational basic degrees of freedom are electrons (quantum chemistry), atoms (force field), monomers or groups of monomers (mesoscopic models), entire polymer chains (soft fluids) or volume elements (finite elements)[3]. Any one of these computer simulation techniques, individually, is restricted to a much narrower range. Therefore, one needs to simulate polymers with models of several different scales, in order to have a complete picture of their properties. This thesis involves two methods: the atomistic force field and the coarse-grained model (CG). In the atomistic force field, every atom is modelled as a separate interaction site. In the CG model, every interaction centre (also referred to as "bead" or "superatom") contains of the order of 10 non-hydrogen atoms or approximately one chemical repeating unit.[3] Both methods have one common features of retaining the material-specific information, which is neglected in the generic models and is not computational affordable through quantum chemistry approach. Here, term "material-specific information" can be comprehended as chemical composition, tacticity, sequence, and topology. Comparing to the atomistic force field, CG models have been proven to be very efficient in studying the complicated behaviour of polymers. This efficiency comes from the fact that the CG model only takes into account those degrees of freedom deemed relevant for the particular properties studied.

Coarse-grained models are parameterised reproducing structural and thermodynamics properties of polymers.[4-6] Very recently, dynamic properties have been a simulation target in some CG simulations.[7,8]

1.2.1. Structural properties

The structural properties of polymer chains are most conveniently described by distributions of geometric quantities, which can be intramolecular or intermolecular. The intramolecular properties can be distances between two adjacent superatoms, angles between three subsequent superatoms, dihedral angles between four subsequent superatoms, principal values of the radius of gyration tensor and so forth. The intermolecular properties involves distances between the superatoms belonging to different chains, distance between the centres of mass of different chains or chain fragments. All these properties have to be reproduced by the coarse-grained simulations.

If the goal of the coarse-grained model is to reproduce structural distribution from atomistic reference simulation, several computation procedures are available.[14] In particular, iterative Boltzmann inversion[14] is readily adapted to the problem of coarse-graining polymer. This procedure is demonstrated with the example of deriving an effective nonbonded potential from a given radial distribution function as following: If a target radial distribution function $RDF_{tartet}(r)$ is available, one starts the zeroth simulation with a guessed tabulated pair potential $V_0(r)$. Its simulation yields radial distribution function $RDF_0(r)$, which is different from $RDF_{tartet}(r)$. Afterwards, potential is improved by adding to $V_0(r)$ the correction term $-kT\ln\dfrac{RDF_0(r)}{RDF_{t\arg et}(r)}$. This step can be iterated,

$$V_{j+1}(r) = V_j(r) + kT\ln\frac{RDF_j(r)}{RDF_{t\arg et}(r)} \tag{1}$$

until

$$f_{t\arg et} = \int_0^{cutoff} \omega(r)\big[RDF_j(r) - RDF_{t\arg et}(r)\big]^2 dr \tag{2}$$

falls below an initially specified threshold. $\omega(r)$ is weighting function in order to specifically penalize deviations at small distance.

1.2.2. Thermodynamic properties

Thermodynamic properties like the cohesive-energy density, the density (in *NPT* ensemble) or the pressure (in *NVT* ensemble) are also reproduced in the coarse-grained simulations. The simplex method, which was originally developed to adjust atomistic force field parameters to experimental thermodynamics properties of molecular liquids, is brought into CG simulation to reproduce the thermodynamics data.[14] The pressure information can be introduced into polymer systems by the so-called ramp correction: Since the initially optimized structure yield a pressure different from the one at which the atomistic simulation are performed, a weak linear potential term ΔV is added to the attractive long-range part of $V_j(r)$, then the structure is post-optimized according to the iterative Boltzmann inversion until also the pressure matches the atomistic system. The form of ramp correction can be taken as Eqn 3.

$$\Delta V(r) = V_j \left(1 - \frac{r}{r_{cut}} \right) \tag{3}$$

It vanishes at the cutoff $(\Delta V(r_{cutoff}) = 0)$ and $\Delta V = \Delta V_j$ $(r = 0)$ is the only parameter.

1.2.3. Dynamics and transport properties

So far, there are but few explicit studies of dynamic properties by means of coarse-grained simulations. Most investigations are limited to an analysis of self-diffusion coefficients. The self-diffusion coefficient of the CG model depends on the parameterization of CG force field. There are two different approaches for developing the CG force field:

1. In the first approach, both static and dynamics properties are used to develop the CG force field. The dynamics in the CG model is matched with atomistic one by an appropriate selection of friction constants appearing in Langevin's equations of motion. Following this approach, Padding and Briels[5] proposed a method to define the friction within the CG model using underlying short atomistic simulation. Moreover, they introduced an uncrossability constraint into their CG equation of motion to prevent

unphysical bond crossing. They proved that the dynamics and the zero-shear viscosity of their CG model agree with experimental findings.[6]

2. In the second approach, only static properties are utilized in the force field parameterization, and Newton's equation of motion is used to evolve the system. The CG model developed from this approach can accurately describe the static properties, while on the other hand, the dynamics is generally too fast. Depa and Maranas[7] have proven that there is a robust scaling factor in the CG dynamics by mapping the self-diffusion coefficient of the CG model to the one of underlying atomistic model.

1.3. Back to the atomistic description: backmapping

As the way of coarse-graining an atomistic model into mesoscopic one is not unique, it is much more complicated to refine a CG model back to an atomistic one. Santangelo[8] *et al* introduced a systematic procedure to obtain well-relaxed atomistic melt structures from mesoscale models of vinyl polymers based on sequence of diad. This method is based on a fully geometrical approach and does not involve expensive potential energy and force evaluations. Kotelyanskii[13] *et al* proposed a refining procedure in order to introduce atoms into their lattice model of polystyrene. They used a coordinate template of the building block, and place it on top of the lattice site (equivalent to a super-atom) which they wanted to refine. Then, they rotated it by taking into account the orientation with respect to its two nearest neighbours along the chain.

1.4. Algorithms used to compute the viscosity

One aspect of this thesis is investigating the viscosities of polymers. The algorithms used to compute the viscosity are briefly reviewed here.

1.4.1 Equilibrium molecular dynamics: the Green-Kubo method

The Green-Kubo method simply consists of simulating an equilibrium fluid under periodic boundary conditions and making the appropriate analysis of the time-dependent stress fluctuations.[11] The Kubo relation predicting the viscosity is given by Eqn. 4

$$\eta = \beta V \int_0^\infty dt \langle P_{xy}(0)P_{xy}(t) \rangle \tag{4}$$

where, $\beta = 1 / (kT)$ with the Boltzmann constant k and V is the system volume. The integral is over the equilibrium time autocorrelation function of the xy component of the pressure tensor P_{xy}. The Green-Kubo technique is restricted to only linear transport coefficients.

1.4.2. Nonequilibrium molecular dynamics

The non-Newtonian character of most complex fluids and their resulting unique properties manifest themselves only beyond the linear response regime. To study these, nonequilibrium molecular dynamics (NEMD) simulations are necessary. The conventional NEMD methods are similar in spirit to real experiments: the cause is an appropriate field or gradient which is imposed on the system, then the ensemble average of the effect, the resulting flux, is measure and the ratio of flux and field gives the viscosity. In the NEMD simulations, one has to tackle two problems: First, one must mechanically impose the shear. Second, the shear is enforced by constantly pumping energy into the system. Hence one must get rid of the heat by applying an appropriate thermostat. One exception is the reverse nonequilibrium molecular dynamics (RNEMD).

Surface-driven method. The most direct way of imposing a shear is to confine the system between two rough walls, and either move one of them (for Couette flow), or apply a pressure gradient (for Poiseuille flow). The virtue of this method is of being physical: Strain is enforced physically, and the heat can be removed in a physical way by coupling a thermostat to the walls. On the other hand, the system contains two surfaces, and depending on the material under consideration, one may encounter strong surface effects.[10]Varnik and Binder[9] have shown that surface-driven methods can be used to measure the shear viscosity in polymer melts.

Homogenous shear method An alternative way to generate planar Couette flow is to use moving periodic boundary conditions as illustrated in Fig. 1.1 (Lees-Edwards

boundary condition). In order to enforce the shear flow $\vec{u} = (u_x, 0, 0)$ with an average strain rate $\dot{\gamma} = \partial u_x / \partial y$, one proceeds as follows: One replicates the particles in the x and the z direction like in regular periodic boundary conditions. In the y-direction, the replicated particles acquire an additional velocity $v_x = \dot{\gamma} L_y$. One particularly popular algorithm of this kind is the SLLOD[11] algorithm. For the imposed flow $\vec{u}(\vec{r}) = \dot{\gamma} y \vec{e}$, the SSLOD equations of motion for atom i is

$$\frac{d\vec{r}_i}{dt} = \frac{\vec{p}_i}{m_i} + \dot{\gamma} y_i \vec{e}_x \tag{5}$$

$$\frac{d\vec{p}_i}{dt} = \vec{F}_i - \dot{\gamma} y_i' \vec{e}_x \tag{6}$$

where, $\vec{p}_i = m_i(\vec{v}_i - \vec{u}(\vec{r}_i))$ is the momentum of atom i in a reference frame moving with the local flow velocity $\vec{u}(\vec{r}_i)$, and $\vec{F}_i$ is the regular force acting on the atom i. The equations of motion can be integrated with standard techniques.
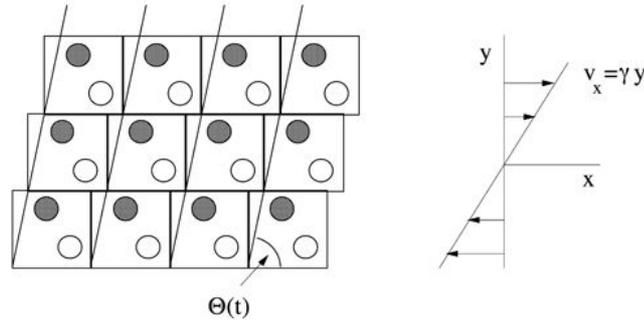
Figure 1.1. Schematic view of Lees Edwards periodic boundary condition (reproduce from ref.12).

 Reverse nonequilibrium molecular dynamics The shear algorithm used in this study is the reverse nonequilibrium molecular dynamics (RNEMD) method.[15] The RNEMD method reverses the experimental cause-and-effect picture: the effect (momentum flux or stress) is imposed, whereas the cause (velocity gradient or shear rate) is obtained from simulation. The details of RNEMD are elucidated in Chapter 2.

1.5. References

(1)   Müller-Plathe, F. *ChemPhysChem* **2002**, *3*, 754-769.

(2)   Kremer, K.; Müller-Plathe, F. *MRS Bulletin* **2001**, *26*, 205-210.

(3)   Müller-Plathe, F. *Soft Mater.* **2003**, *1*, 1-31.

(4)   Reith, D.; Meyer, H.; Müller-Plathe, F. *Macromolecules* **2001**, *34*, 2335-2345.

(5)   Padding, J. T.; Briels, W. J. *J. Chem. Phys.* **2001**, *115*, 2846-2859.

(6)   Padding, J. T.; Briels, W. J. *J. Chem. Phys.* **2003**, *118*, 10276-10286.

(7)   Depa, P. K.; Maranas, J. K. *J. Chem. Phys.* **2005**, *123*, 094901.

(8)   Santangelo, G.; Matteo, A. D.; Müller-Plathe, F.; Milano, G. *J. Phys. Chem. B* **2007**, *111*, 2765 -2773.

(9)   Varnik, F.; Binder, K. *J. Chem. Phys.* **2002**, *117*, 6336-6349.

(10)   Hess, B. *J. Chem. Phys.* **2002**, *116*, 209-217.

(11)   Allen, M. P.; Tildesley, D. J. *Computer Simulation of Liquids*; Oxford University Press, 1987.

(12)   D. J. Evans and T. P. Morriss . **1990** *Statistical Mechanics of Nonequilibrium Fluids*. Academic Press, San Diego

(13)   Kotelyanskii, M.; Wagner, N. J.; Paulaitis, M. E. *Macromolecules* **1996**, *29*, 8497-8506.

(14)   Reith, D.; Pütz, M.; Müller-Plathe, F. *J. Comput. Chem.* **2003**, *24*, 1624-1636.

(15)   Müller-Plathe, F. *Phys. Rev. E* **1999**, *59*, 4894-4898.

2. Viscosity and structure alteration of a coarse-grained model of polystyrene under steady shear flow studied by reverse nonequilibrium molecular dynamics

2.1. Introduction

In the last two decades, several simulation methods for the prediction of shear viscosities have been proposed. In equilibrium molecular dynamics (EMD), the shear viscosity is obtained from pressure or momentum fluctuations based on the Einstein and Green-Kubo relations;[1] In conventional non-equilibrium molecular dynamics (NEMD),[2] the shear viscosity can be calculated by reproducing the experimental setup; i.e., an appropriate perturbation is applied, the ensemble averages of the resulting flux and the corresponding field are measured, the ratio of flux and field gives the shear viscosity. The most widely used NEMD methods are homogeneous shear (HS) and surface-driven shear methods (SD). In HS method, the shear flow is imposed by modifying the equation of motion of the molecules and using sliding-wall periodic boundary conditions. In SD method, the shear is imparted on the fluid through the actual motion of the confining walls. A comparison of the applicability, accuracy and efficiency for these methods can be found in ref. 3.

A more recent alternative is the reverse nonequilibrium molecular dynamics (RNEMD) method,[4,5] which is used here. It reverses the experimental cause-and-effect picture: the momentum flux (stress) is imposed by a Maxwell daemon and the corresponding field (velocity gradient) is measured. Compared to the more traditional NEMD techniques, RNEMD offers certain advantages, but also has its shortcomings. They have been discussed in more detail elsewhere.[5] Its chief advantage is the fact, that no energy is deposited into the simulation, in contrast to other NEMD methods, and

hence no energy need be removed by an external thermostat. As most thermostats interfere with the linear momentum, they are a potential error source in viscosity calculations. Further advantages are the absence of boundary regions (as in SD method), the ease of implementation and analysis, and parallelisability.[6] The major shortcoming of RNEMD is that the temperature in the system is not uniform but develops a stationary quadratic profile.[4] As a consequence, the density is also not uniform, so that the calculated viscosity is an average over different temperatures and densities. This aspect requires great care in designing the perturbation to be small enough for these variations to be numerically irrelevant. As one usually attempts anyway in NEMD to make the perturbation as small as possible, in order to have linear-response conditions, this is not a serious restriction, but more a point to be watched. RNEMD has been very successfully applied to predict the viscosity of Lennard-Jones liquids,[4] atomistic models of molecular liquids[7], simplified models of amphiphiles[8], liquid crystals[9] and Yukawa liquids.[10] In particular, ref 10 shows that for small shear rates the viscosity values calculated via RNEMD and NEMD simulations are mutually consistent and also in agreement with equilibrium MD calculations. So far, the RNEMD method has not been tried for the calculation of polymer viscosities.

The viscosities of polymer melts and structural changes under shear flow are of great practical importance in manufacturing and processing of polymers. Viscosity and structure of polymer melts under shear were intensively studied by conventional NEMD in previous work. Among these studies, some simple and general models have successfully captured the rheological properties and contributed to the understanding of their physical origin.[11-15] A detailed review on simple models for complex non-equilibrium fluids can be found in ref. 16. However, the generic models have not been designed to provide quantitative properties of *specific* polymer melts. Some studies on specific macromolecules, which were based on realistic models, have also been carried out.[17-19] The presence of many different time and length scales and the associated computational costs usually preclude the use of fully atomistic force fields. One, therefore, tries to find a coarse-grained (CG) model at a level between atomistic and generic. It should be detailed enough to be material-specific and simple enough to be

computationally viable. One way to approach the problem is to reduce the degrees of freedom by coarsening the models, keeping only those degrees of freedom deemed relevant for the particular properties of interest. Parameterization of coarse-grained force fields can be roughly classified into two different approaches. In the first, both static and dynamics properties are used to develop the force field and the dynamics is matched by an appropriate selection of friction constant appearing in Langevin's equations of motion at the coarse-grained scale.[20,21] In the second approach, only static properties are utilized in the force field parameterization and Newton's equations of motion are used to evolve the system.[22,23] The coarse-grained models developed from this approach can accurately describe the static properties, while on the other hand the dynamics is generally too fast.[24] In some cases it was possible to recover the dynamical properties by appropriate time scaling.[25] The dynamical properties predicted by such CG model are based on the philosophy that the same basic mechanisms are still operative at a different time rate when the molecular mobility changes. Therefore, the accelerated dynamics is expected to retain some reality of the motion in the system. Ideally, one would like structurally optimised models to also be able to predict polymer viscosities without any further calibration. Finding out whether this is possible is one aspect of the current investigation.

The aim of this study is therefore twofold. First, the applicability of the RNEMD algorithm to the prediction of the viscosity of polymers is investigated. We compare the shear behaviour to previous studies of similar models, where conventional NEMD methods have been used. Second, we study the rheological behaviour of the specific, realistic coarse-grained model of polystyrene, which has been developed taking only structural information into account. For the shortest polymer chain the zero-shear viscosity is compared to recent experimental results. The material functions (first and second normal stress difference) are briefly discussed and structural properties of polystyrene under shear are also quantitatively characterized in this work.

2.2. Reverse nonequilibrium molecular dynamics

The RNEMD method for calculating shear viscosity is briefly reviewed in this section, for details, see ref. 4 and ref. 5. The shear viscosity η relates the transverse momentum flux $j_z(p_x)$ and the flow velocity gradient $\partial \bar{v}_x / \partial z$ via Eq. (1).

$$j_z(p_x) = -\eta \frac{\partial \bar{v}_x}{\partial z} \qquad (1)$$

The magnitude of momentum flux $|j_z(p_x)|$ is equal to the off-diagonal (xz) component of the stress tensor τ_{xz}, and $\partial \bar{v}_x / \partial z$ is also called the shear rate $\dot{\gamma}$. The momentum flux $j_z(p_x)$ can be described as a transport through a surface perpendicular to its direction within a certain time. In RNEMD, $j_z(p_x)$ is imposed in an unphysical way, and the flow field corresponds to two symmetric planar Couette flows, with a shear flow in the x direction and the velocity gradient in the z direction, as illustrated in Fig. 2.1.
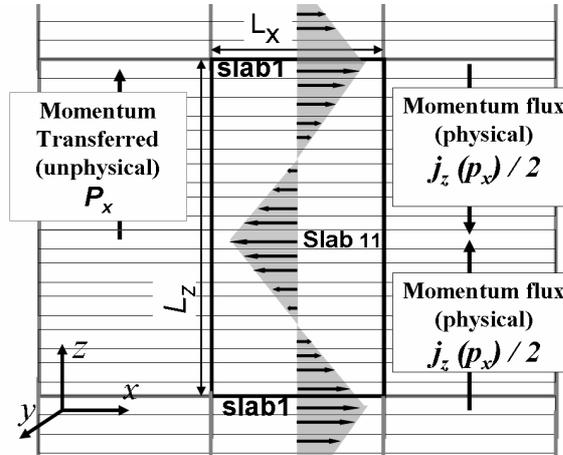
Figure 2.1. Sketch of the RNEMD method for calculating the shear viscosity. The flow field imposed on the system corresponds to two symmetric planar Couette flows, which have the shear flow in the x direction, and the velocity gradient is in z direction. Horizontal arrows in the simulation cell indicate the velocity field. The periodic

orthorhombic simulation cell with size of L_x, L_y, and L_z ($L_x = L_y = L_z / 3$) in periodic system is partitioned into 20 slabs in z direction. For details, see text.

The orthorhombic simulation cell with size of L_x, L_y, L_z in the periodic system is partitioned into an even number of slabs, here 20 , in z direction. One selects in slab 1 the atom with the *largest* negative x component of momentum (mv_{x1}) and in the central slab (slab 11) the atom with the *largest* positive x component of momentum (mv_{x2}). These two atoms must have the same mass m. One exchanges the x component of the velocity vector between these two atoms. As the two atoms have the same mass m, the unphysical momentum swap conserves both the total linear momentum and the total kinetic energy. The exchanged quantity Δp_x is the x component of the momentum,

$$\Delta p_x = mv_{x1} - mv_{x2} \tag{2}$$

By such velocity swap, momentum (Δp_x) is transferred unphysically across the system. The velocity swap is performed every W time steps; so the time elapsed between two velocity swaps is $W \cdot \Delta t$, with Δt being the lengths of the time step. The total transferred momentum during the simulation is given by $p_x = \Sigma \Delta p_x$. The response of the system to this nonequilibrium perturbation is a momentum flux $j_z(p_x)$ in the opposite direction via a physical mechanism, the friction. In the steady state, the unphysical and the physical momentum flux are balanced, and $j_z(p_x)$ can be evaluated by Eq. (3)

$$j_z(p_x) = \frac{p_x}{2tL_xL_y} \tag{3}$$

The factor 2 arises because of the periodicity of the system, and t is the duration of the simulation. The momentum flux $j_z(p_x)$ leads to a continuous velocity gradient $\partial \overline{v}_x / \partial z$ in the fluid except slab 1 and slab 11 where velocities are not differentiable. The local flow velocity in slab n, $\overline{v}_x(n)$ is determined by averaging over the particles in this slab.

13

$$\bar{v}_x(n) = \langle v_{x,i} \rangle, \quad i \in \text{slab } n \tag{4}$$

The velocity profile is linear and it slope $\langle \partial \bar{v}/\partial z \rangle$ can be extracted by a linear least-squares fit. The local temperature in slab n, $T(n)$, is evaluated from peculiar velocities, i.e. the difference between the actual velocities and the local flow velocities, as Eq(5).

$$T(n) = \frac{1}{3N_{bead}k_B} \sum_{i=1}^{N_{bead}} [(v_{x,i} - \bar{v}_x(n))^2 + v_{y,i}^2 + v_{z,i}^2], \quad i \in \text{slab n} \tag{5}$$

where, k_B is Boltzmann's constant, N_{bead} is total number of beads in slab n, m_i and v_i denote the mass and actual velocity of ith bead. The temperature profile is parabolic in both upper and lower halves of simulation cell, with cooling in the exchange slabs 1 and 11 and heating in between.[6,] As the transport of momentum p_x is exactly known, the shear viscosity η at a given shear rate $\dot{\gamma} = \langle \partial \bar{v}/\partial z \rangle$ can be calculated by Eq. (6).

$$\eta = \frac{p_x}{2tL_xL_y \langle \partial \bar{v}_x/\partial z \rangle} \tag{6}$$

The momentum flux $j_z(p_x)$ is controlled by adjusting the time elapsed between two velocity swaps $W \cdot \Delta t$. As a result, different shear rates $\dot{\gamma}$ are achieved.

It is worth considering the influence of the thermostat. As the total linear momentum and total energy are conserved, the RNEMD method, in contrast to other NEMD methods, does not need any external thermostat. However, calculations on realistic systems often necessitate a thermostat for reasons unrelated to the RNEMD scheme, because either *NVT* conditions are explicitly required, or temperature shifts due to round-off or cutoff noise need to be corrected. As any thermostat introduces an artificial dissipation of momentum, the calculated viscosities may carry an intrinsic error. We use an atomic version of Berendsen's thermostat,[26] i.e. the actual temperature is calculated from atomic velocities, rather than centre-of-mass velocities, and the atomic velocities are being rescaled. An atom-based thermostat is dictated by the system

being a melt of long, flexible and entwined polymer chains. Firstly, in contrast to fluids of small rigid molecules, they create no problems from rotational motion, as they reorient much slower than they thermalise. Secondly, confining the temperature analysis and control only to the centre-of-mass velocities (one hundredth of all degrees of freedom for chain of 100 beads, namely PS-100, see Section 3) would lead to large statistical uncertainties. Finally, we need the thermostat only to counteract a very slow drift due to round-off errors. The usual main source of spurious heat generation, namely cutoff noise, plays a minor role here, since our cutoff is long and the nonbonded potentials have a finite range. As the Berendsen thermostat applies a uniform scaling to all velocities, it may change velocity profiles only uniformly and only by a small amount, avoiding local artefacts. In this sense, it might have an advantage over alternative thermostats, which perform velocity scaling on an individual-atom basis.[27] In Figure 2.2, we report the rate of energy input into or removal from the system by the thermostat in the simulation of the biggest system (PS-100, Section 3) at the highest shear rate. It is evident that, in the steady state, the average kinetic energy added/removed by the thermostat is zero.
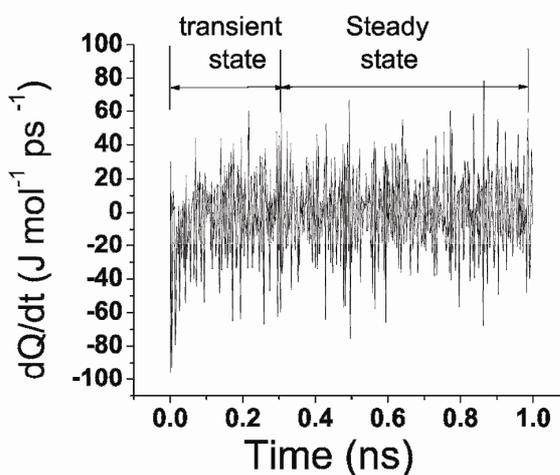
Figure 2.2. Evolution of the rate of heat energy (dQ/dt) input to the system by the thermostat during the simulation for PS-100 system at the highest shear rate $5.06 \times 10^{10} s^{-1}$.

2.3. Model and computational technique

References 24 and 28 report, respectively, the CG model of atactic polystyrene and the corresponding force field parameters used in this work. The most important characteristics of this model are: the polystyrene diad is coarse-grained as a superatom in the mesoscale effective force field; the center of the superatom is placed at the methylene carbon; two different types of superatoms can be designated according to the configuration of two adjacent pseudoasymmetric –CHR– methyne groups, either *meso* (same configurations *RR* or *SS*) or *racemo* (opposite configurations *RS* or *SR*), as shown in Fig. 2.3; the corresponding force-field contains three different bonds, six angles and three nonbonded terms. This model has been successfully tested against structural properties of polystyrene melts with different chain lengths, the dynamical behaviour can be properly evaluated by taking into account the time scale.
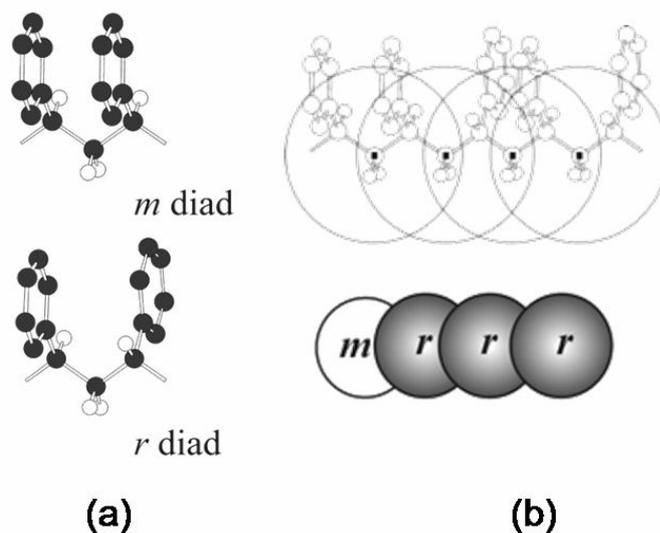
Figure 2.3. Illustration of the coarse-grained model of atactic polystyrene: (a) the *meso* (*m*) and *racemo* (*r*) of diads in transplanar conformation (hydrogen atoms on phenyl rings are omitted for clarity) (b) one superatom corresponding to a diadic *m* or *r* unit.

The centres of these superatoms, as indicated by filled squares, are the methylene carbons. Reproduced from ref. 24.

The RNEMD simulations of monodisperse polystyrene melts are performed for four different chain lengths. Every system consists of N_{chain} polystyrene chains of N_{bead} beads, where N_{bead} is taken to be 9, 20, 30 and 100. These systems are referred to as PS-9, PS-20, PS-30, and PS-100, respectively. They are all unentangled systems. The densities of the systems are obtained from equilibrium simulations at constant temperature 500 K and constant pressure 1 atm. The relaxation time of a chain τ is obtained by time integration of the autocorrelation function for the end-to-end vector $\mathbf{s}$, as given by Eq. (7).

$$\tau = \int_0^\infty C(t)\mathrm{d}t = \int_0^\infty \left\langle \mathbf{s}(0) \cdot \mathbf{s}(t) \right\rangle / \left\langle s^2 \right\rangle \mathrm{d}t \tag{7}$$

The correlation function is noisy, so the long-time behaviour is hard to take into account. To arrive at practical estimates for comparing the dynamics, we have integrated $C(t)$ until it reaches zero for the first time. The parameters of these systems are summarised in Table 2.1. These well-equilibrated systems are used as initial configurations of the RNEMD calculations.

17

Table 2.1. Parameters of the coarse-grained model system used. Polymer systems, the number of beads per chain N_{bead}, the molecular weight MW, the number of chains N_{chain}, density ρ, simulation cell with size of L_x, L_y, and L_z, equilibrium root mean-squared gyration radius $\langle R^2 \rangle^{1/2}_{eq}$, the chain relaxation time τ.

System	N_{bead}	MW (g/mol)	N_{chain}	ρ (kg/m³)	$L_x \times L_z \times Lz$ (nm)	$\langle R^2 \rangle^{1/2}_{eq}$ (nm)	τ (ps)
PS-9	9	1043	150	929.8	4.534×4.534×13.602	0.549	~15
PS-20	20	2189	120	940.6	5.367×5.367×16.101	0.975	~70
PS-30	30	3230	120	945.4	6.099×6.099×18.297	1.276	~160
PS-100	100	10520	60	951.0	7.161×7.161×21.483	2.648	~2000

All RNEMD simulations are carried out with the modified GMQ_num code, the numerical version of the molecular dynamics simulation software package GMQ.[29,30] In this modified code, orthorhombic periodic boundary conditions are applied. The simulation cells are elongated in the z direction ($L_x = L_y = L_z/3$), in which the momentum flux is imposed. The equations of motion are numerically integrated by the Verlet algorithm, the loose-coupling method of Berendsen[26] is used to control the temperature of the system, and neighbour lists[1] are used to speed up the computation of the nonbonded potential. The cutoff for the nonbonded potential is $r_c = 1.5$ nm. The simulations are performed at constant temperature $T = 500$ K. The momentum flux is imposed by exchanging the x component of the velocity of beads as described in the section 2. In order to cover a wide shear rate window, different velocity swap intervals $W \cdot \Delta t$ are applied: Δt is taken in the range of 1–7 fs, W in the range of every 60 to 500 time steps. The velocity profile sampling rate $W' = W + 1$ is in the range of every 61– 501 time steps for the production runs. The velocity profiles are sampled only in those time steps in which no velocity swap is performed. Table 2 lists all the RNEMD control parameters. The system takes a certain time to reach the steady state after the perturbation is applied; this time depends on the chain length and perturbation strength. The steady state can be monitored from the time evolution of the momentum flux during the simulation, which decays to a stable average. The initial transient stage has been excluded when calculating viscosity and analyzing structural changes. The resulting shear rates for different systems are: PS-9 in the range of $1.7 \times 10^{10} - 1.3 \times 10^{11} s^{-1}$, PS-20 in the range of $1.0 \times 10^{10} - 6.6 \times 10^{10} s^{-1}$, PS-30 in the range of $5.3 \times 10^{9} - 5.7 \times 10^{10} s^{-1}$, PS-100 in the range of $1.2 \times 10^{9} - 5.1 \times 10^{10} s^{-1}$.

It should be pointed out that the shear rates used in this work are very large compared to experiment. This results from (i) a short simulation time, compared to experimental time, and (ii) the requirement of a reasonable signal-to-noise ratio during the accessible simulation time. Lower shear rates, could, in principle, be achieved by increasing the velocity swap interval $W \cdot \Delta t$ at the expense of a less well defined temperature gradient.[4] The same is true for the algorithmic alternative of more often selecting an atom pair for exchange with a smaller velocity difference.[5] As a

consequence, some of the simulations are beyond the Newtonian regime. The shear rate where shear thinning sets in can be roughly estimated as the inverse of the chain relaxation time τ^{-1},[17,18,31] for PS-9 $\tau^{-1} \sim 6.7 \times 10^{10}$, for PS-20 $\tau^{-1} \sim 1.4 \times 10^{10}$ s^{-1}, for PS-30 $\tau^{-1} \sim 6.3 \times 10^{9}$ s^{-1}, for PS-100 $\tau^{-1} \sim 5.0 \times 10^{8}$ s^{-1}. Thus, it drastically decreases with increasing molecular weight. This is a problem common to all non-equilibrium simulations. With any method, one has to simulate long enough for polymer chains to move past each other, and one has to accumulate enough such events for a well-converged viscosity. Methods, such as the use of non-linear response theory and transient time correlation functions have been used recently for molecular fluids such as n-decane, [32], but are still waiting to be tried on high-molecular-weight polymers. Therefore, there are but few reports on molecular dynamics simulation of direct observation of the shear thinning onset for *realistic* polymer models, with one exception being the work on polyethylene chains by Padding and Briels.[18]

The error bar of the shear viscosity is calculated according to Eq. (7).

$$\Delta \eta \leq \langle \eta \rangle \left(\left| \frac{\Delta j_z (p_x)}{\langle j_z (p_x) \rangle} \right| + \left| \frac{\Delta \dot{\gamma}}{\langle \dot{\gamma} \rangle} \right| \right) \tag{7}$$

where, $\langle \eta \rangle$ is the average viscosity; $\langle j_z (p_x) \rangle$ is the momentum flux averaged over the production run and $\Delta j_z (p_x)$ is the standard deviation of the average $\langle j_z (p_x) \rangle$; $\langle \dot{\gamma} \rangle$ is the shear rate averaged over the production run and $\Delta \dot{\gamma}$ is the standard deviation of the average $\langle \dot{\gamma} \rangle$.

2.4. Results and discussion

2.4.1. Shear viscosity and material functions.

Here we briefly give the definition of some quantities used to analyze the results of our simulations. The apparent viscosity is calculated according to Eq. (1). The first and second normal stress differences $N_1(\dot{\gamma})$ and $N_2(\dot{\gamma})$ are calculated from diagonal elements of the stress tensor using the following equation:

$$N_1 = P_{zz} - P_{xx} \tag{8}$$

20

$$N_2 = P_{yy} - P_{zz} \tag{9}$$

$P_{\alpha\alpha}(\alpha = x, y, z)$ is calculated from the atomic implementation of virial-theorem expression:

$$P_{\alpha\alpha} = \frac{1}{V}\left(\sum_i^N m_i(v_i^\alpha - \bar{v}_i^\alpha)^2 + \sum_i^N \sum_{j>i}^N r_{ij}^\alpha F_{ij}^\alpha \right) \tag{10}$$

where, V is the volume of the simulation cell, N is the total number of beads, m_i and v_i denote the mass and actual velocity of ith bead, r_{ij} denotes the distance between bead i and j, F_{ij} is the force exerted on bead i by bead j, α refers to x, y, z components in the Cartesian coordinate system, $\bar{v}_i$ is the local flow velocity of ith bead, which is given by $\bar{v}_i = (\bar{v}_{x,i}, 0, 0)$. The first and second normal stress differences $N_1(\dot{\gamma})$ and $N_2(\dot{\gamma})$ are presented here, rather than the first and the second normal stress coefficients $\Psi_1(\dot{\gamma})$ and $\Psi_2(\dot{\gamma})$ ($\Psi_1 = N_1/\dot{\gamma}^2$, $\Psi_2 = N_2/\dot{\gamma}^2$), which are sometimes reported, because N_1 and N_2 obtained from the simulations are associated with their relative errors (particularly at low shear rate) and the division of N_1 and N_2 by a very small shear rate($\dot{\gamma} \to 0$) leads to large uncertainties in Ψ_1 and Ψ_2. In addition, the hydrostatic pressure P is computed from the normal stresses by Eq. (11).

$$P(\dot{\gamma}) = \frac{1}{3}\left(P_{xx} + P_{yy} + P_{zz} \right) \tag{11}$$

Viscosity. Fig. 2.4 shows the shear viscosity as a function of the shear rate for polymer melts with different chain lengths. For PS-9, PS-20 and PS-30, the shear viscosity functions exhibit two distinct regimes: a visible plateau at lower shear rates and a shear-thinning regime at higher shear rates. For PS-100, the shear-thinning region is dominant and the Newtonian regime is inaccessible in the given shear rate window.

The viscosity dependence on shear rate in the shear-thinning regime is often empirically described as a power-law relation, in the form $\eta \propto \dot{\gamma}^{-n}$.[33] The exponent n of the power-law can be obtained from the linear region in the log-log plot of the viscosity versus the shear rate. For comparison, the exponents obtained from this work and from some previous simulations on modelled polymers are collected in Table 2.3.
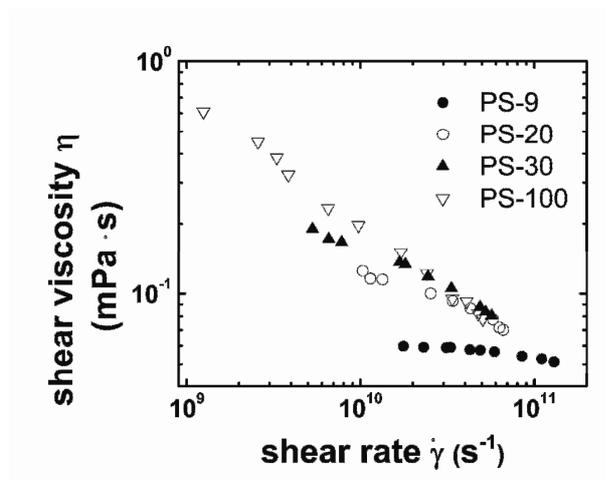
Figure 2.4. Shear-rate dependence of the shear viscosity for PS-9, PS-20, PS-30, and PS-100. Error bars are approximately the same size as the symbols and have been omitted for clarity.

Table 2.2. The RNEMD control parameters: the length of the time step Δt, the velocity swap interval W for PS-9, PS-20, PS-30, and PS-100.

PS-9		PS-20		PS-30		PS-100	
Δt (fs)	W	Δt (fs)	W	Δt (fs)	W	Δt (fs)	W
1	60	1	60	1	60	1	60
2	60	2	60	2	60	2	60
4	60	3	60	3	60	3	60
7	60	7	60	7	60	5	60
7	75	7	90	7	90	5	90
7	90	7	120	7	120	5	120
7	120	7	180	7	180	5	180
7	180	7	240	7	240	5	240
7	240	7	400	7	300	5	300
				7	347	5	330
						5	360
						5	500

Table 2.3. Exponent n of the power law ($\eta \propto \dot{\gamma}^{-n}$) in the shear thinning region for different chain length N_{bead} from this work and some other conventional NEMD simulations.

Author	Model	Force field	Ensemble and density	Exponent n (chain-length N_{bead})
this work	Realistic linear polymer	Coarse-grained force field contains three different bonds, six angles and three nonbonded terms for the non-bonded part.	NVT Different densities for different chain lengths	0.12± 5.2 % (N=9) 0.34 ± 5.6 % (N=20) 0.43 ±6.0 % (N=30) 0.56 ± 7% (N=100)
Xu. et al.[a]	Model linear chain	LJ for any two beads interaction and FENE potential used for adjacent beads interaction	NVT Same density for different chain lengths	0.25 (N=10) 0.35 (N=20) 0.42 (N=50) 0.30 (N=10)
Kröger et al.[b]	Model linear chain	All beads interact with a repulsive LJ and FENE potential is added for adjacent beads along a chain interaction	NVT Same density for different chain length	0.45 (N=30) 0.46 (N=60) 0.47 (N=100)

Bosko *et al.*[c]	Model chain	linear	WCA potential for all two beads interaction, FENE potential for adjacent beads along a chain interaction	NVT	Same density for different chain lengths	0.321±2% (N=19) 0.413±5% (N=43) 0.523±2% (N=91) 0.743±3% (N=187)
Daivis *et al.*[d]	Model chain	linear	WCA potential for all two beads interaction except the those which are bonded to each other within a molecule, rigidly constrained bonds	NVT	Same density for different chain lengths	0.45 (N=4) 0.43 (N=10) 0.42 (N=20) 0.45 (N=50)
Kröger and Hess[e]	Model chain	linear	All beads interact with a repulsive LJ and FENE potential is added for adjacent beads along a chain interaction	NVT	Same density for different chain length	0.60 ±0.10 (N=20~400) weak shear dilatancy (N< 20)

LJ potential refers to Lennard-Jones potential, WCA potential refers to Weeks-Chandler-Anderson potential, FENE potential refers to finitely extensible nonlinear elastic potential.

[a]Ref. 15, [b]Ref. 11, [c]Ref. 14, [d]Ref. 12, [e]Ref. 13

Our results suggest that the exponent n increases with molecular weight. This dependence is more pronounced for the shorter chains (PS-9 and PS-20) than for larger molecular weights. The data qualitatively agree with Xu et al.[15], Bosko et al.[14], while Kröger and Hess[13] and Daivis et al.[12] found invariant exponents, and a weak shear dilatancy is detected for short chain (N< 20) in the work of Kröger and Hess.[13] In particular, Kröger et al.[11] show a tiny dependence on short chain-lengths and almost the same exponent for longer chains. One should anyway be aware that these simulations were performed at different conditions and using different models. Moreover, the determination of the exponents is extremely sensitive to where on the shear rate curve one assumes the power law to be valid.[14] The exponent n for PS-100 lies within the experimental values reported for polymeric liquids (n in the range 0.4–0.9).[34] The exponent derived by Doi and Edwards[35] from reptation dynamics is much higher ($n \cong 1.5$). Exponents reported from simulations are generally in the range of 0.20–0.74, which are much lower than that predicted by reptation theory. The basic assumption of reptation theory in an entangled network of polymer chains, whereas chain lengths used in simulations are often too short to form entanglements. This could be one reason for the discrepancy.

The zero-shear viscosity η_0 is of both theoretical and industrial interest. It is defined as the melt viscosity in the limit of $\dot{\gamma} \to 0$ and it is a function of temperature and molecular weight. Since in molecular dynamics simulation very low shear rates are not accessible for complex liquids, the way to extrapolate the data to low shear rates becomes a key issue when estimating the η_0. The extrapolation schemes used in previous simulation are not entirely consistent. Cummings et al.[36] evaluated the η_0 for liquid rubidium by using the scheme $\eta = \eta_0 - A\dot{\gamma}^{1/2}$, which is based on the mode-coupling theory of Kawasaki and Gunton.[37] Evans and Morriss[2] confirm this theoretical prediction via NEMD simulation for the triple-point Lennard-Jones fluid. However, this $\dot{\gamma}^{1/2}$ dependence of shear viscosity has not been confirmed for complex molecular fluids. Moreover, recent work questions such dependence.[38-40] Daivis et al.[12] evaluated

the η_0 for the modeled polymer by the extrapolation scheme $\eta = \eta_0 - A\dot{\gamma}^2$, which is based on the retarded motion expansion (RME) for a third-order fluid. Bosko *et al.* determined the η_0 for dendrimer by taking the average of several extrapolation schemes.[14] As RME offers a systematic and model-independent description of an arbitrary viscoelastic fluid at low shear rates,[41] it would be reasonable to evaluate the η_0 of polymer by $\eta = \eta_0 - A\dot{\gamma}^2$ scheme. The η_0 value of polymers has also been obtained from experimental work by the extrapolation scheme $\log(\eta^{-1}) = \log(\eta_0^{-1}) - A\tau_{xz}$,[42-44] where τ_{xz} is the off-diagonal component (xz) of the stress tensor. In this work, the η_0 is determined as an average of values by using 2 different extrapolation schemes, as demonstrated for the case of PS-9 in Fig. 2.5: (1) $\eta = \eta_0 - A\dot{\gamma}^2$ and (2) $\log(\eta^{-1}) = \log(\eta_0^{-1}) - A\tau_{xz}$. For the latter extrapolation, we use the momentum flux $|j_z(p_x)|$ instead of the shear stress τ_{xz}. The η_0 determined for all systems are summarized in table 4, except for PS-100, because the given shear rate window for PS-100 is unable to reach the Newtonian regime. The η_0 determined by these 2 extrapolation schemes agree well with each other in the uncertainty limit. The dependence of η_0 on the molecular weight is linear ($\eta_0 \propto M$) for short chains.[45] Such dependence on the molecular weight is predicted by the Rouse model. As shown in Fig. 2.6, one observes an almost linear dependence of η_0 on the molecular weight with the slopes of 0.98 and 1.10 obtained from both extrapolation schemes.

Experiment[46] indicates that the zero shear viscosity for polystyrene of molecular weight ~1000g/mol at 500 K is around $15 \times 10^{-3}\,\mathrm{Pa \cdot s}$. Comparing the η_0 for the similar molecular weight of PS-9 in this work, the simulation result ($\sim 0.06 \times 10^{-3}\,\mathrm{Pa \cdot s}$) is much lower than the experiment, by a factor of ~250. As predicted by hydrodynamics, the zero-shear viscosity and the self-diffusion coefficient are approximately reciprocal.[47] The self-diffusion coefficient of the coarse-grained model used in this work is, indeed, found to be a factor of ~200 higher than that of the fully atomistic model of the PS-9 system.[24] Therefore, the difference of the zero-shear

viscosity between simulation and experiment can be traced mainly to the fast dynamics of the coarse-grained model used. There could be two possible explanations: (1). The reduction of the number of degrees of freedom upon coarse-graining eliminates the fluctuating force associated with those missing molecular degrees of freedom.[48] (2). The coarse-grained force field is generally very soft. This leads to the reduction of nearest-neighbor interactions, particularly of their repulsion, and thereby atoms can more easily escape from the local cages formed by their neighbors.[25] According to Boltzmann's superposition principle, the zero-shear viscosity can be deduced from the time dependent shear modulus $G(t)$,[49] i.e.,

$$\eta_0 = \int_0^\infty G(t)dt \qquad (12)$$

Hence, the fast dynamics of the coarse-grained model can effect η_0 through the shear modulus. Two parts contribute to the shear modulus in an unentangled system [49]

$$G(t) = G_{mic}(t) + G_{Rouse}(t) \qquad (13)$$

The first term $G_{mic}(t)$ accounts for the short-time behavior, which is controlled by the internal degrees of freedom or microstructure. This contribution cannot be reproduced well by a coarse-grained model, because short-time degrees have been eliminated in order to improve the computational efficiency. The second term $G_{Rouse}(t)$ accounts for the generic Rouse dynamics, which can be reproduced by the coarse-grained model taking into account a time scale factor. Both terms complicate the viscosity prediction in coarse-grained model, and for details a further study is required. Still, the agreement of η_0 with Rouse theory and experiment is encouraging when the time scale factor is taken into account.

Normal stress difference. As in experimental[33] and previous NEMD simulation data,[15,19] the first normal stress difference N_1 predicted from this work is positive for all cases, as shown in Fig. 2.7, This validates the theoretical prediction that simple shear is accompanied by a non-vanishing normal stress difference.[49] Physically, this corresponds to a compressing force perpendicular to the plane in which shear flow take

place. As the shear rate increases, N_1 increases significantly, following a power law in the shear-thinning region in the form: $N_1 \propto \dot{\gamma}^\alpha$ (For PS-9, 20, 30, 100, $\alpha = 1.0, \ 0.72, \ 0.66, 0.53$). A similar behavior has been observed for polyethylene by Jabbarazadeh et $al.$ in their NEMD simulation.[19] Concerning the second normal stress difference N_2, both experimental and simulation work provide only limited data. However, it is has been pointed out[33] based on experimental findings, that N_2 is negative for homogeneous polymer liquids, that $-N_2/N_1$ typically lies in the range $0.2 \sim 0.3$, and that it is insensitive to the shear rate. Fig. 2.8 indicates that N_2 is negative for nearly all the systems and it increases with the shear rate in the shear-thinning region. The values of $-N_2/N_1$ in the shear-thinning region for PS-9, 20, 30 are in the range of $0.2 \sim 0.3$, for PS-100 is 0.1~0.2.

Hydrostatic pressure. Fig. 2.9 shows the dependence of the hydrostatic pressure on the shear rate. Two different regimes are visible. At higher shear rate, the hydrostatic pressure increases with the shear rate, and it seems again to follow the power law $P = P_0 + \dot{\gamma}^\beta$. Similar behavior was found for polyethylene[17,19] and dendrimers.[14] At lower shear rate, there is a small, if any, increase of the hydrostatic pressure, and it is close to the equilibrium value. Moore $et \ al.$[17] have found a minimum of the hydrostatic pressure before a rapid increase, and this pressure minimum occurs at the same shear rate in which the intermolecular LJ potential energy has a minimum. Due to uncertainty at the low shear rate in our result, the existence of such a minimum can neither be confirmed nor ruled out.

Table 2.4. Estimated values of the zero-shear viscosity (η_0) by the different extrapolation scheme (1) $\eta = \eta_0 - A\dot{\gamma}^2$,(2) $\log(\eta^{-1}) = \log(\eta_0^{-1}) - A|j_z(p_x)|$.

Extrapolation scheme	PS-9 ($mPa \cdot s$)	PS-20 ($mPa \cdot s$)	PS-30 ($mPa \cdot s$)
1	$0.060 \pm 0.3\%$	$0.122 \pm 0.5\%$	$0.182 \pm 2\%$
2	$0.061 \pm 8.0\%$	$0.148 \pm 10\%$	$0.208 \pm 12\%$
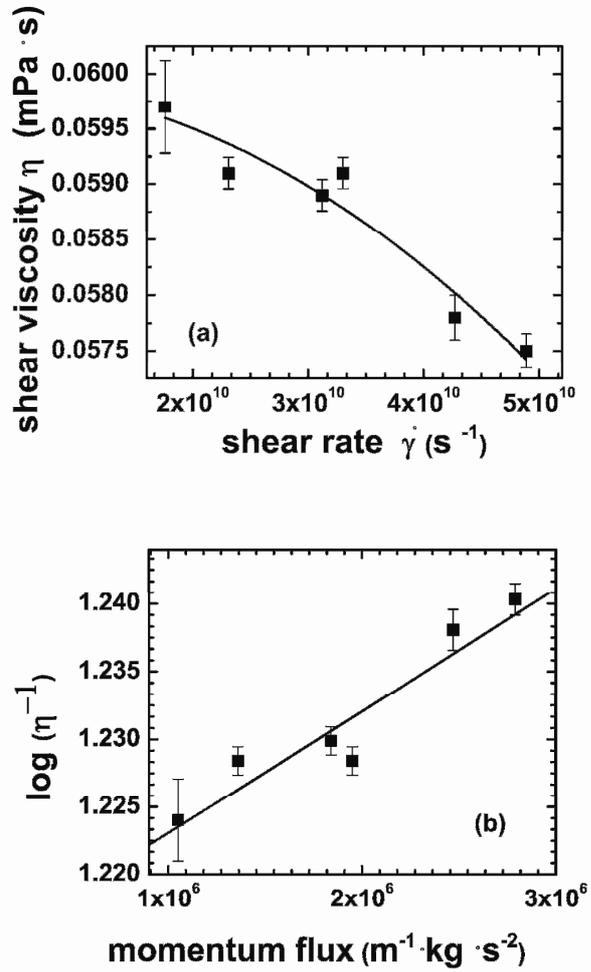
Figure 2.5. Demonstration of the extrapolation schemes used to obtain the zero-shear viscosity from simulation for the PS-9 system. (a) Scheme 1: $\eta = \eta_0 - A\dot{\gamma}^2$ (b) scheme 2: $\log(\eta^{-1}) = \log(\eta_0^{-1}) - A\left|j_z\left(p_x\right)\right|$.
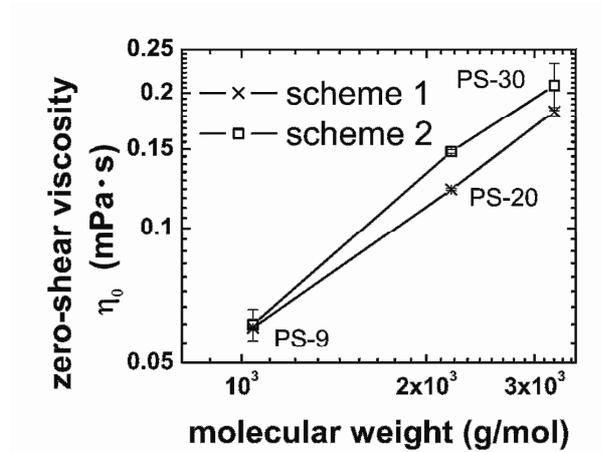
Figure 2.6. Zero-shear viscosity versus molecular weight. Data used from extrapolation scheme (1) $\eta = \eta_0 - A\dot{\gamma}^2$, (2) $\log(\eta^{-1}) = \log(\eta_0^{-1}) - A|j_z(p_x)|$. The slopes of linear fits for these data are $0.98 \pm 0.1\%$, $1.10 \pm 0.3\%$, respectively. Solid lines are used to guide eyes.
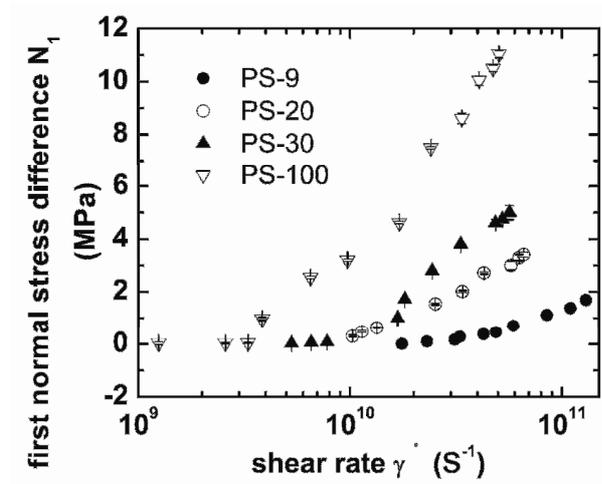
Figure 2.7. First normal stress difference N_1 versus shear rate $\dot{\gamma}$ for polystyrene melts of PS-9, PS-20, PS-30, and PS-100.
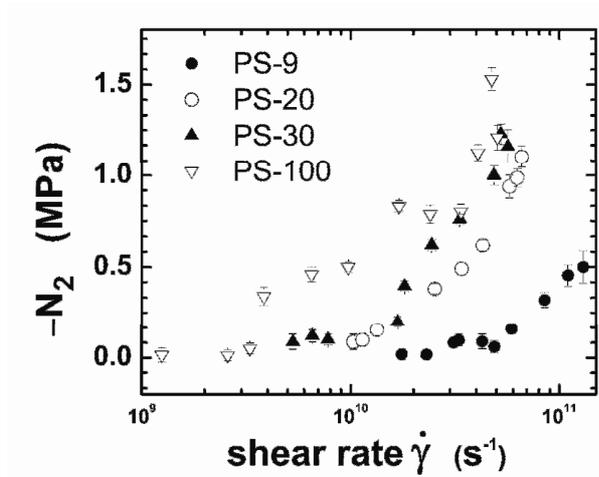
Figure 2.8. Second normal stress difference N_2 versus shear rate $\dot{\gamma}$ for polystyrene melts of PS-9, PS-20, PS-30, and PS-100.
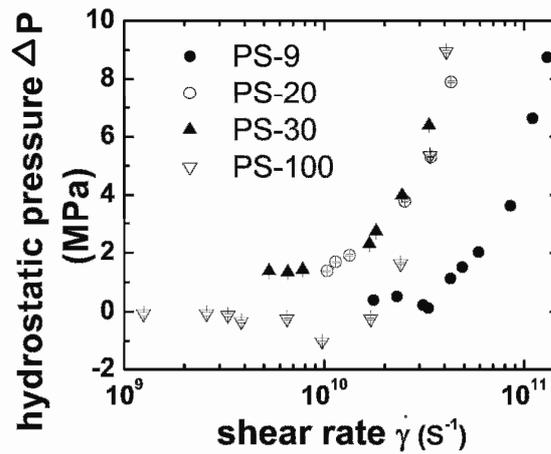
Figure 2.9. Hydrostatic pressure difference $\Delta P = P(\dot{\gamma}) - P(0)$ versus shear rate for polystyrene melts of PS-9, PS-20, PS-30, and PS-100.

2.4.2. Structural alteration under shear

The dependence of the molecular configurations and alignment on the shear rate is covered in this section. In the following analyses, the molecules, whose centres of mass are in the velocity-exchange slabs (slab1 and slab 11), have been excluded.

Average chain dimension. Fig. 2.10. shows the root mean-squared gyration radius $\langle R^2 \rangle^{1/2}$ as a function of the shear rate for different chain lengths. Fig. 2.11 shows the configurations of a single chain of PS-100 under different shear rate. At low shear rates, $\langle R^2 \rangle^{1/2}$ approaches its equilibrium value. As the shear rate increases, the shear field deforms the configuration and elongates the chain. These changes are more marked for the long chains.

Shear-induced alignment. Shear-induced alignment is investigated in term of birefringence extinction angle χ. As in RNEMD, the flow field imposed on the system corresponds to two symmetric planar Couette flows, the momentum fluxes $j_z(p_x)$ in the upper and lower halves are equal in magnitude but opposite in direction. Both half cells have the same shear rate, but the velocity profiles are symmetric. As a consequence, polymer chains are aligned symmetrically in the two halves of the simulation cell. This is found, indeed, in the distribution of the single-molecule alignment angle θ, the angle between the end to end vector and the flow direction x, as shown for the case of PS-30 in Fig. 2.12. Therefore, the birefringence extinction angle χ should be calculated from both halves of cell separately. One can take the average of χ from both half cells to improve the statistics. To describe the shear-induced alignment, we calculate an order tensor **S** defined in Eq. (14).

$$\mathbf{S} = \frac{1}{N} \left\langle \sum_{i=1}^{N} \left(\mathbf{u}_i \otimes \mathbf{u}_i - \frac{1}{3} \mathbf{I} \right) \right\rangle \tag{14}$$

Where, $\mathbf{u}_i$ is unit vector along the end-to-end direction of the molecule i, **I** is the unit tensor. The angle brackets indicate an ensemble average. The birefringence extinction angle χ is calculated as the angle between the eigenvector of **S** corresponding to the largest eigenvalue of the order tensor and the shear flow direction x. As shown in Fig. 2.13, the birefringence extinction angle decreases as the shear rate increases. These changes describe quantitatively the alignment of the system with respect to the flow direction. The process of chain alignment, in combination with chain stretching, leads to a macroscopic anisotropy of the material. It is expected that the birefringence

extinction angle converges to 45^0 in the Newtonian regime.[35] The birefringence extinction angles of PS-9 and PS-20 system at low shear rates are close to 45^0, but the birefringence extinction angle of PS-100 is still far from 45^0. This indicates again that the shear rates used in this work are not low enough to reach the Newtonian regime for the long chains. Note that, for PS-100 at the highest shear rate of $\dot{\gamma} = 5.06 \times 10^{10} s^{-1}$, the root mean-squared gyration radius $\langle R^2 \rangle^{1/2}$ is larger than the half length of the simulation cell ($L_x / 2$ and $L_y / 2$), and the finite box size limits the minimum flow alignment angle to around 5^0.

2.5. Summary

The RNEMD method has been used to calculate the viscosity of a coarse-grained model of short-chain polystyrene. The simulations were performed at constant temperature and constant volume. The viscometric functions obtained in this paper can be summarized as follows: 1. The zero-shear viscosity is linearly dependent on the molecular weight for PS-9, PS-20, and PS-30 systems; this agrees with experiments and the theoretical prediction of the Rouse model. 2. The shear-thinning behaviour for all studied systems follows a power law. The exponent of the power law increases with the molecular weight, and this dependence is more pronounced for short chains (PS-9 and PS-20). 3. The first normal stress difference is positive and the second normal stress is negative for all systems. The first normal stress difference follows the power law of form of $N_1 \propto \dot{\gamma}^\alpha$ at higher shear rates. 4. The hydrostatic pressure increases at higher shear rates. The structural changes under shear are quantitatively investigated. The analysis of these effects indicates that the process of chain alignment, in combination with chain stretching, leads to a macroscopic anisotropy of the material. The reverse non-equilibrium molecular dynamics method gives reliable results in the Newtonian regime, and a still reasonable agreement with homogeneous-shear NEMD methods at higher shear rates. As other methods, it has problems when the shear rates are extremely high.

The extrapolated zero shear viscosity is linearly dependent on the molecular weight, even though its absolute value is lower than the experiments by a factor of ~200 for the shortest chain length. This scaling factor is probably due to the well-known intrinsic speed up of the coarse-grained model. The scaling factor found for the viscosity is close to that of the diffusion coefficient calculated from equilibrium MD simulations of the same model. This result indicates the CG model which has been developed taking only structural information into account can reproduce the generic Rouse behaviour, and those short-time degrees which have been actively removed in the CG model are responsible for the larger difference of zero-shear viscosity between simulation and experiment.
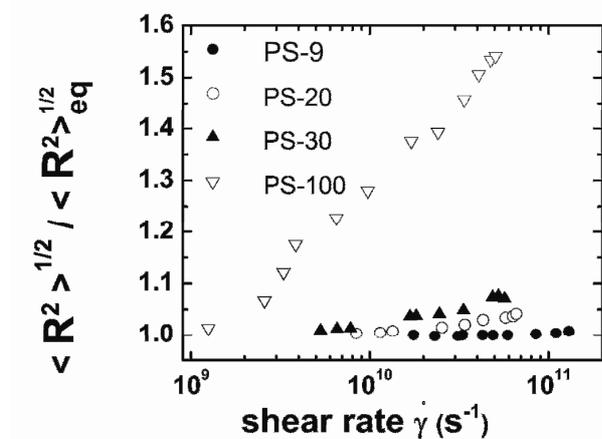
Figure 2.10. Root mean-squared gyration radius, $\langle R^2 \rangle^{1/2}$, versus shear rate for PS-9, PS-20, PS-30, and PS-100. $\langle R^2 \rangle^{1/2}$ is normalized by its equilibrium value $\langle R^2 \rangle^{1/2}_{eq}$ (no shear) .

$$\dot{\gamma} = 1.25 \times 10^9 s^{-1} \qquad \dot{\gamma} = 5.06 \times 10^{10} s^{-1}$$
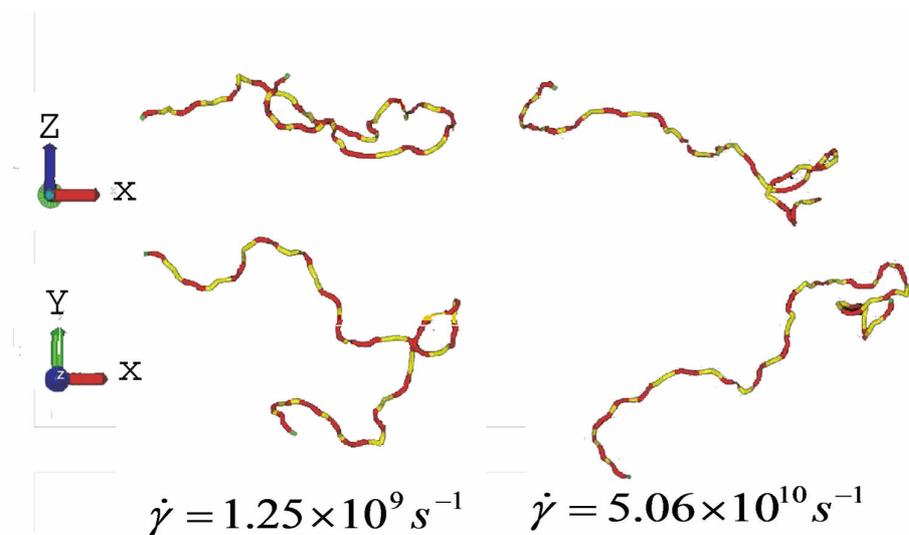
Figure 2.11. Typical configurations of individual chains of PS-100 under different shear rates.

37
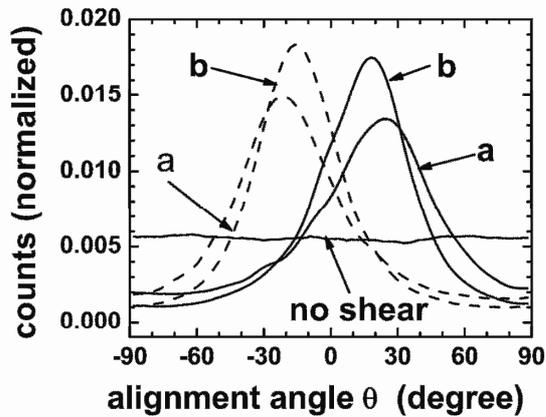
Figure 2.12. Distributions of the single molecule alignment angle θ at various shear rates $\dot{\gamma}$ for the PS-30 system. The solid lines are from the upper half of the simulation cell, the dashed lines from the lower half. The distribution is weighted by a factor of $1/\sin\theta$. For (a) shear rate $\dot{\gamma} = 1.82 \times 10^{10}$ s-1, the distribution maxima obtained from the upper and lower halves of the simulation cell are 22.9^0 and -22.0^0, respectively. For (b) shear rate $\dot{\gamma} = 3.34 \times 10^{10}$ s-1, the maxima are 16.5^0 and -16.1^0, respectively.
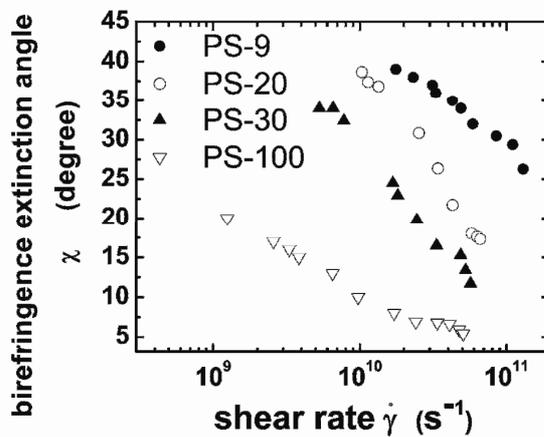
Figure 2.13. Birefringence extinction angle χ as a function of the shear rate for PS-9, PS-20, PS-30, and PS-100.

38

2.6. References and notes

(1)   Allen, M. P.; Tildesley, D. J. *Computer Simulation of Liquids*; Oxford University Press, 1987.

(2)   Evans, D. J.; Morriss, G. P. *Statistical Mechanics of Nonequilibrium Liquids*; Academic Press, London, 1990.

(3)   Hess, B. *J. Chem. Phys.* **2002**, *116*, 209-217.

(4)   Müller-Plathe, F. *Phys. Rev. E* **1999**, *59*, 4894-4898.

(5)   Müller-Plathe, F.; Bordat, P. Reverse Non-Equilibrium Molecular Dynamics, In *Lecture Notes in Physics*, 2004; Vol. 640, pp 310-326.

(6)   Soddemann, T., Ph.D. thesis, Johannes Gutenberg-Universität Mainz , Germany, 2001.

(7)   Bordat, P.; Müller-Plathe, F. *J. Chem Phys.* **2002**, *116*, 3362–3369.

(8)   Guo, H.; Kremer, K.; Soddemann, T. *Phys. Rev. E* **2002**. 66, 061503.

(9)   Soddemann, T.; Auernhammer, G. K.; Guo, H.; Dünweg, B.; Kremer, K. *Eur. Phys. J. E* **2004**. 13, 141-151

(10)   Donkó, Z.; Goree, J.; Hartmann, P.; Kutasi, K. *Phys. Rev. Lett.* **2006**, *96*, 145003.

(11)   Kröger, M.; Loose, W.; Hess, S. *J. Rheol.* **1993**, *37*, 1057-1079.

(12)   Daivis, P. J.; Matin, M. L.; Todd, B. D. *J. Non-Newtonian Fluid Mech.* **2003**, *111*, 1-18.

(13)   Kröger, M.; Hess, S. *Phys. Rev. Lett* **2000**, *86*, 1128 - 1131.

(14)   Bosko, J. T.; Todd, B. D.; Sadus, R. J. *J. Chem. Phys.* **2004**, *121*, 12050-12059.

(15)   Xu, Z.; de Pablo, J. J.; Kim, S. *J. Chem. Phys.* **1995**, *102*, 5836-5844.

(16)   Kröger, M. *Phys. Rep.* **2004**, *390*, 453-551.

(17)   Moore, J. D.; Cui, S. T.; Cochran, H. D.; Cummings, P. T. *J. Non-Newtonian Fluid Mech.* **2000**, *93*, 83-99.

(18)   Padding, J. T.; Briels, W. J. *J. Chem. Phys.* **2003**, *118*, 10276-10286.

(19)   Jabbarzadeh, A.; Atkinson, J. D.; Tanner, R. I. *Macromolecules* **2003**, *36*, 5020 -5031.

(20)   Padding, J. T.; Briels, W. J. *J. Chem. Phys.* **2001**, *115*, 2846-2859.

(21)   Akkermans, R. L. C.; Briels, W. J. *J. Chem. Phys.* **2000**, *113*, 6409-6422.

(22)   Fukunaga, H.; Takimoto, J.; Doi, M. *J. Chem. Phys.* **2002**, *116*, 8183-8190.

(23)   Kremer, K.; Müller-Plathe, F. *MRS Bulletin* **2001**, *26*, 205-210.

(24)   Milano, G.; Müller-Plathe, F. *J. Phys. Chem. B* **2005**, *109*, 18609 -18619.

(25)   Depa, P. K.; Maranas, J. K. *J. Chem. Phys.* **2005**, *123*, 094901.

(26)   Berendsen, H. J. C.; Postma, J. P. M.; van-Gunsteren, W. F.; DiNola, A.;
        Haak, J. R. *J. Chem. Phys.* **1984**, *81*, 3684-3690.

(27)   Zhang, M.; Lussetti, E.; Souza, L. E. S. d.; Müller-Plathe, F. *J. Phys. Chem. B*
        2005, *109*, 15060 -15067.

(28)   Spyriouni, T.; Tzoumanekas, C.; Theodorou, D.; Müller-Plathe, F.; Milano, G.
        Macromolecules **2007**, *40*, 3876.

(29)   Brown, D., *The gmq Manual Version 3*, *http://uni-
        savioe.fr/labos/mops/brown/gmq.html*

(30)   Queyroy, S., Simulations moléculaires dynamiques de surfaces de polymère
        amorphe: cas de la cellulose, Ph.D. thesis,Université de Savoie, 2004.

(31)   Cui, S. T.; Cummings, P. T.; Cochran, H. D.; Moore, J. D.; Gupta, S. A.
        International Journal of Thermophysics **1998**, *Volume 19*, 449-459.

(32)   Pan, G.; McCabe, C. *J. Chem Phys.* **2006**, *125*, 194527.

(33)   Mark, J.; Ngai, K.; Graessley, W.; Mandelkern, L.; Samulski, E.; Koenig, J.;
        Wignall, G. *Physical Properties of Polymers*, 3rd ed.; Cambridge University
        Press, 2004.

(34)   Bird, R. R.; Curtis, C. F.; Armstrong, R. C.; Hassager, O. *Dynamics of
        polymeric liquids, Fluid Mechanics*; John Wiley & Sons, Inc., New York, 1987;
        Vol. 1.

(35)   Doi, M.; Edwards, S. F. *The Theory of Polymer Dynamics*; Oxford University
        Press, 1988.

(36)   Cummings, P. T.; Morriss, G. P. *J. Phys. F* **1987**, *17*, 593-604.

(37)   Kawasaki, K.; Gunton, J. D. *Phys. Rev. A* **1973**, *8*, 2048 - 2064.

(38) Ryckaert, J.-P.; Bellemans, A.; Ciccotti, G.; Paolini, G. V. *Phys. Rev. Lett.* **1988**, *60*, 128 - 131.

(39) Pierleoni, C.; Ryckaert, J.-P. *Phys. Rev. A* **1991**, *44*, 5314 - 5317.

(40) Todd, B. D. *Phys. Rev. E* **2005**, *72*, 041204.

(41) Bird, R. R.; Curtis, C. F.; Armstrong, R. C.; Hassager, O. *Dynamics of polymeric liquids, Kinetic Theory*, 2nd ed.; John Wiley & Sons, Inc., New York, 1987; Vol. 2.

(42) Spencer, R. S.; Dillon, R. E. *Journal of Colloid Science* **1948**, *3*, 163-180.

(43) Spencer, R. S.; Dillon, R. E. *Journal of Colloid Science* **1949**, *4*, 241-255.

(44) Vinogradov, G. V.; Malkin, A. Y. *J. Polymer Sci. Part A* **1964**, *2*, 2357-2372.

(45) Bicerano, J. *Prediction of Polymer Properties, Revised and Expanded*, 2nd ed.; Marcel Dekker, 1996.

(46) Viscosity data of short-chain polystyrene (1000g/mol) measured at 80 ^{o}C (207.3 Pa s), 110 ^{o}C (2.9 Pa s), 130 ^{o}C (0.57 Pa s) and 145 ^{o}C (0.23 Pa s) were extrapolated to 500 K using the Williams-Landel-Ferry equation. The experimental data were provided by BASF AG (M. Rüllmann, personal communication).

(47) Phillies, G. D. J. *Macromolecules* **2002**, *35*, 7414 - 7418.

(48) Izvekov, S.; Voth, G. A. *J. Chem. Phys.* **2006**, *125*, 151101.

(49) Strobl, G. R. *The Physics of Polymers : Concepts for Understanding Their Structures and Behavior*; Springer-Verlag, New York, 1996.

3. Backmapping coarse-grained polymer models under sheared nonequilibrium conditions

3.1. Introduction

Polymers exhibit physical properties in a broad range of length and time scale, and these properties cannot be viewed on one length scale alone. However, any individual molecular simulation technique is restricted to much narrower range. In order to have a complete picture of the polymers, much effort has been made to study them by means of molecular simulation through a hierarchical approach.[1,2-5] Multiscale simulation is a neither unique nor trivial path from one scale to another. Coarse-graining is the process of "zooming-out": the "forward-mapping" process, passes from a detailed model to a simpler one. Often, the terms "coarse-grained" (CG) and "mesoscopic" are used indiscriminately and can mean different things. In this paper, we define the term "coarse-grained" following ref. 5: One interaction centre (also referred to as "bead" or "superatom") contains of the order of 10 real non-hydrogen atoms or approximately one chemical repeating unit. CG models employed here retain some chemical individualities. Therefore, they are not generic models, but material-specific. CG models have been proven to be very efficient in studying the complicated behaviour of polymers. This efficiency comes from the fact that CG models only take into account those degrees of freedom deemed relevant for the particular properties studied.[6,7,8] On the other hand, the amount of detailed information lumped in one single CG bead can obscure some fundamental aspects, and it can preclude the calculation of polymer properties, which depend on the positions of atoms. Therefore, one also needs a "zoom-in" procedure which restores the atomistic features to a CG model. Indeed, the chemical details discarded in the CG model can be reproduced by reinserting the atoms. This method is called fine-graining, reverse-mapping or backmapping. The main applications of backmapping are listed below:

(1) Making different kinds of analyses at different levels[7]. Refining a CG model is a reliable method to generate atomistic structures, at least as probed by neutrons, positronium and small penetrants[3,9,10]. By tracing the CG model, which depends on the properties of entire chain, back to atomistic level, the "atomistic" properties, which depend on the behaviour of individual atoms, can be also calculated. For example, the structure factor calculated from backmapped bisphenol-A polycarbonate melt agrees with neutron scattering,[3] the properties probed by atomic motion agree with the diffusion of penetrants through polymer.[9]

(2) Generating equilibrated ensembles with atomistic details for conducting further atomistic simulation or predicting properties for which atomistic details are important. In this case, CG model plays a role as means of relaxing the atomistic structure. By refining CG structure from a CG trajectory which has already undergone relaxation, a great computation cost is saved.

As most CG simulation studies focus on reproducing static structural properties, such as distributions of geometric quantities, and thermodynamic properties, like cohesive-energy, density and pressure, the simulations are performed under equilibrium conditions. Accordingly, efforts in developing backmapping method are pursued on equilibrium systems. Early attempts at the backmapping method have been made by Tschöp et al. [3] and Kotelyanskii et al.[11] In particular the latter proposed a specific fine-graining procedure in order to introduce atoms into their lattice model of polystyrene. Presently, backmapping has been widely used to generate atomistic structures from CG equilibrium ensembles.[2,12,13] On the other hand, dynamic properties, in particular melt viscosities under shear or elongational flow, are of great interest to the polymer manufacturing and processing. Recently, these dynamic properties have been a simulation target in some CG simulations[1,14], which were performed under nonequilibrium conditions. To the best of our knowledge, so far no attempts have been made to develop backmapping methods for the nonequilibrium situations. Thus, a robust backmapping method for nonequilibrium systems is still needed.

In a typical protocol, backmapping an equilibrium system involves two steps:

(1). Each CG bead is reconstructed in atomistic detail. To do this, templates of many possible atomistic structures are set up and the CG beads are replaced by a proper selection from one of these templates which fits the contour of the underlying CG chain. The template library is generally extracted from a (preceding) atomistic equilibrium simulation. If several atomistic configurations fit one CG bead, the atomistic structure is chosen, which allows the best superposition also for the bead's neighbourhood. The construction of the other monomers continues until the end of the chain. In this step, only geometric criteria are used, no force and potential energy calculations are involved, which leads to a high backmapping efficiency. If a CG bead contains a complex atomic structure with bulky side groups, a straightforward reinsertion of atomistic details often leads to artificial interlocks of side groups, for example, the catenation or spearing of phenyl rings. In this case, a strategy is needed to avoid interlocking. In ref 13, the catenation of phenyl ring is removed in the following way: add fictitious Lennard-Jones particles centred in the phenyl rings; the non-bonded interactions are gradually introduced on both fictions and genuine atoms until to their full values: afterwards, the fictitious particles are removed. In this stage, avoiding interlocking of side groups needs force and potential energy calculations. We refer to this preparatory stage as a pre-process for the structural optimization.

(2). Collective and local relaxation are performed with energy minimization, molecular dynamics or Monte Carlo optimization. The atomistic configuration generated in step (1) is not the most 'comfortable' one in its local environment. Atom overlaps may have been generated. The reason is that the CG force field is derived from average atomic distributions. The cross dependence between different distributions in the atomistic description is generally neglected. Harmandaris et al [12] have pointed out that this approximation may lead to conformations, which do not exist in the atomistic description, still being sampled in the CG model. When atomistic details are re-inserted into such CG conformation, strong overlaps may result. This happens more often in coarser CG models. Therefore, relaxation by energy minimization (EM), molecular dynamics (MD) or Monte Carlo (MC) is required to eliminate such artefacts. Generally, EM leads to the nearest local energy minimum, while MD and MC can, in principle,

reach the global energy minimum. Further relaxation of the atomistic structure is achieved post-processing it with atomistic MD run or sometimes a combination of EM and MD, or even MC[11].

There are two additional requirements in backmapping a nonequilibrium CG system: (1) The deformed CG configurations need to be retained in the atomistic picture. Usually, stretched and sheared polymer configurations in nonequilibrium systems are different from equilibrium ones. The backmapped atomistic configurations should be able to reflect these features. The backmapping process must therefore relax the polymer locally but not its global structure. (2) The deformation energy stored in the chain of the CG model should be passed to the atomistic level. In an atomistic molecular mechanics model[15,16] of a deformed chain, three types of valence coordinates (bond length r_i, bending angle α_i and torsional angle φ_i) deviate from the equilibrium values and the deformation energy stored in the chain is dissipated in them. These deformations have been recorded in the CG structure during the nonequilibrium process, and a proper backmapping method should be able to translate these CG coordinates into atomistic ones. Obviously, the common backmapping methods cannot meet these requirements for two main reasons: (1) During EM or equilibrium MD or MC runs applied to the system after remapping (step 1), the conformation generated from the nonequilibrium CG simulation is unstable and relaxes quickly toward energetically more favourable structures, which are no longer stretched. (2) The atomistic coordinates r_i, α_i and φ_i, which are obtained by reinserting the atomistic equilibrium templates, do not correspond to the parent deformed CG conformation. In this paper, we propose three strategies and a new backmapping procedure to meet the above mentioned requirements. An application to atactic polystyrene melts under steady shear flow is demonstrated.

3.2. Strategies and procedure

3.2.1. Strategy 1: Preserving globally sheared configurations in the backmapping procedure by applying position restraints.

To meet the first requirement, i.e. to retain the global stretched configuration from the CG simulation, we apply position restraints to all those atoms which coincide with locations of CG beads. The position restraint potential V_{pr} is given by

$$V_{pr} = \frac{1}{2} k_{pr} \left(\mathbf{r}_i - \mathbf{R}_i \right)^2 \tag{1}$$

where, k_{pr} is the force constant, $\mathbf{r}_i$ is the coordinate of particle i, $\mathbf{R}_i$ is its fixed reference position. Two remarks are necessary here: (1) In this study, the force constant k_{pr} is taken as 10000 kJ mol $^{-1}$ nm $^{-2}$, which is sufficiently stiff to preserve the configuration from the CG run while its contribution to total energy is fairly small (see below). This values, however, is probably not transferable to other CG models. It, in principle, may depend on polymer stiffness, nonequilibrium conditions, mapping scheme and other system peculiarities. (2) In the present study, the CG beads are located on real atoms. Therefore, the CG coordinates can be directly used as reference positions. Depending on the CG mapping scheme, the CG coordinates may be located on the centre of geometry or centre of mass of the group of atoms and not coincide with any real atoms. In this case, the reference positions need to be recalculated and the method elaborated here is still adaptable.

3.2.2. Strategy 2: Achieving a globally deformed, but locally relaxed atomistic structure through a molecular mechanics approach.

In the molecular mechanics force field, the total potential energy V of deformed molecules can be decomposed into two terms:

$$V = U_{con} + V_{ex} \tag{2}$$

where, V_{ex}, is the imposed external field, U_{con} is the conformational energies of chains, [17]. i.e.

$$U = \sum_r U(r) + \sum_\alpha U(\alpha) + \sum_\varphi U(\varphi) + \sum_l U(l) \qquad (3)$$

The first two terms $U(r)$ and $U(\alpha)$ express the contributions to the potential energy of the molecules due to the deviation of bond lengths and valence angles from the reference (relaxed) values r_i and α_i respectively. The third term $U(\varphi)$ is the torsional potential and $U(l)$ is the nonbonded interaction between particle pairs i and j as the function of distance l_{ij}. The structure of the deformed molecules can be generated by minimizing the conformational energy in the presence of an applied external force. This procedure has been adapted in generating deformed polymers [16,17]. We borrow this idea to generate the deformed local atomistic structures out of template structures from an equilibrium (undeformed) simulation. Here, the external potential is the position restraint potential. The procedure is illustrated in Fig. 3.1: we insert atomistic equilibrium templates in place of the CG beads and restrain all atoms coinciding with bead locations. Then we energy-minimise in the presence of the position restraints until the total energy converges. If one neglects the weak energy contribution from the position restraints, the conformational energy is approximately the total energy. This approximation is reasonable, as in this study, the contribution from position restraints to the total energy is less than 4% in the first EM step and less than 1% in the final step.

47
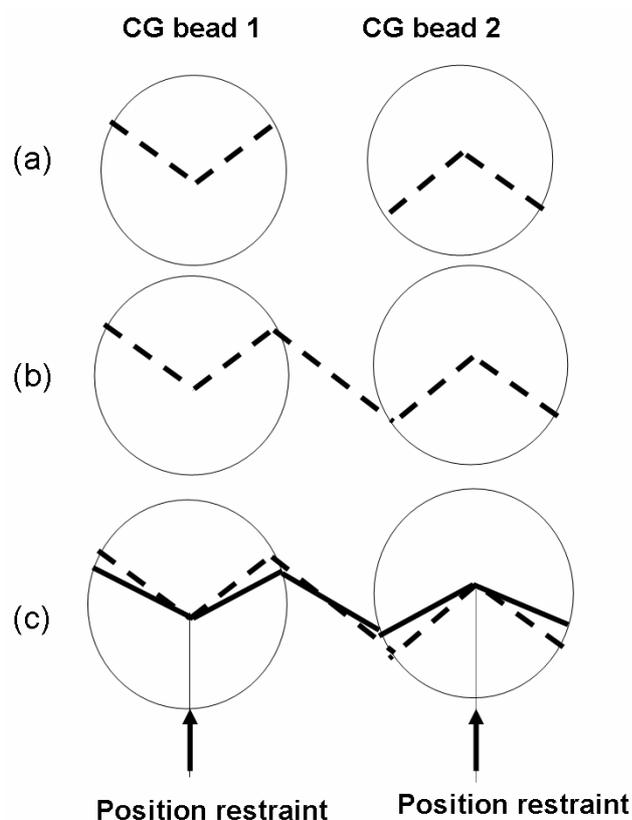
Figure 3.1. llustration of rebuilding the atomistic details for coarse-grained (CG) beads within a deformed chain conformation. For simplicity, one CG bead is assumed to contain a 3-carbon paraffin-like structure. One CG bead is indicated by one circle. (a) Atomistic equilibrium templates (dashed line) are inserted in places of their corresponding CG beads. (b) Atomistic structure before structure optimization (dashed line). (c) Atomistic structure after optimization with applying position restraints (solid line); arrows indicate the position restraints applied. For comparison, the atomistic structure before optimization (dashed line) is also shown in (c).

3.2.3. Strategy 3: Minimizing the isolation of segments introduced by the position restraints via an iterative procedure.

An additional problem arises when one attempts to meet both requirements simultaneously: One needs more position restraints to preserve the global configuration as precisely as possible, and at the same time as few as possible for optimizing the deformed atomistic structure, because they hinder also the *local* rearrangement of chain segments. The atomistic structure so generated (via strategy 2) is only locally optimized. i.e. stresses within the chains are not transmitted across a restrained atom and the local conformation does not feel that it is part of a long chain; we refer to this effect as segment isolation. Therefore, we attempt to find a compromise between the two requirements. We are interested in the average properties of the nonequilibrium system, which are not seriously be affected by the local conformation of an individual segment. Based on this consideration, we use fewer position restraints and distribute them evenly over the whole polymer chain. In this way, the global conformation is still preserved although not all atomistic segments are fixed precisely to the positions of their parent CG beads. We optimize the structure until the energy converges. The conformation so generated still suffers from segment isolation but to a smaller extent. A remedy is to shift the restraints and repeat the energy minimisation: We use same number of position restraints but move them to those atoms, which were free in the previous EM run, and optimise again until the energy converges. We repeat the EM runs until the energy is converged in the presence of various position restraints. The final conformations can be regarded as independent of the locations of position restraints.

3.2.4. Backmapping procedure

Our backmapping procedure for a nonequilibrium system involves three steps, as is outlined in Fig. 3.2. In the first step, each bead of the CG model is replaced by an atomistic segment, whose conformation is extracted from the library of average equilibrium conformations. A pre-processing for avoiding interlocking of bulky side

groups is also included in this step. At this step, the usual recipe for backmapping is followed. In the second step, the atomistic structure is energy-minimised while applying position restraints to all atoms coinciding with the locations of their parent CG beads (in the example of polystyrene, these are all methylene carbons). In the third step, the atomistic structure is re-optimized with fewer position restraints. Several position restraint schemes can be alternated during the structure optimization. The conformation whose energy converges in the presence of various position restraint schemes is accepted as the final one. This procedure can have problems at the chain end, since a chain end has more freedom and a behaviour different from the central segments. The longer the chain length is, the less important these problems become. In this study, no position restraints are applied to the chain ends.
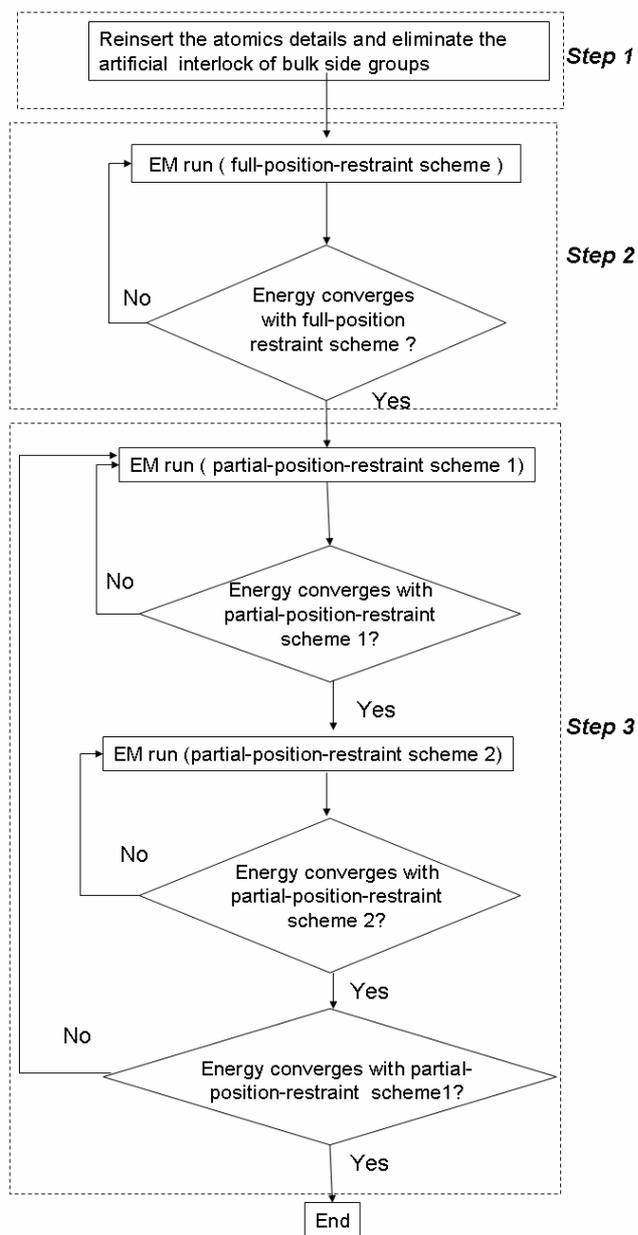
Figure 3.2. The workflow of the backmapping procedure of a coarse-grained sheared nonequilibrium conformation. The position restraint schemes are explained in Figure 3.3.

3.3. Mesoscale models of vinyl polymers and the structural alteration under steady shear flow studied by reverse nonequilibrium molecular dynamics

This section is intended to guide readers quickly to the earlier work that is essential for understanding the present investigation. Extensive details can be found in ref. 18 and ref. 1.

A systematic procedure to coarse-grain atomistic models of vinyl polymers into off-lattice mesoscopic models was developed in our earlier work.[18] This model is able to keep informations about the polymer's stereosequence. A diad is considered as the shortest distinguishing piece of a stereosequence. If a diad contains two consecutive same absolute configurations (*RR* or *SS*), the diad is labelled as *meso* (*m* diad); if they are different (*RS* or *SR*), it is labelled as *racemo* (*r* diad). The basic idea of this mapping scheme is to consider a diad as a superatom. Accordingly, a CG bead of polystyrene corresponds to a diadic m or r unit, and the centre of this CG bead is the methylene carbon, as illustrated in Fig. 3.3. The force field of this CG model has two types of particles (m and r), three different bond types (*mm, rr, mr*), six angle types (*mmm, mmr, mrm, mrr, rmr, rrr*). Bonds and angle distributions and intermolecular radial distribution functions extracted from atomistic simulation are considered as target distribution. The CG bond and angle potentials were obtained via direct Boltzmann inversion of their multi-peaked distributions, which, for computational convenience, were approximated as sums of several Gaussian functions.[19] The CG nonbonded pair potentials of each pair of beads are obtained by iterative Boltzmann inversion of the corresponding radial distribution functions, the pressure information is incorporated into the optimization of nonbonded potential by means of a so-called ramp correction.[18] For ease of reference, the parameters of CG force field used in this work are reproduced in Appendix 3.
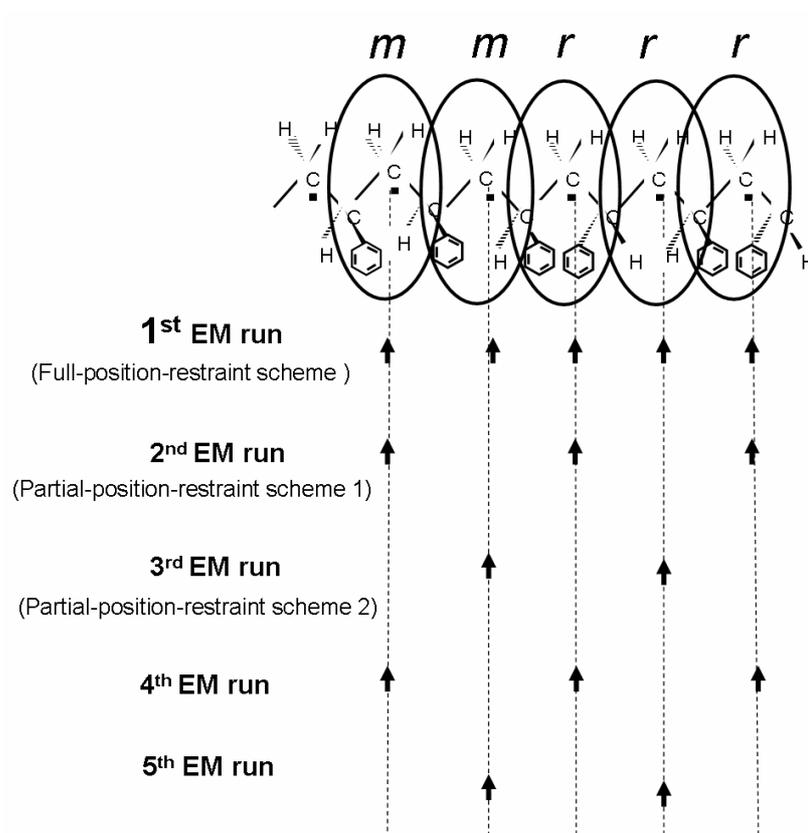
Figure 3.3. Illustration of the atomistic-to-coarse-grained mapping scheme for atactic polystyrene and the position restraint scheme used during energy minimization of a backmapped sheared nonequilibrium system. Coarse-grained beads are indicated by ovals corresponding to *meso* (*m*) or *racemo* (*r*) diads. The centres of these superatoms, indicated by filled squares, are the methylene carbons. The arrows along the dashed lines indicate the position restraints used in the successive EM runs. For details, see text.

The reverse nonequilibrium molecular dynamics (RNEMD)[20] was used to investigate the rheological behaviour of the CG model of polystyrene under steady shear flow. The RNEMD algorithm for shear flow by is illustrated in Fig. 3.4. The simulation box is partitioned into an even number of slabs along the z direction. One periodically searches in the first slab for the atom with largest negative x component of the momentum, and in the central slab for the atom with largest positive x component. If these two atoms have same mass, one exchanges their momenta. By repeating this procedure periodically, an unphysical momentum flux is imposed and a velocity gradient or shear field results.

In RNEMD, the flow field imposed on the system corresponds to two symmetric planar Couette flows, the momentum fluxes in the upper and lower halves are equal in magnitude but opposite in direction. Both half cells have the same shear rate, but the velocity profile is symmetric. As a consequence, polymer chains are aligned symmetrically in the two halves of the simulation cell. We have quantitatively characterized the structural alteration of a CG model under steady shear flow. The average chain dimension was characterized by the root mean-square gyration radius and the shear-induced alignment by the birefringence extinction angle χ.[1] In order to obtain χ, we first calculate an order tensor S

$$\mathbf{S} = \frac{1}{N} \left\langle \sum_{i=1}^{N} \left(\mathbf{u}_i \otimes \mathbf{u}_i - \frac{1}{3} \mathbf{I} \right) \right\rangle$$

(4)

where $\mathbf{u}_i$ is the unit vector along the end-to-end direction of molecule i, and I is the unit tensor. The angle brackets indicate an ensemble average. The birefringence extinction angle χ is calculated as the angle between the eigenvector of S corresponding to the largest eigenvalue of the order tensor and the shear flow direction X. The birefringence extinction angle χ gives the preferred alignment direction respective to the flow. In ref. 1, χ was calculated from both the upper and lower halves of cell separately, the reported values were the average of χ from both half cells.
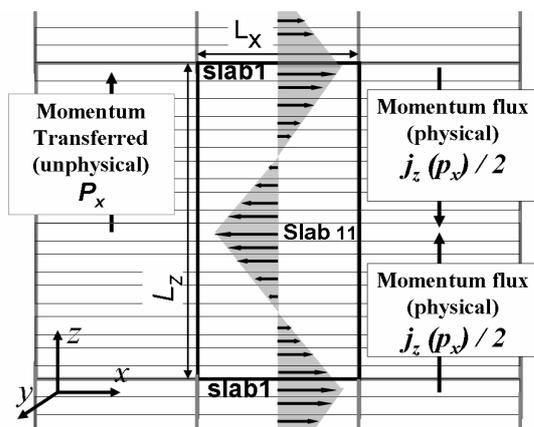
Figure 3.4. Sketch of the RNEMD method for calculating the shear viscosity. The flow field imposed on the system corresponds to two symmetric planar Couette flows, which have the shear flow in the x direction, and the velocity gradient is in z direction. Horizontal arrows in the simulation cell indicate the velocity field. The periodic orthorhombic simulation cell is partitioned into 20 slabs in the z direction. Reproduced from ref. 1.

3.4. Model and computational details

3.4.1. Coarse-grained potential and generation CG configurations under steady shear flow

      References 18 and 2 report, respectively, the CG model of atactic polystyrene and the corresponding force field parameters used in this work. In this CG model, the bond stretching and the bond bending potential were parameterized to reproduce the corresponding distribution functions (bonds, bond angles and radial distribution functions) of an atomistic melt of short chains. The nonbonded potentials were derived by iterative Boltzmann inversion to reproduce the chain packing of the short chain melt. The most important characteristics of this model are: the polystyrene diad is coarse-grained as a superatom (bead) in the mesoscale effective force field; the center of the superatom is placed at the methylene carbon; two different types of superatoms are designated according to the configuration of two adjacent pseudoasymmetric –CHR–

methyne groups, either meso (same configurations *RR* or *SS*) or racemo (opposite configurations *RS* or *SR*), as shown in Fig. 3.3; the corresponding force-field contains three different bonds, six angles and three nonbonded terms. This CG model retains the tacticity of polystyrene, so we are in a comfortable situation of being able to map the CG monomers back onto the different groups of the underlying atomistic structure.

The deformed CG conformations were generated by reverse nonequilibrium molecular dynamics (RNEMD) simulations.[20] Ref. 1 gives the details about how we generate the CG conformations under a steady shear flow by RNEMD simulation. The RNEMD simulations were performed at constant temperature (T= 500 K) and constant volume. The global features of the deformed CG system such as the root mean-square gyration radius and the birefringence extinction angles followed the expected trends.[1] Two sheared nonequilibrium systems are selected to be studied. We refer as PS-30 and PS100 to these systems containing 30 and 100 CG beads per chain, respectively, corresponding to molecular weights of 3.23 kDa and 10.52 kDa. For the sheared PS-30 and PS-100 systems studied here, the momentum fluxes are imposed in RNEMD by velocity swapping every 60 time steps with the time step length of 1 fs. All CG calculations were carried out with the modified GMQ_num code. The final CG configurations, deformed by a steady shear flow of 1 ns, are selected to be backmapped. For comparison, the unperturbed CG structures from an equilibrium run of 2.4 ns are also backmapped. The backmappep systems are characterised in Table 3.1.

Table 3.1. Characteristics of the coarse-grained systems, which are being backmapped: number of beads per chain N_{bead}, molecular weight MW, number of chains N_{chain}, mass density ρ, simulation cell sizes L_x, L_y, and L_z, root mean-square gyration radii of polymer chains in the unperturbed systems $\langle R^2 \rangle^{1/2}_{eq}$ and sheared nonequilibrium systems $\langle R^2 \rangle^{1/2}_{shear}$, averaged birefringence extinction angles χ from the upper and lower halves of simulation cell in the sheared nonequilibrium system.

System	N_{bead}	MW (g/mol)	N_{chain}	ρ (kg/m³)	$L_x \times L_z \times Lz$ (nm)	$\langle R^2 \rangle^{1/2}_{eq}$ (nm)	$\langle R^2 \rangle^{1/2}_{shear}$ (nm)	χ (degree)
PS-30	30	3230	120	945.4	$6.099 \times 6.099 \times 18.297$	1.28	1.38	11.5^o
PS-100	100	10520	60	951.0	$7.161 \times 7.161 \times 21.483$	2.65	4.08	5.9^o

3.4.2. Technical details of energy minimization run for the backmapped nonequilibrium structures and molecular dynamics run for the backmapped unperturbed ensembles.

The molecular simulation package GROMACS [21,22] is used for both EM and MD under constant volume and constant temperature (500 K). All bond lengths are kept rigid by the SHAKE procedure[23]. The cutoff for Coulombic and Lennard-Jones interaction is 1.35 nm with a Verlet neighbour list [24]cutoff of 1.38 nm. The atomistic force field used here is the one reported in reference 13. For ease of reference, the parameters of atomistic force field used in this work are reproduced in Appendix 2. For energy minimisation, the steepest descent method[25] is used for finding a local potential-energy minimum. The convergence threshold for the maximum force is set as 100 kJ mol $^{-1}$ nm $^{-1}$. The force constant for the position restraint potential is 10000 kJ mol $^{-1}$ nm $^{-2}$. Since the bond-stretching potential is much stiffer than the ones of angle bending and torsions, the dominating changes of coordinates in the deformed atomistic structure are expected in the torsional angle φ and the bending angle α. The changes of bond coordinates are negligible; therefore the use of bond constraints is justified. For MD runs for the unperturbed PS-30 and PS-100 systems, simulation lengths are over 2.4 ns, the Berendsen thermostat[26] is used to control the temperature of the system, with a temperature coupling time of 0.2 ps at a time step of 2 fs.

3.5. Backmapping procedure for atactic polystyrene under shear flow

3.5.1. Reconstructing the atomistic details using equilibrium structural templates

Here we follow the same strategy as ref. 13 to rebuild the atomistic details. We use quaternions to dock atomistic diads into the coarse-grained conformations. First, the

absolute chirality of one end group is chosen as R or S with equal probability, since this is not determined by the CG model. Once the chirality of the end group is fixed, the chirality of the other repeating units can be established by the sequence of superatoms in the CG model. This chirality can be translated into an atomistic structure according to the mapping rules, which defines the sequence of three successive atomistic chiralities when backmapping two successive CG beads, as given as Table 3.3 in ref. 13. Second, the atomistic end group is rebuilt by superposing the three superatom centers with the corresponding three methylene groups (indicated by filled squares in Fig. 3.3). In a similar way, the following CG diads are replaced by the three methylene groups of the atomistic diad model. The replacement continues until the end of the chain. Afterwards, according to the mapping rule above, atomistic diads of different chiralities and different dihedral conformations are selected from a library containing possible structures. Each atomistic structure in the library is in the minimum-energy geometry for the given dihedral conformation of the isolated diad.

Some catenations of phenyl rings occur after reconstruction of atomistic details as described above. They are eliminated in the following way: We introduce the additional fictitious Lennard-Jones particles centered in the phenyl ring. The nonbonded interaction is turned on for both fictitious and genuine atoms sites. EM runs perform with gradually increasing the nonbonded parameters epsilon and sigma of these atoms sites until the catenations of phenyl rings disappear. Afterwards, the nonbonded interactions on the fictitious atoms are turned off, the nonbonded interactions on genuine atoms sites (including the genuine atoms on the phenyl ring) are left on. EM runs are repeated with gradually increasing the epsilon and sigma parameters until they reach the full values as reported in Table 3.1 of reference 13. Finally, the fictitious particles are removed. Note that during this preprocessing for eliminating phenyl ring catenations, the positions of all backbone atoms (methylene and methyne carbons) are fixed by position restraints.

3.5.2. Structure optimization by energy minimization

The EM run procedure is illustrated in Fig. 3.3. In the first EM run, position restraints are applied to all methylene carbons, which correspond to the centres of CG beads, except the methylene carbons at the chain ends. The aim of the first EM run is to regularize local structures which come from equilibrium structural templates. One can speculate that the motion of phenyl side groups is decoupled from the motion of the backbone by the presence of the position restraints, which isolate the motions of neighbouring segments from each other. It has been demonstrated by Lyulin et al [27] that there is a strong coupling between motions of the backbone and the pendant phenyl groups even at high temperature (650 K). We minimize the segment isolation effect by several EM run, each EM run being characterized by one of two different types of restraint schemes. In the second EM run, position restraints are still apply to methylene carbons but only of every other unit. In the third EM run, position restraints are shifted by one repeating unit to those atoms which were free in the previous EM run. This process is iterated until the energy converges under both partial-position-restraint schemes. In our test, 10 EM runs are sufficient to reach energy convergence with two partial-position-restraint schemes for both PS30 and PS100 systems. An atomistic chain, backmapped from the sheared CG PS100 system, is illustrated in Fig. 3.5.
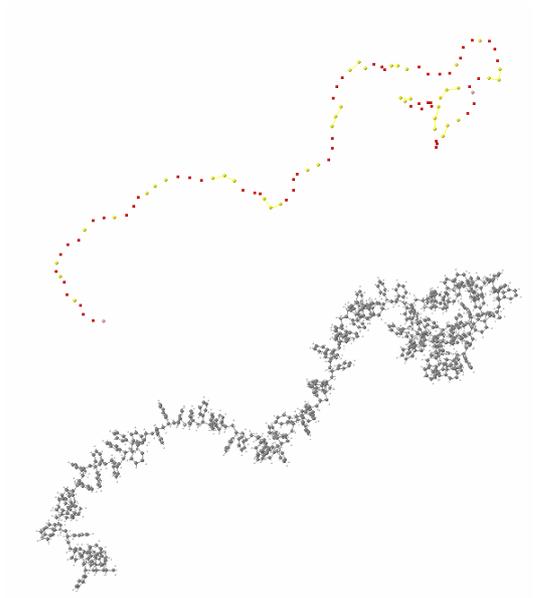
Figure 3.5. A backmapped chain (bottom) from a corresponding coarse-grained chain of 100 repeating units (top). The red beads are the *meso* and the yellow ones the *racemo* superatoms.

In order to demonstrate the influence of an initial EM run on the dynamics of polymer chains, we perform stress relaxation by molecular dynamics over a short period of 300 ps for two different *NVT* ensembles: one has the initial configurations optimized by the proposed method; the second one has the initial conformations generated by simply reinserting the atomistic details without any EM run. We analyze the reorientation dynamics of local chain segments and the end-to-end vector for both simulations by means of the autocorrelation function of the second Legendre polynomial P_2 of chain segment vectors.

$$C_{reor}(t) = \left\langle \frac{1}{2}\left[3(\vec{u}_d(t)\vec{u}_d(0))^2 - 1\right]\right\rangle = \left\langle P_2\left[\vec{u}_d(t)\vec{u}_d(0)\right]\right\rangle \tag{5}$$

As chain segment vector $\vec{u}_d$, we take the normalized vector connecting two atoms along backbone.

$$\vec{u}_d = \frac{\vec{r}_i - \vec{r}_{i-d}}{\left|\vec{r}_i - \vec{r}_{i-d}\right|} \tag{6}$$

where, $\vec{r}_i$ denotes the coordinate of atom i, the subscript d denotes the number of atoms from atom i. Here, we take d as 1 and 4, the chain segment vectors $\vec{u}_1$ and $\vec{u}_4$ are illustrated in Fig. 3.6.
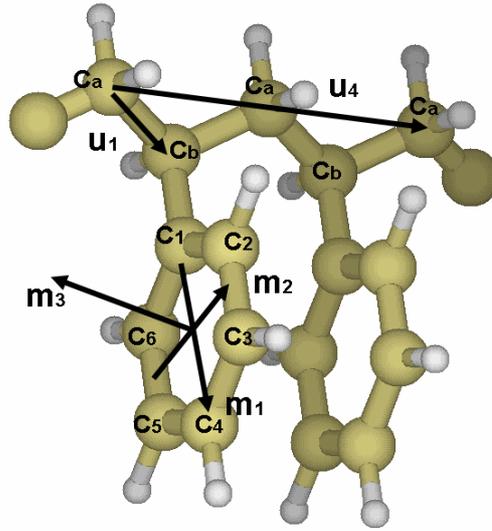
Figure 3.6. Atom labelling and orientational vectors for polystyrene used in this work.

The influence of the protocol used to prepare the initial structure on the short-time reorientation dynamics is shown in Fig. 3.7. The reorientation dynamics deviates from a simple exponential decay ($C_{reor}(t) \sim e^{-t/\tau}$). Nonetheless, we use an exponential fit to obtain very rough estimates of the reorientation times τ (Table 3.2). For all chain vectors investigated, the τ values of those conformations generated with optimization are longer than the one without optimization. It is evident that the pre-optimized conformation has a higher relative conformational stability, in other words, a large fraction of the local relaxation has already taken place during the EM runs.
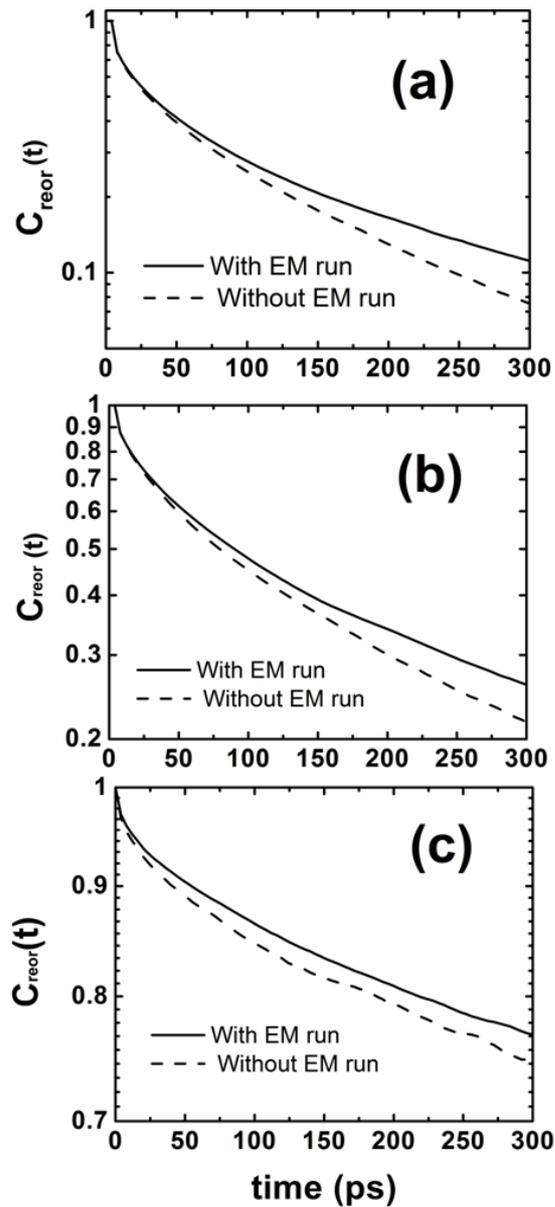
Figure 3.7. Chain segment autocorrelation function of the chain vector (a) $\vec{u}_1$, (b) $\vec{u}_4$ and (c) end-to-end vector for different polystyrene-30 systems under *NVT* conditions (T=500K): initial conformations optimized by EM runs with the proposed method (solid line) and initial conformation generated by simply reinserting the atomistic details without any EM runs (dashed line).

Table 3.2. orientation relaxation times τ (ps) obtained by fitting an exponential ($C_{reor}(t) \sim e^{-t/\tau}$) to the curves in Fig. 3.7 between 150 ps and 300 ps.

System	$\vec{u}_1$	$\vec{u}_4$	End-to-end
backmapped without energy minimisation	175	294	1615
backmapped followed by the energy minimization protocol	244	399	1828

3.6. Local characterization of the backmapped structure

The root mean-square gyration radius obtained from the backmapped structure for PS-30 system is 13.9 ± 0.2 nm, the CG value 13.8 ± 0.1 nm, the difference being negligible. The perfect agreement comes from the fact that the backmapping method preserves all global features of the CG structure; therefore, here the only interesting characterization involves the local structure of the sheared polymer chains.

One possibility to validate the ability of the backmapping method is to compare the so-called reduced intensity function (or interference function) calculated from simulation with that from wide angle X-ray scattering (WAXS). The experimental reduced intensity function is defined by Eqn. (7)[28]

$$I(q) = kI_{corr}(q) - \sum_j f_j^2(q) - I_{comp}(q) \tag{7}$$

where, $I_{corr}(q)$ is the fully corrected intensity, k is a normalization factor needed to place the intensity on an absolute scale (in electron units per atom). $\sum_{j} f_j^2(q)$ is the independent atomic scattering. $I_{comp}(q)$ is the Compton scattering. Unoriented high-molecular-weight atactic polystyrene X-ray structures are characterized by a diffuse halo (referred to as the polymerization peak) at around $q = 7.5\ nm^{-1}$ and a ubiquitous "amorphous halo" at $q = 14\ nm^{-1}$. It has been pointed out that the X-ray density profile of oriented atactic polystyrene is anisotropic:[30] Intrachain peaks intensify in the extension direction (meridian), and interchain peaks intensify perpendicular to the extension direction (equator). Fig. 3.8 shows the q-weight reduced WAXS intensities $(q \cdot I(q))$ in equatorial and meridional sections for atactic polystyrene, which was oriented at 358 K with an extension rate 3 by extrusion in a channel die. The experimental data indicate that the polymerization peak ($q = 7.5\ nm^{-1}$) is intensified in the equatorial section.[28] Ayyagari et al. [31] quantitatively analyzed the intramolecular and intermolecular contributions to the X-ray structure factor of unorientedatactic polystyrene by means of molecular dynamics simulation. They concluded that there are important intramolecular and intermolecular contributions to the high-q peak, while the structure in the low-q peak region appears to be primarily of intermolecular origin. Therefore, we may infer that the intensification of the polymerization peak in the equatorial section indicates intermolecular packing in the direction normal to the chain extension.
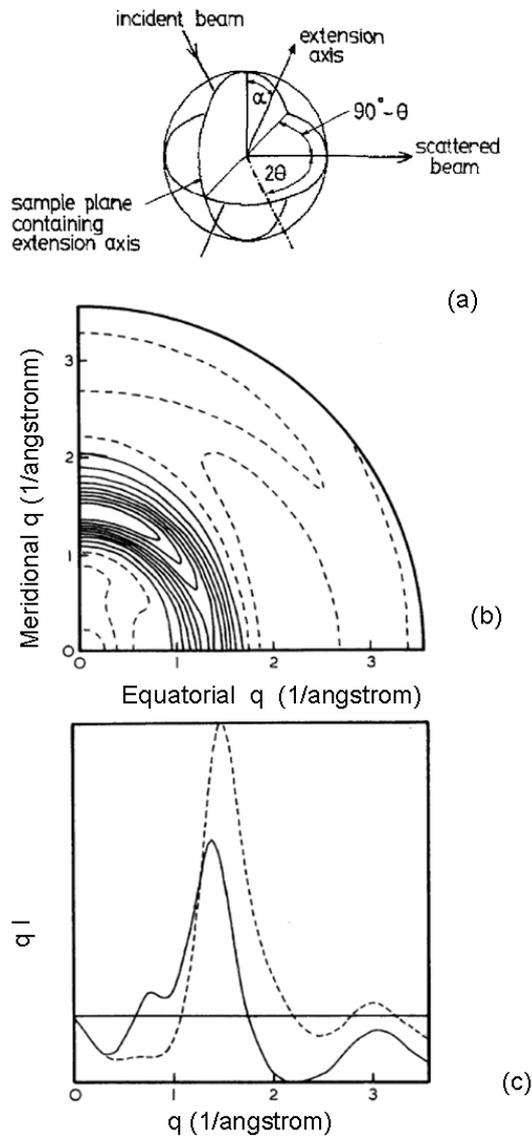
Figure 3.8. Experimental WAXS data for atactic polystyrene oriented at 358K by extrusion in a channel die. Rproduced with permission from ref. 28.) (b) q-weighted reduced intensity function $(q \cdot I(q))$. The dashed contours represent negative values. (c) plot of meridional ($\alpha = 0^o$, solid line) and equatorial ($\alpha = 90^o$, dashed line) sections of Fig. 3.8 (b). The X-ray scattering intensity was measured using a symmetrical transmission diffractometer, as shown in Fig. 3.8 (a). (Reproduced with permission from ref. 29).

The X-ray intensity can be also calculated by Fourier-transforming pair distribution functions obtained from simulations. For oriented polymers, this intensity is explicitly dependent on the direction of the vector $\vec{q}$ in reciprocal space, or equivalently the vector $\vec{r}$ in real space. In order to compare with the experimental data, we need to calculate the X-ray intensity profile along the planes parallel ($\alpha = 0^o$, meridian) and perpendicular ($\alpha = 90^o$, equator) to the chain extension direction. As we have mentioned in section 3, the polymer chains are aligned symmetrically in the two halves of the simulation cell and the birefringence extinction angle χ gives the preferred alignment direction with respective to the flow. For the sheared PS-30 system studied here, the χ averaged from the upper and lower halves of simulation cell is 11.5^0. It is convenient to define the alignment direction as $\widetilde{X}$ axis of a new coordinate system $\left(\widetilde{X}, \widetilde{Y}, \widetilde{Z}\right)$, as shown in Fig. 3.9, then the $\widetilde{X}\widetilde{Y}$ and $\widetilde{Y}\widetilde{Z}$ planes correspond the planes parallel and perpendicular to the chain extension direction. We compute the X-ray intensities for both planes from all-carbon atom sites. For both planes, the calculation of the radial distribution functions is done in an angle of 5 degree above and below the plane. Fig. 3.9 shows the calculated scattering intensities profiles parallel and perpendicular to the chain extension. It indicates an intensification of polymerization peak normal to chain extension, which agrees well with the experimental findings.
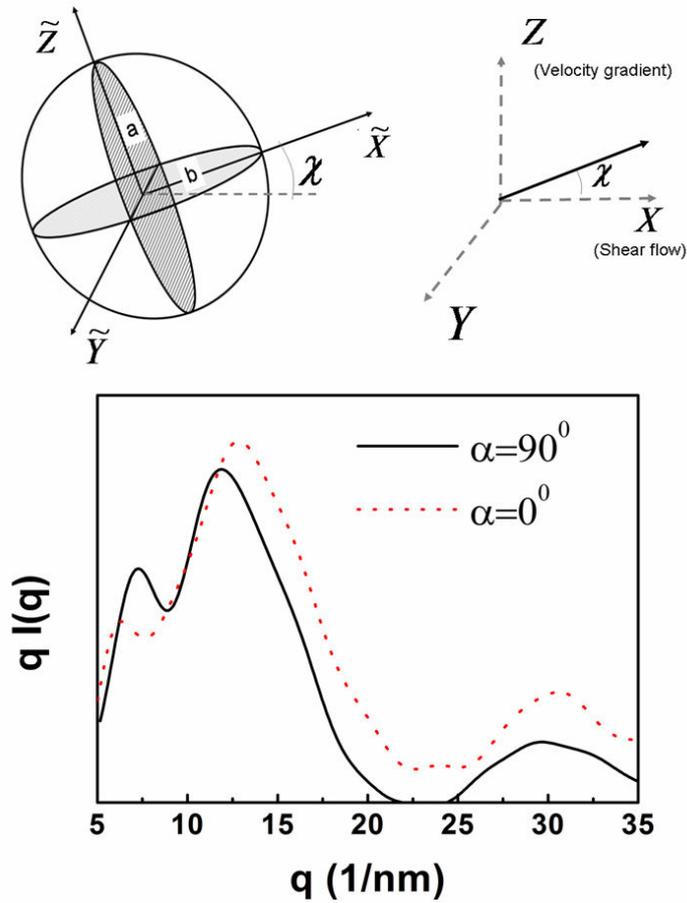
Figure 3.9. Calculated q-weighted reduced scattering intensity profile for a melt of backmapped chains of PS-30 at 500 K under a steady shear flow. The lower part of the plot shows the two section: meridion ($\alpha = 0^o$, dashed line) and equator ($\alpha = 90^o$, solid line). The laboratory coordinate system (X,Y,Z) is indicated as the right side of the upper part: The X axis denotes the shear flow direction, Z axis denotes the velocity gradient direction. The birefringence extinction angle ($\chi = 11.5^o$) gives the preferred alignment direction with respect to the flow. The rotated coordinate system ($(\tilde{X}, \tilde{Y}, \tilde{Z})$ is illustrated in the upper left side, $\tilde{X}$ is the direction of the chain alignment.

.

The pair distribution function can offer the structural information more directly than the X-ray scattering patterns. The chain configurations under steady shear flow are highly anisotropic. Thus, the pair distribution function $g(\vec{r})$ is also anisotropic. Fig. 3.10 reports $g(\vec{r})$ for interchain backbone-backbone, phenyl-phenyl and backbone-phenyl carbon along the vector perpendicular and parallel to the chain preferred alignment (orientation). For comparison, the corresponding distributions for an unperturbed system (no shear) are also shown. Fig. 3.10 clearly shows a noticeable increase of interchain neighbors in the direction perpendicular to chain orientation and a decrease in the direction parallel to the orientation. These features manifest a strong packing effect introduced by shear flow.
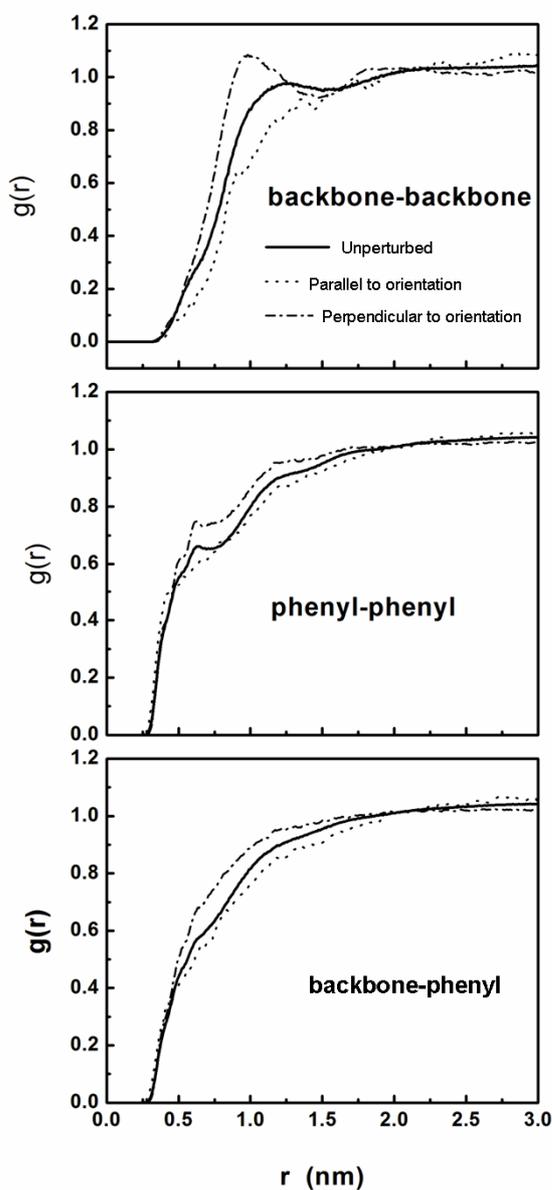
Figure 3.10. Interchain carbon-carbon pair distribution functions (backbone-backbone, phenyl-phenyl, backbone-phenyl) along the directions parallel (dotted line) and perpendicular (dash-dotted line) to the chain orientation direction for the sheared PS-30 system. For comparison, the isotropic distribution of the unperturbed system (equilibrium, no shear) is also shown (solid line).

After backmapping, it is possible to take a closer look at the mutual orientation of phenyl side groups under strong shear flow. We define this orientation by measuring the cosine of the angle between the phenyl ring normals m_3. The orientational vectors used are illustrated in Fig. 3.6: The unit vector $\mathbf{m}_1$ is the in-plane vector from C_1 to C_4, the other in-plane vector m_2 is perpendicular to $\mathbf{m}_1$, the orientation vector $\mathbf{m}_3$ is the ring normal. The average of the scalar product between two unit vectors $\mathbf{m}_{3,\,i}$ and $\mathbf{m}_{3,\,j}$ describes the dominating angle between different ring normals.

$$\cos\beta = \left\langle \left| \mathbf{m}_{3,i} \cdot \mathbf{m}_{3,j} \right| \right\rangle \tag{8}$$

Here, we use the absolute value of the scalar product of $\left| \mathbf{m}_{3,i} \cdot \mathbf{m}_{3,j} \right|$ since we do not distinguish between symmetrically equivalent orientations (one ring turned by 180°). This value is 1 for coplanar rings, 0 for a T-shape arrangement, and 0.5 for a random arrangement. The orientation distribution functions (ODF) are shown in Fig. 3.11 as a function of ring-ring (centre of mass) distance for the unperturbed and the sheared systems. The curve of the unperturbed polystyrene agrees well with the finding in ref. 32: The orientation correlation is quickly lost with increasing distance and no structure is visible beyond 0.9 nm. The first strong peak occurs at around 0.27 nm and the second weak peak occurs at around 0.7 nm. Within the short distance of 0.5 nm, the dominant arrangement of phenyl rings is coplanar due to steric constraints (note that there are very few pairs of rings at this short distance.). As a general observation, the shape of the sheared curve is very similar to the unperturbed one; however, subtle differences are still visible. There is a distinct although small shift of the first peak for the nonequilibrium system (at 0.30 nm) compared to the unperturbed one (at 0.27 nm). If one makes the reasonable assumption that the normal of a phenyl ring is parallel to the direction of chain backbone of each repeating unit[33], then this peak shift indicates the elongation of backbone. The unperturbed ODF converges to 0.5 for distances beyond 0.9 nm, indicating that beyond this distance the mutual orientations are completely random in amorphous polystyrene. The sheared system shows an ODF above 0.5 at all distances (see the inset of Fig. 3.11), indicating that shear flow introduces mutual

71

orientation of phenyl ring within a larger range, and that there is a small prevalence of coplanarity.
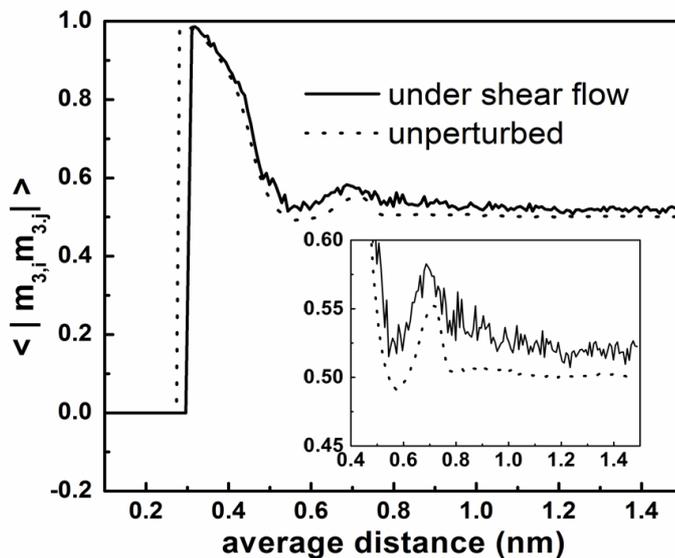
Figure 3.11. Orientation distribution function (ODF) describing the mutual orientation of the phenyl rings obtained from the unperturbed (dotted line) and nonequilibrium systems (solid line), respectively. The inset shows ODF in the average distance domain between 0.4 nm and 1.5 nm. A value of 0 corresponds to perpendicular orientation (T-shape), a value of 0.5 to a random distribution, a value of 1 to a coplanar arrangement.

Capturing the correct backbone torsional angle distribution is a stringent test for the backmapping method. Robyr *et al.*[34] have compared NMR measurements with atomistic simulations of atactic polystyrene and found out noticeable deviations between experimental findings and predictions from atomistic models of bulk structures. As the purpose of this study is to develop a backmapping method instead of examining the atomistic force field, we mainly compare the torsional distributions between the reverse mapped unperturbed and backmapped sheared structures. The convention used to define the torsional angle follows refs. 35 and 36, a right-hand reference frame is used for bond i and a left-hand one for bond $i+1$, and the cis conformation corresponds to 180°. Accordingly, φ_i is measured in the right-handed

sense and φ_{i+1} in the left-handed sense.[36] Fig. 3.12 shows an all-trans meso diad of polystyrene where all torsion angles are zero. The state relative frequencies of torsional angles in the unperturbed and the nonequilibrium structures are listed together with the integrated areas in Table 3.3, the definitions of the integrated areas follows reference 33. The calculated trans fraction is $(57 \pm 5)\%$ in the nonequilibrium structure, which is equal within the errors bar with the value in the unperturbed structure ($(59 \pm 5)\%$). Fig. 3.13 gives the distributions of backbone torsional angles. The coalescence of the trans, gauche (+) and gauche (-) states occurs for both the unperturbed and the nonequilibrium structures, and the distributions are symmetric around 0^0. Compared to the unperturbed distribution, the nonequilibrium distribution is intensified around 0^0 (pure trans conformation), which again indicates the elongation of polymer chain; simultaneously, the gauche states in the range of $-180^0 \sim -120^0$ and the range of $+120^0 \sim +180^0$ are also enriched. It should be noted, however, that conformational differences between unperturbed and sheared structures are small.

Table 3.3. Relative frequencies of backbone torsional angle states and angle ranges.

State	Angle range	Relative frequency in % (Unperturbed structure)	Relative frequency in % (Nonequilibrium structure)
trans (t)	$-60^o \leq \varphi_i \geq +60^o$	59 ± 5	57 ± 5
gauche (g)	$+60^o < \varphi_i \leq +180^o$	22 ± 3	23 ± 3
gauche ($\bar{g}$)	$-180^o \leq \varphi_i < -60^o$	19 ± 3	20 ± 3

Figure 3.12. Meso diad of polystyrene in the all trans-trans conformation.
($\varphi_{i-1} = \varphi_i = \varphi_{i+1} = \varphi_{i+2} = 0$).
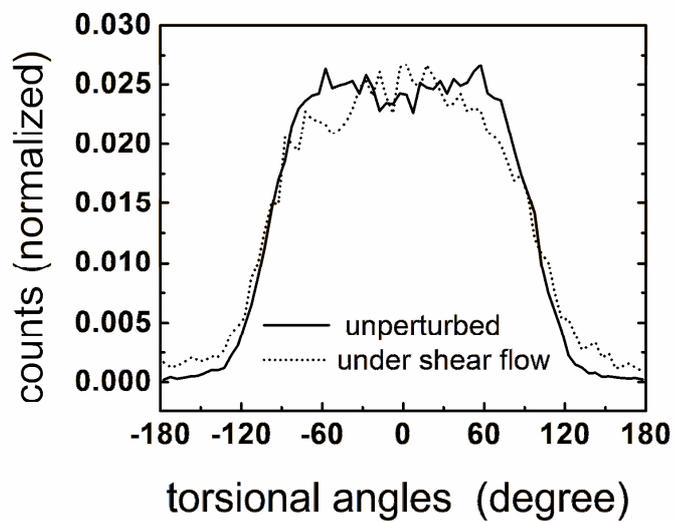
Figure 3.13. Distribution of backbone torsional angles for the PS-30 NVT ensembles (T=500K): under the unperturbed (equilibrium, no shear) condition (solid line) and the sheared nonequilibrium condition (dotted line).

Fig. 3.14 and Fig. 3.15 show the distributions of backbone torsional angle pairs (φ_i, φ_{i+1}) for the meso and racemo diads in the unperturbed and the nonequilibrium system, respectively. As a general observation for both cases, the distributions of racemo and meso diads are very similar. This analogy can be attributed to the strong inter-molecular packing effect over those dictated by the local intramolecular interaction[33,34]. However, compared to the corresponding unperturbed ensemble, the distribution of torsional angle pairs of backmapped sheared structures is more diffuse. It has been found through rotational-isomeric-state (RIS) theory[36] that the three main energy minima are tg, gt, and gg for the meso diad and the two important states are tt and gg for racemo diad. In the backmapped nonequilibrium ensemble, many diad angle pairs fall outside the region of low energy. Especially, the $\overline{gg}$ population becomes abundant in the nonequilibrium ensemble, despite its high intramolecular energy. As experimental observations of torsional angle pairs in nonequilibrium ensembles are lacking, it is not clear whether this observation is due to (physical) conformational defects induced by strong shear flow, or to deficiencies of the atomistic force field used, or to artifacts of the backmapping procedure. It still remains to be clarified in further investigations. For the time being, we report it as a phenomenon.
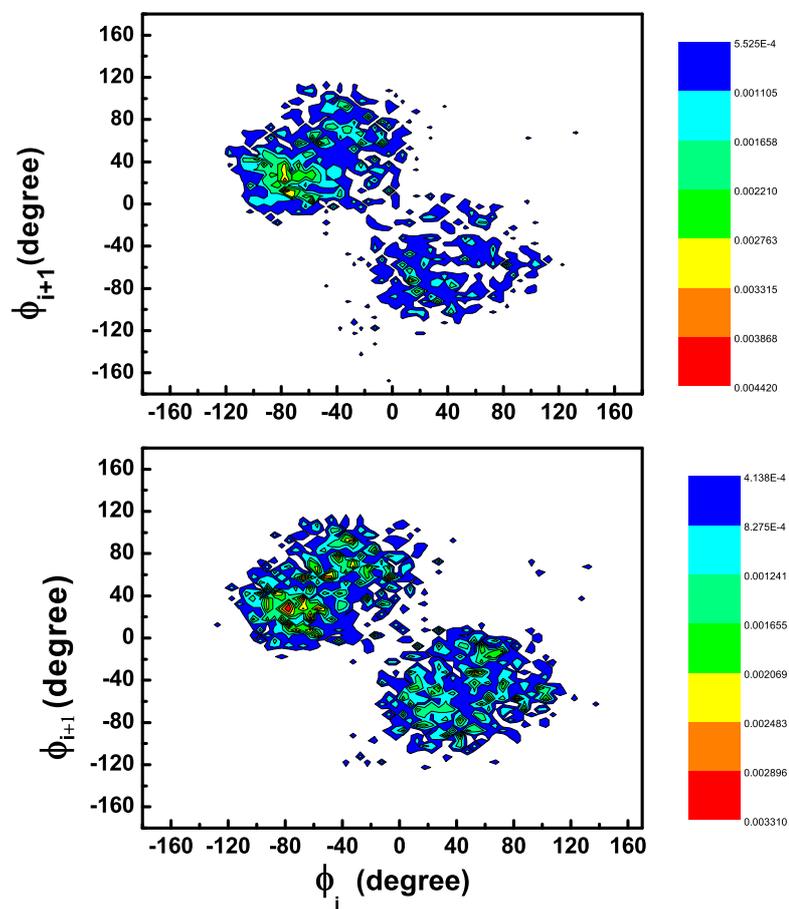
Figure 3.14. Torsional angles pairs (φ_i, φ_{i+1}) distribution of *meso* (upper) and *racemo* (lower) diad in the backmapped unperturbed ensemble of PS-30.
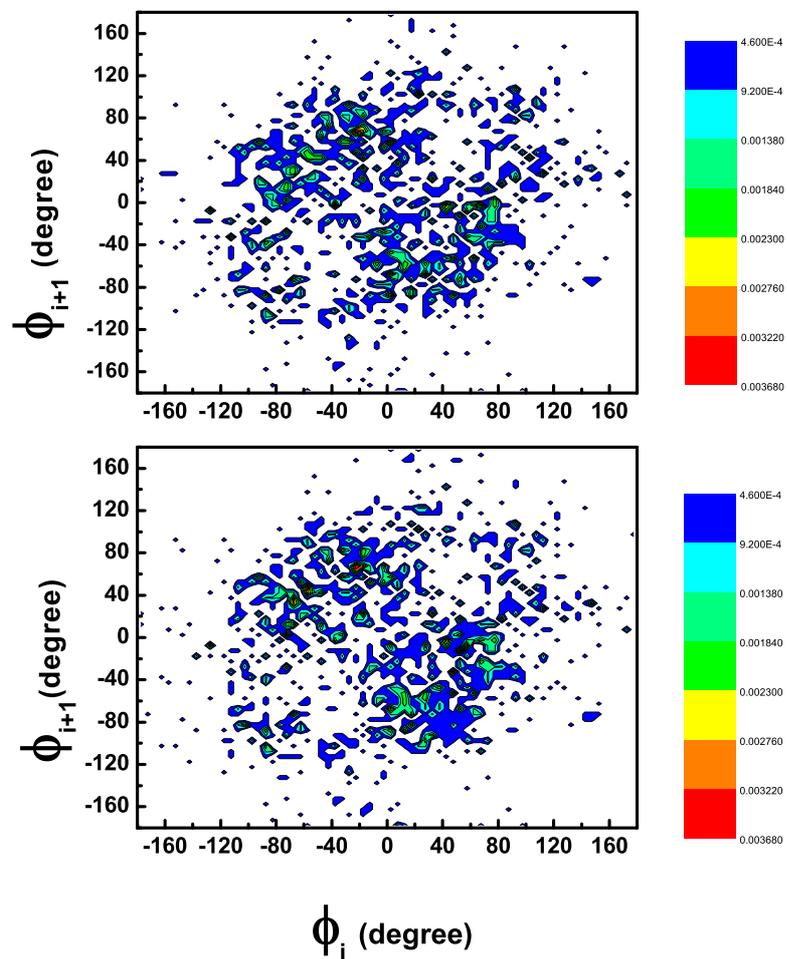
Figure 3.15. Torsional angles pairs (φ_i, φ_{i+1}) distribution of meso (upper) and racemo (lower) diad in the backmapped nonequilibrium ensemble of PS-30.

3.7. Conclusions

The backmapping method has been extended to the situation of a nonequilibrium mesoscale polymer model, on which a nonequilibrium shear flow is imposed. Two basic requirements in backmapping non-equilibrium system need to be fulfilled: (1). The sheared CG configurations need to be retained in the atomistic picture. (2).The deformation energy stored in the chain of CG model should be passed on to the atomistic level. In order to meet the above two requirements, we propose three strategies: (1) Preserving globally sheared configurations by applying position restraints. We apply position restraints to all those atoms which coincide with the locations of CG beads. Thus, the global configuration of every individual chain is preserved. (2) Achieving the locally relaxed atomistic structures through a molecular mechanics approach. The structure of the deformed molecules is generated by minimizing the conformational energy in the presence of an applied external force. This approach is transferred here in generating the deformed atomistic structures out of template structures from an equilibrium (undeformed) simulation. (3) Minimization of the artificial segment isolation introduced by the position restraints via an iterative procedure. Position restraints hinder the rearrangements of chain segments when optimizing deformed atomistic structure also at a local level; the segments become "isolated" from each other. This effect is counteracted by performing several EM runs with shifting position restraint schemes. This process is iterated until the energy converges under different partial-position-restraint schemes. We presume that the final configuration is independent on the locations of position restraints. Based on the strategies above, we propose a new workflow for backmapping nonequilibrium CG system.

The proposed new procedure is demonstrated on atactic polystyrene melts under steady shear flow. The backmapped local structures are structurally characterized and compared to experimental data where available. The calculated X-ray scattering profiles parallel and perpendicular to the chain-extension direction compare well with

experiment. Parallel packing induced by the shear flow manifests itself in the intensification of the polymerization peak in the parallel direction. The shear flow also introduces elongation of the backbone and, as a consequence, a longer range of the mutual orientation of phenyl rings as well as a small prevalence of coplanarity. The backbone torsional angle distribution of the sheared structure has an equivalent integrated distribution of trans and gauche states as the unperturbed one. A more detailed investigation of the distribution, however, reveals a sharpening of the trans peak and a blurring of the gauche distributions.

3.8. References

(1)   Chen, X.; Carbone, P.; Cavalcanti, W. L.; Milano, G.; Müller-Plathe, F. *Macromolecules* **2007**, *40,* 8087-8095.

(2)   Spyriouni, T.; Tzoumanekas, C.; Theodorou, D.; Müller-Plathe, F.; Milano, G. *Macromolecules* **2007**, *40,* 3876-3885.

(3)   Tschöp, W.; Kremer, K.; Hahn, O.; Batoulis, J.; Bürger, T. *Acta Polymer.* **1998**, *49,* 75-79.

(4)   Müller-Plathe, F. *ChemPhysChem* **2002**, *3*, 754-769.

(5)   Müller-Plathe, F. *Soft Mater.* **2003**, *1*, 1-31.

(6)   Reith, D.; Pütz, M.; Müller-Plathe, F. *J. Comput. Chem.* **2003**, *24*, 1624-1636.

(7)   Girard, S.; Müller-Plathe, F. Coarse-Graining in Polymer Simulations , Lecture Notes in Physics, In *Novel Methods in Soft Matter Simulations*; Springer Berlin / Heidelberg, 2004.

(8)   Carbone, P.; Negri, F.; Müller-Plathe, F. *Macromolecules* **2007**, *40*, 7044 - 7055.

(9)   Müller-Plathe, F. *Acta Polymer.* **1994**, *45*, 259-293.

(10)   Tschöp, W.; Kremer, K.; Batoulis, J.; Bürger, T.; Hahn, O. *Acta Polymer.* **1998**, *49*, 61-74.

(11)   Kotelyanskii, M.; Wagner, N. J.; Paulaitis, M. E. *Macromolecules* **1996**, *29*, 8497-8506.

(12)   Harmandaris, V. A.; Mavrantzas, V. G.; Theodorou, D. N. *Macromolecules* **2000**, *33*, 8062 -8076.

(13)   Santangelo, G.; Di Matteo, A.; Müller-Plathe, F.; Milano, G. *J. Phys. Chem. B* **2007**, *111*, 2765 -2773.

(14)   Padding, J. T.; Briels, W. J. *J. Chem. Phys.* **2003**, *118*, 10276-10286.

(15)   Bleha, T.; Gajods, J. *Colloid Polym. Sci.* **1988**, *266*, 405-410.

(16)   Bleha, T.; Gajdos, J.; Karasz, F. E. *Macromolecules* **1990**, *23*, 4076-4082.

(17)   Wool, R. P.; Boyd, R. H. *J. Appl. Phys.* **1980**, *51*, 5116.

(18)   Milano, G.; Müller-Plathe, F. *J. Phys. Chem. B* **2005**, *109*, 18609 -18619.

(19)   Milano, G.; Goudeau, S.; Müller-Plathe, F. *J. Polym. Sci. Part B: Poly. Phys.* **2005**, *43*, 871-885.

(20)   Müller-Plathe, F. *Phys. Rev. E* **1999**, *59*, 4894 - 4898.

(21)   Berendsen, H. J. C.; van der Spoel, D.; van Drunen, R. *Comput. Phys.Commun.* **1995**, *91*, 43-56.

(22)   Lindahl, E.; Hess, B.; van der Spoel, D. *J. Mol. Model.* **2001**, *7*, 306-317.

(23)   Ryckaert, J.-P.; Ciccotti, G.; Berendsen, H. J. C. *J. Comput. Phys.* **1977**, *23*, 327-341.

(24)   Allen, M. P.; Tildesley, D. J. *Computer Simulation of Liquids*; Oxford University Press, 1987.

(25)   Vetterling, W. T.; Press, W. H.; Teukolsky, S. A.; Flannery, B. P. *Numerical.Recipes*; Cambridge University Press U.K., 1996.

(26)   Berendsen, H. J. C.; Postma, J. P. M.; van Gunsteren, W. F.; DiNola, A.; Haak, J. R. *J. Chem. Phys.* **1984**, *81*, 3684-3690.

(27)   Lyulin, A. V.; Balabaev, N. K.; Michels, M. A. J. *Macromolecules* **2002**, *35*, 9595 -9604.

(28)   Mitchell, G. R.; Windle, A. H. *Polymer* **1984**, *25*, 906-920.

(29)   Mitchell, G. R.; Windle, A. H. *Colloid Poly. Sci.* **1982**, *260*, 754-761.

(30)   Mitchell, G. R.; Lovell, R. *Acta Cryst.* **1981**, *A 37*, 189-196.

(31)   Ayyagari, C.; Bedrov, D.; Smith, G. D. *Macromolecules* **2000**, *33*, 6194-6199.

(32)   Müller-Plathe, F. *Macromolecules* **1996**, *29*, 4782 -4791.

(33)   Rapold, R. F.; Suter, U. W. *Macromol. Theory Simul.* **1994**, *3*, 19-43.

(34)   Robyr, P.; Gan, Z.; Suter, U. W. *Macromolecules* **1998**, *31*, 8918-8923.

(35)   Flory, P. J.; Sundararajan, P. R.; DeBolt, L. C. *J. Am. Chem. Soc.* **1974**, *96*, 5015-5024.

(36)   Rapold, R. F.; Suter, U. W. *Macromol. Theory Simul.* **1994**, *3*, 1-17.

4. Developing a simulation tool for coarse-grained polymeric system

4.1. Implementation of the reverse nonequilibrium molecular dynamics (RNEMD)

Before extending the RNMED method to polymeric and other complex system, one needs a reliable simulation tool. The RNMED method has implemented in molecular dynamics package YASP[1], which works on analytical potentials. YASP is a reliable and efficient tool for atomistic MD simulation, but not designed for CG simulations. In atomistic simulations, apart the cases of very complex systems, particle interactions have a very regular behaviour and can be well reproduced by simple analytical potentials. However, at mesoscale level, potentials have a very complicated form and in most cases it is not easy to find a simple function to describe these potentials. The CG molecular dynamics code IBIsCo[2] is designed to meet such need. In this code, the potential is described in a flexible tabulated numerical form. As part of this work, the RNEMD algorithm has been embedded into IBIsCo.

The fundamentals of RNEMD are elucidated in Chapter 2. The basic workflow of RNEMD for shear works as follows:

1. Search in the first slab for the atom with largest negative x component of the momentum, and in the central slab for the super-atom with largest positive x component.

2. Swap the velocities between the atom in the first slab and atom in the central slabs.

3. Record the mean velocity, temperature, and density in every slab (the output file is called *md.prf*); Record the trajectory of momentum flux, velocity gradient, viscosity. (the output file is called *md.trj*).

4. Repeat the 1-3 steps according to the requested exchange frequency.

Appendix 1.1 gives the outline of the RNEMD algorithm in the serial and parallel versions of IBIsCo. Appendix 1.3 gives the details of the input and output files for conducting the RNEMD simulation.

4.2. Implementation of the standard and the transverse dissipative particle dynamics (DPD) for use as a thermostat

In molecular dynamics, the algorithm for controlling the temperature to the required value is called thermostat. Temperature control is commonly achieved by adjusting the kinetic energy. In a flowing fluid with flow velocity $\vec{u}(\vec{r})$, the kinetic energy has a flow contribution and a thermal contribution. Therefore, thermostat is requested to be defined in a frame that moves with the fluid, i.e., to couple it to the "peculiar" velocities $\vec{v}_i' = \vec{v}_i - \vec{u}(\vec{r}_i)$, rather than to the absolute velocities $\vec{v}_i$. However, most thermostats don't take this request into account automatically, and one has to put in the flow profile manually. The dissipative particle dynamics (DPD) thermostat has been developed to cure this problem.[3] DPD is a very useful thermostat for molecular dynamics, which should be used whenever momentum transport is important, since it does not screen the hydrodynamic correlations.

4.2.1. The standard DPD for use as a thermostat

In DPD, the time evolution of a set of interacting particles is governed by Newton's equation of motion. The force acting on a particle has three parts: conservative force, drag force and random force. Drag force represented as a Brownian dash-pot, which damps out the relative approaching velocity, and random force introduces a noise term that keeps the system at constant temperature. The DPD equations of motion for used as a thermostat are then given by ref. 3

$$\dot{\vec{r}} = \frac{\vec{p}_i}{m_i} \tag{1}$$

and

$$\dot{\vec{p}} = \vec{F}_i^C + \vec{F}_i^D + \vec{F}_i^R \tag{2}$$

where, $\vec{F}_i^C$, $\vec{F}_i^D$, $\vec{F}_i^R$ denote the conservative force, drag force and random force on i-th particle, respectively. The drag force and random force are sum of particle-pair forces as

$$\vec{F}_i^D = \sum_{j \neq i} \vec{F}_{ij}^D \tag{3}$$

$$\vec{F}_i^R = \sum_{j \neq i} \vec{F}_{ij}^R \tag{4}$$

where, $\vec{F}_{ij}^D$ and $\vec{F}_{ij}^R$ force compute as

$$\vec{F}_{ij}^D = -\zeta \omega^D (r_{ij})(\hat{r}_{ij} \cdot \vec{v}_{ij})\hat{r}_{ij} \tag{5}$$

$$\vec{F}_{ij}^R = \sigma \omega^R (r_{ij})\theta_{ij}\hat{r}_{ij} \tag{6}$$

where, $\vec{v}_{ij}$ is relative velocity between particle i and particle j, $\vec{v}_{ij} = \vec{v}_i - \vec{v}_j$, $\hat{r}_{ij}$ denotes the unit vector of the interatomic axis $\vec{r}_{ij} = \vec{r}_i - \vec{r}_j$, ζ and σ are the friction constant and the noise strength. ω^R and ω^D are r-dependent weighting functions. The Gaussian white noise θ_{ij} is symmetric in the particle indices ($\theta_{ij} = \theta_{ji}$) and satisfies the following equation.

$$\langle \theta_{ij} \rangle = 0 \tag{7}$$

and the second moment,

$$\langle \theta_{ij}(t)\theta_{kj}(t') \rangle = 2(\delta_{ik}\delta_{ij} + \delta_{il}\delta_{jk})\delta(t - t') \tag{8}$$

According to the fluctuation-dissipation theorem, the following relation between ζ and σ, ω^R and ω^D must fulfilled eqn. 9 and eqn. 10.

$$\left(\sigma\right)^2 = k_B T \zeta \tag{9}$$

$$\left(\omega^R(r)\right)^2 = \omega^D(r) \tag{10}$$

4.2.2. The transverse DPD for use as a thermostat

It turns out, however, the DPD thermostat in its standard form is not capable of controlling liquid properties such as viscosity and diffusion coefficient.[3] Junghans *et al* [4] extended the DPD equations in a way that these quantities can be tuned by changing the parameters of the so-called transverse thermostat. The standard DPD thermostat acts only on a relative velocity along the interatomic axis, while the transverse DPD includes the damping of the perpendicular component of the relative velocity. The basic assumption in the transverse DPD thermostat in contrast to the standard DPD is that the viscosity is very sensitive to the drag force which is perpendicular to the interatomic axis. This drag force mimics the shear on the particle pairs. The random force acts in the same direction as the drag force. Junghans *et al* [4] have demonstrated that the shear viscosity in a simulation with the transverse DPD thermostat is always higher than that with standard DPD, this is also the case in our test simulation. However, a theoretical approach for explaining higher viscosity with the transverse DPD thermostat is still lacking.

The drag force and random force in DPD can be generalized as Eqn. 11 and 12.[4]

$$\vec{F}_{ij}^D = -\zeta \omega^D(r_{ij}) \vec{P}_{ij}(\vec{r}_{ij}) \vec{v}_{ij} \tag{11}$$

$$\vec{F}_{ij}^R = \sigma \omega^R(r_{ij}) \vec{P}_{ij}(\vec{r}_{ij}) \vec{\theta}_{ij} \tag{12}$$

ζ and σ are the friction constant and the noise strength. $\vec{P}_{ij}(\vec{r}_{ij})$ is a projection operator, $\vec{\theta}_{ij}$ is a noise vector. For the case where one chooses projector along the interatomic axis between particle i and j ,

$$\vec{P}(\vec{r}_{ij}) = \hat{r}_{ij} \otimes \hat{r}_{ij} \tag{13}$$

the standard DPD thermostat is recovered. One chooses projector on the plane perpendicular to the interactomic axis,

$$\ddot{P}(\vec{r}_{ij}) = \ddot{I} - \hat{r}_{ij} \otimes \hat{r}_{ij} \tag{14}$$

the space defined by the projector (14) is orthogonal to the case of the standard DPD, and this formulizes the transverse DPD. In the transverse DPD, random force $\vec{F}_{ij}^{R}$ and the drag force $\vec{F}_{ij}^{D}$ are calculated by eqn 11 and 12 with applying Eqn 14 to define the projection operator.

Appendix 1.2 gives the implementatory details of the standard and the transverse DPD for use as a thermostat algorithm in the serial version of IBIsCo.

4.2.3. Temperature and diffusion coefficient controlled by a DPD thermostat

To check whether DPD thermostat works, molecular dynamics simulations on argon system, which has a Lennard-Jones potential (Eqn. 15), are performed.

$$V(r) = 4\varepsilon \left[\left(\frac{\sigma}{r} \right)^{12} - \left(\frac{\sigma}{r} \right)^{6} \right] \tag{15}$$

The system contains 2592 atoms, the argon parameters are: $m = 39.95$ g/mol, $\varepsilon = 0.99707$ kJ/mol and $\sigma = 0.340$ nm. The simulation box size is $L \times L \times 3L$ where $L = 3.425$ nm, the mass density is $1426.621 kg/m^3$. The temperature is 86.5 K, the cutoff is 1.0215 nm, and the time step is 2 fs.

Temperature. Fig. 4.2. and 4.3. show the temperature controlled by the standard and the transverse DPD thermostat with different noise-strengths. For comparison, the temperature controlled by Berendsen thermostat is also shown in Fig.4.1
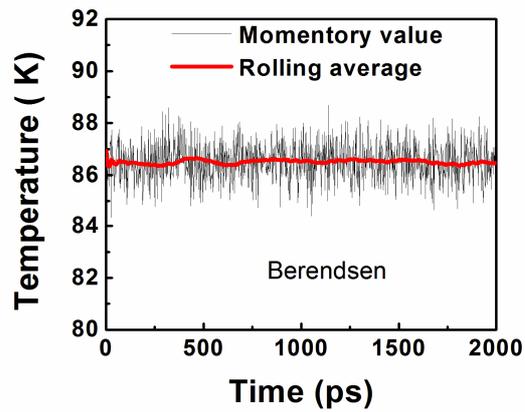
Figure 4.1. Temperature controlled by Berendsen thermostat with a temperature coupling time 0.2 ps.
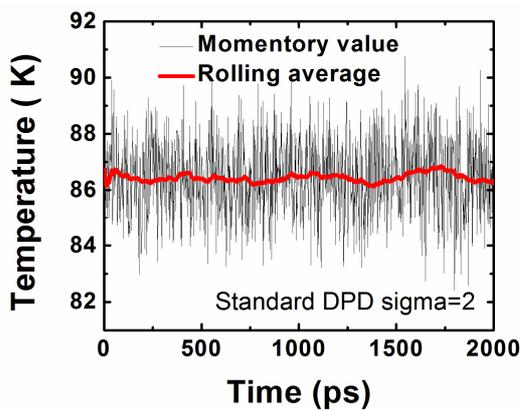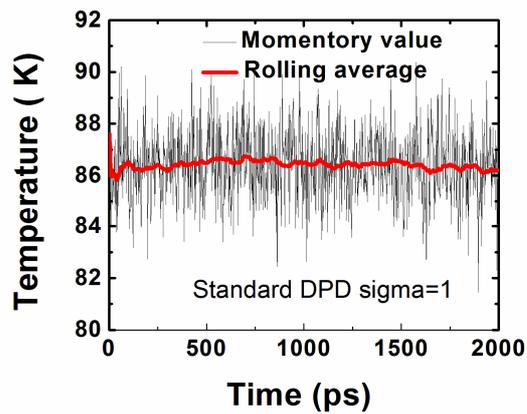
Figure 4.2. Temperature controlled by the standard DPD thermostat with noise strength sigma = 1 (top) and sigma=2 (bottom).
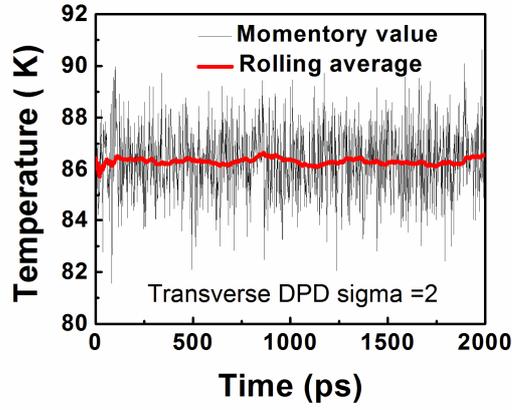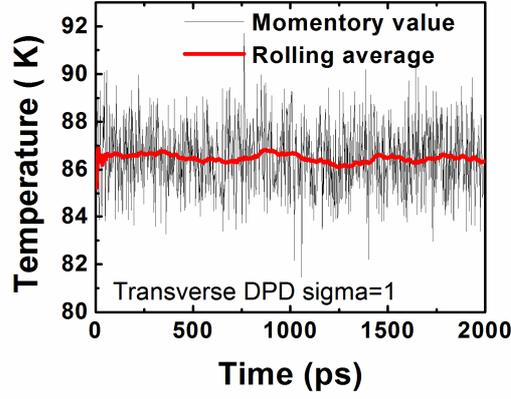
Figure 4.3. Temperature controlled by the transverse DPD thermostat with sigma = 1 (top) and sigma=2 (bottom).

Diffusion coefficient The diffusion coefficient is computed from the mean-square displacement according to the Einstein relation:

$$D = \frac{1}{6}\frac{d}{dt}\left\langle \left| \vec{R}(t) - \vec{R}(0) \right|^2 \right\rangle \tag{16}$$

Fig. 4.4 shows the diffusion coefficient over time for different thermostats. Our results are consistent with the finding in ref. 4: the diffusion coefficient decreases with increasing noise strength for both types of DPD thermostats, compare to the standard one, the transverse DPD thermostat is more sensitive to the noise strength.
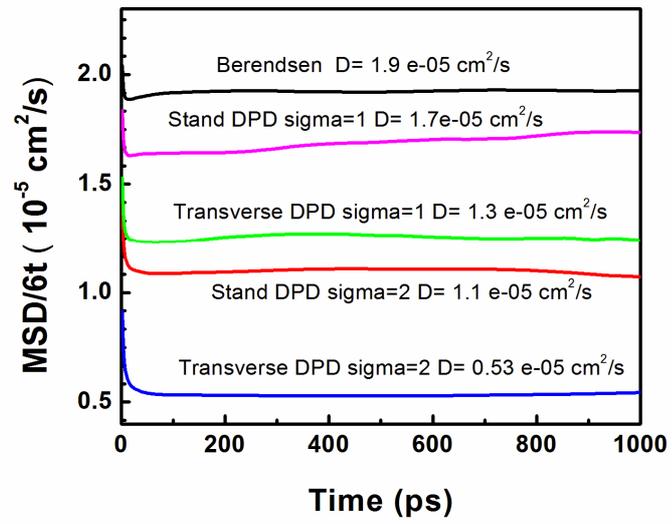
Figure 4.4. The diffusion coefficient over time for different thermostats.

4.3. References

(1)   Müller-Plathe, F. *Comput. Phys. Commum* **1993**, *78*, 77-94.

(2)   Karimi Varzaneh H. A; Müller-Plathe, F., The Temperaory User Manual for IBIsCO, 2007. (private communication)

(3)   Soddemann, T.; Dünweg, B.; Kremer, K. *Phys. Rev. E* **2003**, *68*, 046702

(4)   Junghans, C.; Praprotnik, M.; Kremer, K. *Soft Matter.* **2008**, *4*, 156-161.

5. Outlook

5.1. Viscosities of polymers from coarse-grained simulations

Our results indicate that besides reproducing the structural properties, coarse-grained models have some capabilities in predicting the viscosity of polymers. What are the field's unsolved problems and future challenges?

1. Is the viscosity scaling factor predicted from the shortest chain still valid for longer chain?

In chapter 2, CG simulations show that the extrapolated zero-shear viscosity is linearly dependent on the molecular weight, which agrees with the theoretical prediction. However, its absolute value is lower than the experiment by a factor of ~ 200 for the shortest chain length PS-9. This scaling factor is probably due to the well-known intrinsic speed up of the coarse-grained model. The question remains here: is this scaling factor constant for all unentangled systems studied? This question can be answered, in principle, by comparing to the viscosities of CG models with those of the parent atomistic models. The obstacle is that viscosity calculation with a full-atom model is a very tedious and time-consuming work. The system of PS-9, which is the shortest chain length in all systems studied, it contains 60120 atoms. For calculating a viscosity at a given shear rate, it needs a simulation length beyond 1 ns. Elapsing time on calculation with a parallelized molecular dynamics code, roughly estimated by experience, is beyond two months. For the system of PS-100, the elapsing time is unpredictable. Therefore, the feasible solution needs to be figured out in the future.

2. Can experimental viscosities be reproduced by CG models and RNEMD simulations?

The fast dynamics of CG models leads to much lower viscosities in simulations in contrast to experiments. The fast dynamics of CG model is due to the softness of CG potentials. For large degrees of coarse-graining, they become so soft that essential

polymer physics is lost and must be reintroduced via the equations of motions.[1] Izvekov and Voth[2] matched real dynamics adding friction to the CG system. Their theoretical formalism is base on the generalized Langevin equation and its simpler Langevin equation limit. The friction coefficient is determined in a multiscale fashion from the underlying fully atomistic molecular dynamics simulations using force-velocity and velocity-velocity correlation functions for the CG sites. The self-diffusion and time dependence of the velocity autocorrelation function are reproduced in their resulting CG Brownian dynamics. However, the method they proposed is not applicable in predicting viscosities via the RNEMD method: a fundamental limitation of RNEMD lies in the assumption that, in steady state, the unphysical transfer is balanced by a physical flow. This means that only flows of conserved momentum can be set up in this way. While in their approach, friction is induced deliberately and energy and momentum are not conserved any more. Naturally, one would like to introduce friction to slow down the fast dynamics in the CG model and simultaneously momentum is still conserved. The straightforward choice is dissipative particle dynamics (DPD) as a thermostat in CG simulations. Some efforts have been pursued on this approach. In our preliminary tests, the standard DPD thermostat can slow down the fast dynamics of CG models and the viscosity increases with the noise strength. However, the magnitude of noise strength is restricted in some range: the temperature becomes unstable as increasing noise strength and beyond the certain range the temperature is out of control. Comparing to the standard DPD thermostat, the transverse DPD thermostat can slow down the fast dynamics more efficiently. The problem in the transverse DPD thermostat is that simulation is only stable when a very small time step is applied. A detailed understanding of the time-step-dependent viscosity in the transverse DPD thermostat is required further study and the process is ongoing.

5.2. Backmapping a coarse-grained model under nonequilibrium conditions

As it has been pointed out in Chapter 3, the origin of the diffuse distribution of torsional angle pairs in the nonequilibrium system is still not clear. One possible reason is poor statistics of the backmapped configurations. To clarify the possible origin, one needs to perform more atomistic simulations under nonequilibrium condition to collect abundant configurations. Exactly as the viscosity calculation from fully atomistic model, the main obstacle is a very expensive computational cost.

The backmapping method paves the way for conducting further atomistic simulations involving nonequilibrium process. More information in which atomistic details is important, for example bond orientation decay, can be obtained from this process. The direct application of the reverse-mapped structures is to observe structural changes of the polymers in stress relaxation process.

5.3. References

(1)   Müller-Plathe, F. *Soft Mater*. **2003**, *1*, 1-31.

(2)   Izvekov, S.; Voth, G. A. *J. Chem. Phys*. **2006**, *125*, 151101.

(3)   Soddemann, T.; Dünweg, B.; Kremer, K. *Phys. Rev. E* 2003, *68*, 046702

(4)   Junghans, C.; Praprotnik, M.; Kremer, K. *cond-mat.soft* **2007**, *1*, arXiv:0709.0276v0701 [cond-mat.soft].

(5)   Reith, D.; Pütz, M.; Müller-Plathe, F. J. *Comput. Chem*. **2003**, *24*, 1624-1636.

(6)   Picu, R. C.; Pavel, M. C. *Macromolecules* **2003**, *36*, 9205-9215.

(7)   Gao, J.; Weiner, J.H. *J. Chem. Phys*. **1989***, 90*, 6749

Appendix 1

A.1.1. Schematic representation of the RNEMD algorithm in the serial and parallel version of IBIsCo

Serial version
```
!****************************************************************
    SUBROUTINE VISC_NEMD (TIMESTEP)                          !RNEMD

IF (IFIRST .EQ. 1) THEN                                !Initialization
        NCOUNTCALL = 0
        NTRANSF = 0.0D00
        TTRANSF = 0.0D00
        UTRANSF = 0.0D00
        IFIRST = 0
     DO I = 1, NUMSLAB
        VXMEAN_SLAB (I) = 0.0D00
     ENDDO
ENDIF

IF (ENSEMBLE == 2) THEN
   SLAB_THICKNESS  =  BOXZ/ REAL( NUMSLAB)               !Thickness of slab
ENDIF


IF(MOD(TIMESTEP, NEXCH) .EQ. 0) THEN
CALL VISC_ATOM                                  !  Searching the slowest particle
                                                in first slab and the fast particle
                                                in the central slab
NTRANSF = NTRANSF + 1                           !  accumulating momentum
                                                  and energy transferred

TTRANSF = TTRANSF + TRANSFER
UTRANSF = UTRANSF + TRANSFER * TRANSFER          !accumulating
                                                seconded momentum  transferred
ENDIF

IF (MOD(TIMESTEP, NEMDPROF) .EQ. 0) THEN
  IF (MOD(TIMESTEP, NEXCH) .NE. 0) THEN
    CALL VISC_PROFILE                           !recording mean velocity,
                                                  temperature, density in every slab

  ENDIF
ENDIF


IF (MOD(TIMESTEP, NEMDTRAJ) .EQ. 0)  THEN
    NCOUNTCALL = NCOUNTCALL + 1
     CALL VISC_TRAJ                            !recording momentum flux, velocity
                                               gradient, viscosity
ENDIF

RETURN
END SUBROUTINE
!****************************************************************
```

Parallel version

```
!**************************************************************
         SUBROUTINE VISC_NEMD (TIMESTEP)                    !RNEMD

 IF(MY_ID .EQ. MASTER) THEN                                 ! Initialization
    IF (TIMESTEP .EQ. 1) THEN
            NCOUNTCALL = 0
            NTRANSF =   0
            TTRANSF = 0.0D00
            UTRANSF = 0.0D00
        DO I = 1,  NUMSLAB
            VXMEAN_SLAB (I) =  0.0D00
        ENDDO
      EDIF
    ENDIF

IF (ENSEMBLE == 2) THEN
SLAB_THICKNESS = BOXZ/ REAL( NUMSLAB)                        ! Thickness of slab
ENDIF

IF(MOD(TIMESTEP, NEXCH) .EQ. 0) THEN
   IF (MY_ID .NE. MASTER)  THEN
        CALL VISC_SLABFIRST ( )                             ! Searching the slowest
                                                              particle in the first slab
   ENDIF
       CALL VISC_SLABMIDDLE ( timestep)                     ! Searching the
                                                              fast
                                                              particle in the
                                                              central slab

   IF(MY_ID .EQ. MASTER) THEN
        NTRANSF = NTRANSF + 1
       TTRANSF = TTRANSF + TRANSFER                         ! accumulating momentum
                                                              and energy transferred
        UTRANSF = UTRANSF + TRANSFER * TRANSFER    ! accumulating
                                                     seconded momentum transferred
   ENDIF
 ENDIF

 IF (MOD(TIMESTEP, NEMDPROF) .EQ. 0) THEN
    IF (MOD(TIMESTEP, NEXCH) .NE. 0) THEN
       CALL VISC_PROFILE (TIMESTEP)                         !recording mean velocity,
                                                       temperature, density in every slab
    ENDIF
 ENDIF

 IF (MOD(TIMESTEP, NEMDTRAJ) .EQ. 0) THEN
    NCOUNTCALL = NCOUNTCALL + 1
    CALL VISC_TRAJ (TIMESTEP)                               !recording momentum flux, velocity
                                                                gradient,  viscosity
 ENDIF

RETURN
END SUBROUTINE
!**************************************************************
```

A.1.2. Molecular dynamics simulation with the dissipative particle dynamics (DPD) for use as a thermostat

Both the standard and transverse DPD used as a thermostat are available in the IBIsCo code. One can choose one of them or a combination of both. When any type of DPD thermostat is chosen, Berendsen thermostat is switched off automatically. The input control file for both types of DPD thermostat is demonstrated as Appendix .1.3 The main features of the DPD algorithm for use as a thermostat are listed below:

1. Making the DPD neighbour list. The neighbour list for searching the interacting atom pairs in the random force and drag force is independent from the neighbour list for the common nonbonded interaction; therefore one has more flexible choice in the DPD cutoff. If the size of the box is bigger than three times the DPD-neighbour-list cut off, the link cell algorithm is used to make the DPD neighbour list. The simulation box is divided into cubic cells with the neighbour list cut off length, and searching is restricted to the DPD neighbour cells instead of the whole box. If the box size is smaller than three times the DPD–neighbour-list cut off, updating DPD neighbour list is performed by searching all possible atom pairs.

2. Calculation of the random force $\vec{F}_{ij}^{R}$ and drag force $\vec{F}_{ij}^{D}$ in the DPD thermostat. The random force and drag force are calculated by looping over the DPD neighbour list. In the standard DPD thermostat, random force $\vec{F}_{ij}^{R}$ and drag force $\vec{F}_{ij}^{D}$ are calculated by

$$\vec{F}_{ij}^{D} = -\zeta \omega^{D}(r_{ij})(\hat{r}_{ij} \cdot \vec{v}_{ij})\hat{r}_{ij} \tag{1}$$

$$\vec{F}_{ij}^{R} = \sigma \omega^{R}(r_{ij})\theta_{ij}\hat{r}_{ij} \tag{2}$$

where ζ and σ are the friction constant and the scalar noise strength. In the transverse DPD thermostat, the random force $\vec{F}_{ij}^R$ and drag force $\vec{F}_{ij}^D$ are calculated by

$$\vec{F}_{ij}^D = -\zeta\omega^D(r_{ij})\vec{P}(\vec{r}_{ij})\vec{v}_{ij} \tag{3}$$

$$\vec{F}_{ij}^R = \sigma\omega^R(r_{ij})\vec{P}(\vec{r}_{ij})\vec{\theta}_{ij} \tag{4}$$

where $\vec{P}$ is the projection operator and $\vec{\theta}_{ij}$ is the noise vector.

3. r-dependent weighting function for random force ω^R. There are two options available in IBIsCo code: If the linear weighting function is chosen (key words: Weigh_type = L for the standard DPD and Tran_weigh_type = L for the transverse DPD), the weighting function is defined as

$$\omega^R = 1 - r/r_{cut} \quad r < r_{cut} \tag{5}$$
$$\omega^R = 0 \quad\quad r \geq r_{cut}$$

If the step weighting function is chosen (key words: Weigh_type = S for the standard DPD and Weigh_type = S for the transverse DPD), the weighting function is defined as

$$\omega^R = 1 \quad r < r_{cut} \tag{6}$$
$$\omega^R = 0 \quad r \geq r_{cut}$$

4. r-dependent weighting function for drag force ω^D. ω^D is calculated according to the Eqn. 7.

$$\left(\omega^R(r)\right)^2 = \omega^D(r) \tag{7}$$

5. Integration scheme. A modified DPD velocity-Verlet integration scheme (reference: *J. Phys. Chem.* **1997** *107*, 4423) is used to update the position and velocity. Integration for one single time step can be described as following:

$$r_i(t + \Delta t) = r_i(t) + \Delta t v_i(t) + \frac{1}{2}(\Delta t)^2 f_i(t),$$

$$\tilde{v}_i(t + \Delta t) = v_i(t) + \lambda \Delta t f_i(t),$$

$$f_i(t + \Delta t) = f_i(r(t + \Delta t), \tilde{v}(t + \Delta t)), \tag{8}$$

$$v_i(t + \Delta t) = v_i(t) + \frac{1}{2}\Delta t(f_i(t) + f_i(t + \Delta t)).$$

where, λ is the so-called fudge factor. The actual velocity-Verlet algorithm for a conventional MD is represented with $\lambda = 0.5$. In DPD, the drag force is velocity dependent, which is not consistent with the formulation of the velocity-Verlet algorithm. One makes prediction for a new velocity $\tilde{v}$ and later be corrected in the last step. The properties which are depending on the coordinate differences can be calculated after step 2. and temperature are calculated after last step. The algorithm would be exact to $O(\Delta t^2)\,at\ \lambda = 0.5$ if there were no random and drag force. The numerical order for the proposed algorithm is undefined.

A.1.3. Sample files for conducting a RNEMD simulations and using DPD as a thermostat

The shear viscosity is calculated by the reverse nonequilibrium molecular dynamics (RNEMD) method. In the RNEMD method, the simulation box is partitioned into an even number of slabs along the z direction, one periodically searches in the first slab for the particle with largest negative x component of the momentum, and in the central slab for the particle with largest positive x component. If these two atoms have same mass, one exchanges their momenta. By repeating this procedure periodically, an unphysical momentum flux is imposed and a velocity gradient or shear field results. The momentum flux can be achieved by two different approaches: either by swapping the velocities of atoms or by swapping the centre-of-mass velocities of molecules. At this stage, only the first approach is available in the IBIsCo code. Note that only even number of slabs is suitable for the RNEMD simulation, the shear flow direction is along the X axis and the velocity gradient is along the Z axis.

Four input parameters are required: 1) the number of slabs, 2) the number of time steps between velocity swaps, 3) the number of time steps between two successive samplings of velocity, temperature, and density profile, 4) the number of time steps between two successive frames in the RNEMD trajectory file. Two output files are produced during the RNEMD simulation. One is called md.prf, which records velocity,

temperature, and density profiles, the other is called md.trj, which records trajectory of momentum flux, velocity gradient and viscosity.

Sample Input *Control* file

The input *control* file contains the general parameters for the simulation (time step, ensemble, thermodynamic conditions and so on). The key words in bold are used to conduct the RNEMD simulation and the standard and the transverse dissipative particle dynamics (DPD) thermostat.

Sample *control* file

Ensemble	NVE	(NVE, NPT, NVT)
Temperature	500	(Temperature/K)
Pressure	100	(Pressure/kPa)
Natoms	2400	(Number of atoms)
Nsteps	1000	(Number of time steps)
DT	1	(Time step in fs)
TAUT	1	(Temperature relaxation time in fs)
TAUP	1	(Pressure relaxation time in fs)
Cutoff	1.5	(Cutoff for nonbonded interaction in nm)
Neighbour_list_cutoff	2.3	(The distance in nm, up to where the pairs of particles are included in the neighbor list)
Update_neighbour_list	15	(The interval of time step for updating neighbor list)
Nsampling	1	(Number of time steps between printing the instantaneous values)
Ntrajectory	200	(The interval of time step for storing configuration)
Halt_Drift	10	(The interval of time step for resetting net momentum of the system to zero)
Naverage	100	(Number of time steps between storing average data and restarting file)

Non-Bonded	4	(Use nonbonded potential on 1..4 OR 1..5? 4=1..4, 5=1..5)
Interaction	G	(Option for bond and bend interactions, G = Guassian, T = table)
Standard_DPD	**y**	(y= use standard DPD, n = do not use it)
Lambda	**0.65**	(The parameter for velocity integration)
DPD_cutoff	**1.5**	(The cutoff distance for DPD force, in nm)
DPD_Neighbour_list_cutoff	**1.6**	(Distance in nm, up to where the pairs of particles are included in the neighbor list used in DPD thermostat)
Sigma	**3**	(noise strength for standard DPD thermostat)
Weight_type	**L**	(L = linear weighting function, S = step weighting function)
Tran_DPD	**y**	(y= use transverse DPD, n = do not use it)
Tran_sigma	**0**	(Noise strength for transverse DPD, parameter for drag force, Sigma=0 for normal MD)
Tran_weight_type	**L**	(L = linear weighting function, S = step weighting function)
Shear_viscosity	**y**	(N = no calculation of shear viscosity, Y = calculate shear viscosity by RNEMD)
Num_RNEMD_slab	**20**	(Number of slabs in RNEMD simulation)
Num_RNEMD_exchange	**60**	(Number of time steps between velocity swap in RNEMD simulation)
Num_RNEMD_prof	**61**	(Number of time steps between sampling of velocity, temperature, and density profile in RNEMD simulation)
Num_RNEMD_trj	**61**	(Number of time steps between writing successively the RNEMD trajectory file)
END		

Notes for keywords

1. Ensemble: specify which ensemble you want to use for simulation. Current option include three types: microcanonical (NVE), canonical (NVT) and isobaric-isothermal (NPT) ensemble.

2. Temperature: target temperature in Kelvin. This temperature is used for thermostat and also for calculating the potentials by Boltzmann inversion in the case that one use the Gaussian file for the nonbonded interactions).

3. Pressure: target pressure in kPa (in NPT ensemble).

4. Natoms: the total number of atoms included in the system

5. Nsteps: the total number of time steps of the simulation

6. DT: the simulation time step in fs

7. TAUT: thermostat coupling time in ps

8. TAUP: pressure relaxation time in ps

9. BETA: isothermal compressibility (1/kPa)

10. Cutoff: the cutoff distance for the nonbonded interactions in nm

11. Neighbor_list_cutoff: the distance in nm up to where the pairs of particles are included in the neighbor list

12. Update_neighbor_list: the interval of time step for updating the neighbor list

13. Nsampling: the number of time steps between printing the instantaneous values

14. Ntrajectory: number of time steps between writing the trajectory file

15. Halt_Drift: number of time steps between resetting the net momentum to zero

16. Naverage: number of time steps between calculating the averages as well as printing the restart files

17. Non-Bonded: two possible definitions of nonbonded pairs within same molecule: atoms separated by more than three bonds ('1..5' interactions and above) or atoms separated by more than two bonds ('1..4' interactions and above).

18. Interaction: two options to define the bond and bend interactions. One can prepare Gaussian file, which specifies the Gaussian functions that are fitting to

the bond length and angles distributions, or one can prepare the potential tables for bond and bend interactions.

19. Reset_velocities: by this option one specifies the initial velocity. Option "NO" tells program must use the velocities which are given in the initial coordinate file. Option "YES" tells program initialize the particle velocities according to an Maxwell-Boltzmann distribution.

20. Standard_DPD: this option is to define the dissipative particle (DPD) dynamics in the standard form as thermostat. When this option is chosen, the Berendsen is automatically switched off.

21. Lambda: the parameter for velocity integration when DPD thermostat is chosen. If Lambda = 0.5, the Verlet velocity integration scheme retains.

22. DPD_cutoff: the cutoff in nm for DPD force.

23. DPD_Neighbour_list_cutoff: distance in nm, up to where the pairs of particles are included in the neighbor list used in DPD theomstat)

24. Sigma: noise strength for standard DPD thermostat.

25. Weight_type: the type of weighting function for standard DPD thermostat. Two options are available, liner weighting function (L) and step weighting function (S).

26. Tran_DPD: this option is to define the transverse DPD dynamics as a thermostat. When this option is chosen, Berendsen thermostat is automatically switched off. The transverse DPD can be used in combination with the standard one.

27. Tran_sigma: noise strength for transverse DPD thermostat.

28. Tran_weight_type: the type of weighting function for transverse DPD thermostat. Two options are available, liner weighting function (L) and step weighting function (S).

29. Shear_viscosity: Viscosity is calculated by the RNEMD when this option is chosen.

30. Num_RNEMD_slab: number of slabs in RNEMD simulation.

31. Num_RNEMD_exchange: velocity swap interval in RNEMD simulation.

32. Num_RNEMD_prof: number of time steps between sampling velocity, temperature, and density profile in the RNEMD simulation.

33. Num_RNEMD_trj: number of time steps between writing the RNEMD trajectory file.

34. END: terminate the input *control* file.

Sample *md.prf* file

```
Step:       61
        1   0.53709873E-09   -0.65285951E+01   0.50610220E+03   0.10016588E+04
        2   0.16112962E-08   -0.13858501E+02   0.45943598E+03   0.95451233E+03
        3   0.26854936E-08   -0.22145321E+01   0.50547930E+03   0.10235104E+04
        . ...
       19   0.19872653E-07   -0.54412444E+01   0.51409030E+03   0.92927821E+03
       20   0.20946850E-07   -0.55099505E+01   0.47212377E+03   0.10030761E+04
Step:      122
        1   0.53709873E-09   -0.65285951E+01   0.50610220E+03   0.10016588E+04
        2   0.16112962E-08   -0.13858501E+02   0.45943598E+03   0.95451233E+03
        3   0.26854936E-08   -0.22145321E+01   0.50547930E+03   0.10235104E+04
        . ...
       19   0.19872653E-07   -0.54412444E+01   0.51409030E+03   0.92927821E+03
       20   0.20946850E-07   -0.55099505E+01   0.47212377E+03   0.10030761E+04
        . ...
```

Notes

1. The first line is the time step when the profile is recorded.

There are five columns following the first line: the first column is the index of slab, the second is the z-coordinate of the given slab (in *m*), the third is the average velocity of atoms which belong to the given slab (in *m/s*), the fourth is temperature in the given slab (in *K*), the fifth is the average density of the given slab (in kg/m3).

Sample *md.trj* file

```
61    0.6100000000E-13    0.3320031809E+08    0.3375565672E+08    0.1038293598E+10    -
0.3197860053E+02   -0.3251115821E+02

122   0.1220000000E-12    0.3069612818E+08    0.2865889322E+08    0.1196151511E+10    -
0.2562408810E+02   -0.2116594810E+02

183   0.1830000000E-12    0.3012780908E+08    0.2947435718E+08    0.1098254738E+10    0.9024611172E+09    -
0.2743244198E+02   -0.3265997268E+02

244   0.2440000000E-12    0.2972178688E+08    0.2897878208E+08    0.1018413388E+10    0.7788893228E+09
0.2918440338E+02   -0.3720526298E+02

........
```

Notes

There are eight columns in the *md.trj* file, the fist column is the time step, the second is the elapsing time (in *ps*), the third is the time average flux (in $kg/(m \cdot s^2)$), the fourth is the instantaneous flux (in $kg/(m \cdot s^2)$), the fifth is the time average gradient (in s^{-1}), the sixth is the instantaneous gradient (in s^{-1}), the seventh is the time average viscosity (in *cp*), the eighth is the instantaneous viscosity (in *cp*).

Appendix 2 Parameters of the atomistic force field for polystyrene

The parameters of the atomic force field used in this work were reported in the following references:

1). Müller-Plathe, F. *Macromolecules* **1995**, *28*, 1049-4791

2) Milano, G.; Guerra, G.;Müller-Plathe, F. *Chem. Mater*. **2002**, *14*, 2977-2982

Table A.2.1, A.2.2, A.2.3 A.2.4 and A.2.5 report nonbonded interaction, bond stretching, bond bending, torsion potentials and harmonic dihedrals, respectively.

Table A.2.1. The Lennard-Jones parameters for polystyrene: the nonbonded interactions are given as: $V(r_{ij}) = 4\varepsilon[(\sigma/r_{ij})^{12}-(\sigma/r_{ij})^6]+q_iq_j/4\pi\varepsilon_0 r_{ij}$. A reaction-field correction is applied for the Coulombic interactions. The effective dielectric constant is taken to be 2.5. [a]

Atoms	ε/kJ mol^{-1}	σ/nm	q/e
C_{ali}	0.3519	0.3207	0
H_{ali}	0.318	0.2318	0
C_{aro}	0.294	0.355	-0.115[b]
H_{aro}	0.126	0.242	+0.115

[a]The subscripts ali and aro denote aliphatic and aromatic atoms, respectively. [b]The charge on carbon 1 of the phenyl ring is 0 in the force field. Note here: nonbonded interactions are excluded between first and second neighbors. In addition, nonbonded between all atoms of a given phenyl group are excluded.

Table A.2.2. Bond length and strength.

bonds	r_0/nm
C_{ali}-C_{ali}	0.153
C_{ali}-H_{ali}	0.11
C_{aro}-C_{aro}	0.139
C_{aro}-H_{aro}	0.108
C_{ali}-C_{aro}	0.151

Table A.2.3. Equilibrium bond angles and bond force constants. Angles are described by: $V(\phi) = (k_\phi/2)(\phi-\phi_0)^2$.

bond angle	ϕ_0/deg	k_ϕ /kJ mol^{-1}rad^{-2}
H-C_{ali}-H	109.45	306.4
C_{ali}- C_{ali}-H	109.45	366.9
C_{aro}- C_{ali}-H	109.45	366.9
C_{ali}-C_{ali}-C_{aro}	109.45	482.3
C_{ali}-C_{aro}-C_{aro}	120.0	376.6
C_{aro}-C_{aro}-C_{aro}	120.0	376.6
C_{aro}-C_{aro}-H	120.0	418.8

Table A.2.4. Proper dihedral (torsion) potentials which are described by $V(\tau) = (k_\tau/2)[1-\cos3(\tau-\tau_0)]$ *cis* at 0^0 .

torsion angles	$V(\tau) = (k_\tau/2)[1-\cos3(\tau-\tau_0)]$ *cis* at 0^0	
	τ_0/deg	k_τ /kJ mol^{-1}rad^{-2}
C_{ali} -C_{ali}- C_{ali}- C_{ali}	180	12.0
C_{ali}- C_{ali}-C_{aro} -H (terminal methyl)	180	12.0

Table A.2.5. Harmonic dihedrals which are described by $V(\delta) = (k_\delta/2)(\delta-\delta_0)^2$.

harmonic dihedral angles	δ_0/deg	k_δ /kJ mol^{-1}rad^{-2}
C_{aro}-C_{aro}-C_{aro}- C_{aro}	0.0	167.4
C_{aro}-C_{aro}-C_{aro}-H	0.0	167.4
C_{aro}-C_{aro}-C_{aro}-C_{ali}	0.0	167.4

Appendix 3 Coarse-grained potentials of polystyrene

The coarse-grained (CG) potentials used in this work follow the reference: Milano, G.; Müller-Plathe, F. *J. Phys. Chem. B* **2005**, *109*, 18609 -18619.

Bonded potentials The multi-peaked distribution of a structural parameter, say a bond angle, can be approximated by a sum of n Gaussian functions characterized by their centres (θ_{ci}), total area (A_i), and width (w_i):

$$P(\theta) = \sum_{i=1}^{n} \frac{A_i}{w_i \sqrt{\pi/2}} \exp^{-2(\theta-\theta_{ci})^2/w_i^2} \tag{1}$$

Given a distribution $P(\theta)$ of some structural parameter such as a bond or an angle, say angle θ, a first approximation of the corresponding potential can be derived doing a simple Boltzmann inversion. The corresponding potential obtained by Boltzmann inversion can be written as:

$$V(\theta) = -kT \ln \sum_{i=1}^{n} \frac{A_i}{w_i \sqrt{\pi/2}} \exp^{-2(\theta-\theta_{ci})^2/w_i^2} \tag{2}$$

One defines $g_i(\theta) = A_i / w_i \sqrt{(\pi/2)} \exp^{-2(\theta-\theta_{ci})^2/w_i^2}$, the potential $V(\theta)$ and corresponding force $F(\theta)$ can be written:

$$V(\theta) = -kT \ln \sum_{i=1}^{n} g_i(\theta) \tag{3}$$

$$F(\theta) = -4kT \frac{\sum_{i=1}^{n} g_i(\theta) \frac{(\theta-\theta_{ci})}{w_i^2}}{\sum_{i=1}^{n} g_i(\theta)} \tag{4}$$

Similar equations for bond potentials $V(l)$ and $F(l)$:

$$V(l) = -kT \ln \sum_{i=1}^{n} g_i(l) \tag{5}$$

$$F(l) = -4kT \frac{\displaystyle\sum_{i=1}^{n} g_i(l)\frac{(l-l_{ci})}{w_i^2}}{\displaystyle\sum_{i=1}^{n} g_i(l)} \qquad (6)$$

Table A.3.1 and A.3.2 report the parameters for the CG bond and angle potentials.

Table A.3.1. Parameters of the bond Potential

bond type	n^a	i	A_i	w_i [Å]	l_{ci} [Å]
m-m	1	1	0.015	0.09	2.46
m-r	1	1	0.018	0.09	2.46
r-r	1	1	0.018	0.09	2.46

[a] n is the number of Gaussians used for each force field term.

Table A.3.2. Parameters of the angle potential

angle type	n	i	A_i	w_i [deg]	θ_{ci} [deg]
m-m-m	2	1	0.861	13.7	147.7
		2	0.078	8.9	161.5
m-r-m	2	1	0.042	11.0	142.8
		2	1.283	13.0	165.0
r-r-m	3	1	0.047	18.0	99.6
		2	0.255	14.2	144.1

		3	3.404	13.0	165.4
r-r-r	3	1	0.168	10.1	89.4
		2	0.580	11.0	142.8
		3	0.385	15.2	164.1
r-m-r	3	1	0.043	7.0	87.1
		2	0.913	13.5	136.0
		3	0.167	10.9	158.8
m-m-r	2	1	0.800	12.0	136.2
		2	0.192	13.0	155.0

Nonbonded potentials. Nonbonded potentials are obtained by iterative Boltzmann inversion. The iterative Boltzmann inversion uses the difference in the potential of mean force between the distribution functions generated from a trial potential and the true distribution function to improve the effective potential successively. The pressure information is incorporated into the optimization of nonbonded potential by means of a so-called ramp correction. These techniques have been described in Chapter 1.

The nonbonded tabulated potentials for *rr, mm, mr*. are listed in Table A.3.3.

Table A.3.3. The nonbonded tabulated potentials for *rr, mm, mr*.

Distance [m]	rr [J]	mm [J]	mr [J]
0.0000000	0.385776935E-19	0.563021810000E-19	0.484114215E-19
0.377000000E-11	0.385876747E-19	0.563111181810000E-19	0.484224005E-19
0.754000000E-11	0.385976525E-19	0.563201810000E-19	0.484324378E-19
0.113100000E-10	0.386086316E-19	0.563301810000E-19	0.484423578E-19
0.150700000E-10	0.386186075E-19	0.563391810000E-19	0.484523338E-19
0.188400000E-10	0.386285862E-19	0.563481810000E-19	0.484631322E-19
0.226100000E-10	0.386385648E-19	0.563571810000E-19	0.484742905E-19
0.263800000E-10	0.386485436E-19	0.563671810000E-19	0.484842699E-19
0.301500000E-10	0.386605216E-19	0.563771810000E-19	0.484942475E-19
0.339200000E-10	0.386705006E-19	0.563861810000E-19	0.485042226E-19
0.376900000E-10	0.386804780E-19	0.563951810000E-19	0.485142045E-19
0.414600000E-10	0.386904576E-19	0.564041810000E-19	0.485251835E-19
0.452300000E-10	0.387004356E-19	0.564131810000E-19	0.485351615E-19
0.490000000E-10	0.387114146E-19	0.564221810000E-19	0.485451405E-19
0.527600000E-10	0.387213906E-19	0.564321810000E-19	0.485551165E-19
0.565300000E-10	0.387313686E-19	0.564411810000E-19	0.485650945E-19
0.603000000E-10	0.387413476E-19	0.564501810000E-19	0.485760735E-19
0.640700000E-10	0.387513262E-19	0.564601810000E-19	0.485870525E-19
0.678400000E-10	0.387633046E-19	0.564701810000E-19	0.485970305E-19
0.716100000E-10	0.387732836E-19	0.564791810000E-19	0.486070095E-19
0.753800000E-10	0.387832616E-19	0.564881810000E-19	0.486169875E-19
0.791500000E-10	0.387932406E-19	0.564971810000E-19	0.486269665E-19
0.829200000E-10	0.388032186E-19	0.565061810000E-19	0.486379445E-19
0.866800000E-10	0.388131946E-19	0.565161810000E-19	0.486479205E-19
0.904500000E-10	0.388241736E-19	0.565251810000E-19	0.486578995E-19
0.942200000E-10	0.388341546E-19	0.565341810000E-19	0.486678805E-19
0.980100000E-10	0.388441356E-19	0.565431810000E-19	0.486788615E-19
0.101780000E-09	0.388541146E-19	0.565531810000E-19	0.486898405E-19
0.105550000E-09	0.388650925E-19	0.565621810000E-19	0.486998185E-19

Distance [m]	rr [J]	mm [J]	mr [J]
0.109300000E-09	0.388760666E-19	0.565721810000E-19	0.487097925E-19
0.113050000E-09	0.388860396E-19	0.565811810000E-19	0.487197655E-19
0.116820000E-09	0.388960186E-19	0.565901810000E-19	0.487297445E-19
0.120600000E-09	0.389059996E-19	0.565991810000E-19	0.487407255E-19
0.124370000E-09	0.389159777E-19	0.566081810000E-19	0.487507035E-19
0.128150000E-09	0.389269559E-19	0.566181810000E-19	0.487606855E-19
0.131900000E-09	0.389369342E-19	0.566271810000E-19	0.487706585E-19
0.135680000E-09	0.389469905E-19	0.566361810000E-19	0.487806315E-19
0.139430000E-09	0.389568868E-19	0.566451810000E-19	0.487926125E-19
0.143200000E-09	0.389668656E-19	0.566551810000E-19	0.488025915E-19
0.146980000E-09	0.389788446E-19	0.566651810000E-19	0.488125725E-19
0.150750000E-09	0.389888825E-19	0.566741810000E-19	0.488225515E-19
0.154520000E-09	0.389988803E-19	0.566831810000E-19	0.488325295E-19
0.158300000E-09	0.390088784E-19	0.566921810000E-19	0.488435105E-19
0.162070000E-09	0.390187763E-19	0.567011810000E-19	0.488534895E-19
0.165850000E-09	0.390287644E-19	0.567111810000E-19	0.488634705E-19
0.169600000E-09	0.390390717E-19	0.567201810000E-19	0.488734635E-19
0.173350000E-09	0.390490691E-19	0.567291810000E-19	0.488834175E-19
0.177130000E-09	0.390590672E-19	0.567381810000E-19	0.488953985E-19
0.180900000E-09	0.390690651E-19	0.567481810000E-19	0.488905377E-19
0.184680000E-09	0.390801632E-19	0.567581810000E-19	0.489153585E-19
0.188450000E-09	0.390916100E-19	0.567671810000E-19	0.489253365E-19
0.192220000E-09	0.391018448E-19	0.567761810000E-19	0.489353105E-19
0.195950000E-09	0.391111557E-19	0.567851810000E-19	0.489452835E-19
0.199730000E-09	0.391215338E-19	0.567941810000E-19	0.489562645E-19
0.203500000E-09	0.391315170E-19	0.568041810000E-19	0.489662435E-19
0.207280000E-09	0.391424098E-19	0.568131810000E-19	0.489762245E-19
0.211050000E-09	0.391524076E-19	0.568221810000E-19	0.489862025E-19
0.214830000E-09	0.391624586E-19	0.568311810000E-19	0.489971845E-19

116

Distance [m]	rr [J]	mm [J]	mr [J]
0.21860000E-09	0.39172243E-19	0.56841181000E-19	0.49008162E-19
0.22238000E-09	0.39183417E-19	0.56851181000E-19	0.49018143E-19
0.22615000E-09	0.39194399E-19	0.56860181000E-19	0.49028122E-19
0.22990000E-09	0.39204369E-19	0.56869181000E-19	0.49038095E-19
0.23365000E-09	0.39214343E-19	0.56878181000E-19	0.49048069E-19
0.23742000E-09	0.39224321E-19	0.56887181000E-19	0.49058047E-19
0.24120000E-09	0.39234302E-19	0.56896181000E-19	0.49069028E-19
0.24497000E-09	0.39245281E-19	0.56906181000E-19	0.49079007E-19
0.24875000E-09	0.39255262E-19	0.56915181000E-19	0.49089988E-19
0.25252000E-09	0.39265241E-19	0.56924181000E-19	0.49099967E-19
0.25630000E-09	0.39275222E-19	0.56934181000E-19	0.49110948E-19
0.26007000E-09	0.39286200E-19	0.56943181000E-19	0.49120926E-19
0.26385000E-09	0.39297181E-19	0.56953181000E-19	0.49130907E-19
0.26760000E-09	0.39307155E-19	0.56135181000E-19	0.49140881E-19
0.27135000E-09	0.39317128E-19	0.53990181000E-19	0.49150854E-19
0.27513000E-09	0.39326109E-19	0.51115480300E-19	0.49160835E-19
0.27890000E-09	0.39335088E-19	0.48440708330E-19	0.49170814E-19
0.28268000E-09	0.39347069E-19	0.43187563800E-19	0.52156795E-19
0.28645000E-09	0.39358048E-19	0.39339891500E-19	0.53757774E-19
0.29020000E-09	0.39368021E-19	0.31121866200E-19	0.49951533E-19
0.29395000E-09	0.39377994E-19	0.32484890700E-19	0.48227289E-19
0.29773000E-09	0.39387975E-19	0.30294321900E-19	0.44111397E-19
0.30150000E-09	0.39399954E-19	0.28475480100E-19	0.41080252E-19
0.30528000E-09	0.39409935E-19	0.24776139700E-19	0.32620250E-19
0.30905000E-09	0.39419914E-19	0.22506692900E-19	0.33199702E-19
0.31283000E-09	0.39248895E-19	0.19218924000E-19	0.28430905E-19
0.31660000E-09	0.37725873E-19	0.17446215400E-19	0.28322238E-19
0.32037000E-09	0.32616852E-19	0.14730371600E-19	0.22773596E-19
0.32415000E-09	0.32593833E-19	0.13384840700E-19	0.22740823E-19

Distance [m]	rr [J]	mm [J]	mr [J]
0.32790000E-09	0.28826807E-19	0.10963418500E-19	0.20853659E-19
0.33165000E-09	0.27983780E-19	0.93809108000E-20	0.20067624E-19
0.33542000E-09	0.23533160E-19	0.72629741000E-20	0.18315534E-19
0.33920000E-09	0.21007029E-19	0.52247040000E-20	0.17182581E-19
0.34297000E-09	0.22484823E-19	0.45022172400000E-20	0.15414843E-19
0.34675000E-09	0.20274487E-19	0.35192731100000E-20	0.14242738E-19
0.35050000E-09	0.18407197E-19	0.22394810700000E-20	0.12831389E-19
0.35425000E-09	0.18829195E-19	0.11810951300000E-20	0.12034364E-19
0.35803000E-09	0.15858760E-19	0.47407680000000E-22	0.11038949E-19
0.36180000E-09	0.14242504E-19	-0.78544245600000E-21	0.10342070E-19
0.36558000E-09	0.12046814E-19	-0.16232312200000E-20	0.95544282E-20
0.36935000E-09	0.11514225E-19	-0.20671118070000E-20	0.91853266E-20
0.37313000E-09	0.10100821E-19	-0.25619404600000E-20	0.86365337E-20
0.37690000E-09	0.91009742E-20	-0.30568282830000E-20	0.82962028E-20
0.38068000E-09	0.77042031E-20	-0.35138907100000E-20	0.78093378E-20
0.38445000E-09	0.69619088E-20	-0.39264191400000E-20	0.73448532E-20
0.38820000E-09	0.62566209E-20	-0.42228710600000E-20	0.67922997E-20
0.39195000E-09	0.56985293E-20	-0.44848508020000E-20	0.64495346E-20
0.39573000E-09	0.51929515E-20	-0.46952407800000E-20	0.60478140E-20
0.39950000E-09	0.49340510E-20	-0.48851469000000E-20	0.56277599E-20
0.40328000E-09	0.45407486E-20	-0.49077501100000E-20	0.50867206E-20
0.40705000E-09	0.43368510E-20	-0.55107190000000E-20	0.50207770E-20
0.41080000E-09	0.40047244E-20	-0.56073190000000E-20	0.48929504E-20
0.41455000E-09	0.37129978E-20	-0.54846190000000E-20	0.47642523E-20
0.41833000E-09	0.33267899E-20	-0.52808190000000E-20	0.46630490E-20
0.42210000E-09	0.30519575E-20	-0.49964190000000E-20	0.45782835E-20
0.42587000E-09	0.27373360E-20	-0.48952190000000E-20	0.48586620E-20
0.42965000E-09	0.25816172E-20	-0.47936190000000E-20	0.45248432E-20
0.43343000E-09	0.24235983E-20	-0.46755190000000E-20	0.45168243E-20

Distance (m)	rr (J)	mn (J)	mr (J)
0.43720000E-09	0.23891769E-20	-0.45675190000000E-20	0.45619029E-20
0.44097000E-09	0.23121215E-20	-0.44274190000000E-20	0.44912815E-20
0.44475000E-09	0.22500396E-20	-0.42968190000000E-20	0.44062626E-20
0.44850000E-09	0.20920100E-20	-0.41534190000000E-20	0.43793360E-20
0.45225000E-09	0.19236883E-20	-0.40167190000000E-20	0.44121093E-20
0.45603000E-09	0.17457645E-20	-0.38582190000000E-20	0.44450905E-20
0.45980000E-09	0.16215431E-20	-0.36890810000000E-20	0.44875691E-20
0.46357000E-09	0.16045216E-20	-0.34920190000000E-20	0.45407476E-20
0.46735000E-09	0.16739028E-20	-0.32893190000000E-20	0.45743288E-20
0.47110000E-09	0.17885761E-20	-0.30841190000000E-20	0.45089021E-20
0.47485000E-09	0.18226495E-20	-0.29002190000000E-20	0.44662755E-20
0.47863000E-09	0.17446307E-20	-0.27174190000000E-20	0.44094567E-20
0.48240000E-09	0.16937092E-20	-0.25141190000000E-20	0.44014352E-20
0.48617000E-09	0.16812878E-20	-0.22958190000000E-20	0.43114138E-20
0.48995000E-09	0.17995689E-20	-0.20712190000000E-20	0.42750949E-20
0.49373000E-09	0.18883501E-20	-0.18835190000000E-20	0.41840761E-20
0.49750000E-09	0.19209286E-20	-0.17213190000000E-20	0.41354546E-20
0.50127000E-09	0.18981072E-20	-0.15833190000000E-20	0.40038332E-20
0.50505000E-09	0.18824088E-20	-0.14317190000000E-20	0.39127143E-20
0.50880000E-09	0.18469617E-20	-0.12994190000000E-20	0.37583877E-20
0.51255000E-09	0.18451351E-20	-0.11808190000000E-20	0.36408611E-20
0.51632000E-09	0.18170136E-20	-0.10834190000000E-20	0.35073396E-20
0.52010000E-09	0.18102948E-20	-0.95744900000000E-21	0.33951208E-20
0.52388000E-09	0.17472759E-20	-0.85188990000000E-21	0.32335019E-20
0.52765000E-09	0.16887545E-20	-0.76870900000000E-21	0.30850085E-20
0.53140000E-09	0.16701279E-20	-0.73155500000000E-21	0.29189539E-20
0.53515000E-09	0.17240012E-20	-0.67082900000000E-21	0.28006272E-20
0.53892000E-09	0.17296799E-20	-0.58186900000000E-21	0.26764058E-20
0.54270000E-09	0.17439609E-20	-0.48187900000000E-21	0.25756866E-20

Distance (m)	rr (J)	mn (J)	mr (J)
0.54648000E-09	0.16743421E-20	-0.40709900000000E-21	0.24564681E-20
0.55025000E-09	0.16282207E-20	-0.35772900000000E-21	0.23629467E-20
0.55402000E-09	0.15409992E-20	-0.29991900000000E-21	0.22610255E-20
0.55780000E-09	0.15392804E-20	-0.22632900000000E-21	0.21855064E-20
0.56158000E-09	0.15465615E-20	-0.15726900000000E-21	0.21100875E-20
0.56535000E-09	0.15853401E-20	-0.95119000000000E-22	0.20501661E-20
0.56910000E-09	0.15124134E-20	-0.28546500000000E-22	0.19891394E-20
0.57285000E-09	0.14233868E-20	0.45140000000000E-22	0.19237128E-20
0.57662000E-09	0.12562654E-20	0.11347100000000E-21	0.18836914E-20
0.58040000E-09	0.11281465E-20	0.18107100000000E-21	0.18499725E-20
0.58418000E-09	0.10500277E-20	0.26157100000000E-21	0.18118537E-20
0.58795000E-09	0.10093062E-20	0.34816100000000E-21	0.17645232E-20
0.59170000E-09	0.10089796E-20	0.45484100000000E-21	0.17182058E-20
0.59545000E-09	0.99835297E-21	0.55702100000000E-21	0.16810790E-20
0.59923000E-09	0.97703413E-21	0.66870100000000E-21	0.16733601E-20
0.60300000E-09	0.91351268E-21	0.77940100000000E-21	0.16665387E-20
0.60677000E-09	0.85069124E-21	0.89538100000000E-21	0.16710172E-20
0.61055000E-09	0.83107240E-21	0.10046510000000E-20	0.16563908E-20
0.61433000E-09	0.83065355E-21	0.11050810000000E-20	0.16550795E-20
0.61810000E-09	0.82783211E-21	0.11998100000000E-20	0.16608581E-20
0.62188000E-09	0.84511326E-21	0.12737810000000E-20	0.16747393E-20
0.62565000E-09	0.89361182E-21	0.13482810000000E-20	0.16834178E-20
0.62940000E-09	0.93076519E-21	0.14212810000000E-20	0.16731921E-20
0.63315000E-09	0.95673855E-21	0.15087810000000E-20	0.16599648E-20
0.63630000E-09	0.95801971E-21	0.15887810000000E-20	0.16449457E-20
0.64070000E-09	0.95699826E-21	0.16530810000000E-20	0.16259243E-20
0.64447000E-09	0.95207682E-21	0.17044810000000E-20	0.15973028E-20
0.64825000E-09	0.94565798E-21	0.17694810000000E-20	0.15878840E-20
0.65200000E-09	0.92143134E-21	0.18329810000000E-20	0.15747573E-20

Distance (m)	rr (J)	mm (J)	mr (J)
0.65575000E-09	0.88480471E-21	0.19033810000000E-20	0.15467307E-20
0.65953000E-09	0.86788586E-21	0.19381810000000E-20	0.15104119E-20
0.66330000E-09	0.87566442E-21	0.19887810000000E-20	0.15004904E-20
0.66707000E-09	0.88214298E-21	0.20206810000000E-20	0.15004690E-20
0.67085000E-09	0.87362413E-21	0.20648810000000E-20	0.14863501E-20
0.67463000E-09	0.85800529E-21	0.20536810000000E-20	0.14492313E-20
0.67840000E-09	0.87748388E-21	0.20198810000000E-20	0.14180098E-20
0.68217000E-09	0.89726240E-21	0.19579910000000E-20	0.13947884E-20
0.68595000E-09	0.91784356E-21	0.19063810000000E-20	0.13749699E-20
0.68970000E-09	0.90761692E-21	0.18624810000000E-20	0.13517429E-20
0.69345000E-09	0.91149029E-21	0.18280810000000E-20	0.13479163E-20
0.69722000E-09	0.89286885E-21	0.17831810000000E-20	0.13436948E-20
0.70100000E-09	0.87465000E-21	0.17304810000000E-20	0.13346760E-20
0.70477000E-09	0.87362856E-21	0.16680810000000E-20	0.13206546E-20
0.70850000E-09	0.87930971E-21	0.16283810000000E-20	0.13057357E-20
0.71230000E-09	0.84949087E-21	0.15857810000000E-20	0.12901169E-20
0.71610000E-09	0.79997942E-21	0.15479810000000E-20	0.12709542E-20
0.71987000E-09	0.75928798E-21	0.14819810000000E-20	0.12462740E-20
0.72365000E-09	0.76055914E-21	0.14183810000000E-20	0.12295551E-20
0.72740000E-09	0.75289250E-21	0.13400810000000E-20	0.12062885E-20
0.73115000E-09	0.74266587E-21	0.12626810000000E-20	0.11791019E-20
0.73492000E-09	0.70803443E-21	0.11840810000000E-20	0.11369804E-20
0.73870000E-09	0.65460558E-21	0.11115810000000E-20	0.11054616E-20
0.74248000E-09	0.56604673E-21	0.10413810000000E-20	0.10774427E-20
0.74625000E-09	0.49397529E-21	0.97729100000000E-21	0.10650213E-20
0.75000000E-09	0.41584086E-21	0.90975100000000E-21	0.10365947E-20
0.75375000E-09	0.37612920E-21	0.84488100000000E-21	0.10180680E-20
0.75752000E-09	0.31297058E-21	0.77136100000000E-21	0.97734658E-21
0.76130000E-09	0.24948174E-21	0.70747100000000E-21	0.93922774E-21

Distance (m)	rr (J)	mm (J)	mr (J)
0.76508000E-09	0.18160289E-21	0.63581210000000E-21	0.89040889E-21
0.76885000E-09	0.13382145E-21	0.55620100000000E-21	0.85143748E-21
0.77262000E-09	0.94890007E-22	0.46490010000000E-21	0.79560601E-21
0.77640000E-09	0.26591161E-21	0.37945100000000E-21	0.73822716E-21
0.78018000E-09	0.55947685E-22	0.30245100000000E-21	0.67906831E-21
0.78395000E-09	-0.13280613E-21	0.22119100000000E-21	0.62852687E-21
0.78770000E-09	-0.18113417E-21	0.14312100000000E-21	0.57264024E-21
0.79145000E-09	-0.22322339E-21	0.72657000000000E-22	0.52315363E-21
0.79530000E-09	-0.26151512E-21	0.12257520000000E-22	0.47436476E-21
0.79900000E-09	-0.30351268E-21	-0.50985000000000E-22	0.42225332E-21
0.80278000E-09	-0.34674153E-21	-0.12576900000000E-21	0.36639447E-21
0.80655000E-09	-0.39207297E-21	-0.20313900000000E-21	0.31308303E-21
0.81030000E-09	-0.41933960E-21	-0.27218900000000E-21	0.26869640E-21
0.81405000E-09	-0.43207624E-21	-0.32909000000000E-21	0.22384976E-21
0.81782000E-09	-0.43637768E-21	-0.37265690000000E-21	0.18308932E-21
0.82160000E-09	-0.47266653E-21	-0.42210900000000E-21	0.14413947E-21
0.82537000E-09	-0.49619797E-21	-0.47535900000000E-21	0.10461803E-21
0.82915000E-09	-0.51947681E-21	-0.53209000000000E-21	0.60909186E-22
0.83293000E-09	-0.51906566E-21	-0.57487900000000E-21	0.19000340E-22
0.83670000E-09	-0.53185710E-21	-0.61282900000000E-21	-0.25391102E-22
0.84047000E-09	-0.53462854E-21	-0.63389000000000E-21	-0.60825544E-22
0.84425000E-09	-0.55908739E-21	-0.65574900000000E-21	-0.10705939E-21
0.84800000E-09	-0.51563402E-21	-0.66623900000000E-21	-0.13111042E-21
0.85175000E-09	-0.51207066E-21	-0.68853900000000E-21	-0.15143866E-21
0.85553000E-09	-0.51389590E-21	-0.69743900000000E-21	-0.15171050E-21
0.85930000E-09	-0.52610095E-21	-0.70071900000000E-21	-0.16405695E-21
0.86308000E-09	-0.52576979E-21	-0.68651900000000E-21	-0.16978579E-21
0.86685000E-09	-0.51670123E-21	-0.67037900000000E-21	-0.18326429E-21
0.87060000E-09	-0.48716787E-21	-0.65071900000000E-21	-0.18523387E-21

119

Distance [m]	rr [J]	nn [J]	nr [J]
0.874350000E-09	-0.466604560E-21	-0.637589000000000E-21	-0.184288050E-21
0.878120000E-09	-0.448315940E-21	-0.621199000000000E-21	-0.167633940E-21
0.881900000E-09	-0.436994790E-21	-0.609179000000000E-21	-0.152487790E-21
0.885680000E-09	-0.410080360E-21	-0.580609000000000E-21	-0.141045640E-21
0.889450000E-09	-0.384445080E-21	-0.548079000000000E-21	-0.135629080E-21
0.893230000E-09	-0.358913920E-21	-0.509469000000000E-21	-0.127640920E-21
0.897000000E-09	-0.344009537E-21	-0.475477000000000E-21	-0.125146372E-21
0.900770000E-09	-0.329816810E-21	-0.438110000000000E-21	-0.125216810E-21
0.904550000E-09	-0.310235655E-21	-0.395179000000000E-21	-0.127996652E-21
0.908330000E-09	-0.291692296E-21	-0.350549000000000E-21	-0.127284293E-21
0.912050000E-09	-0.275188952E-21	-0.314019000000000E-21	-0.121215921E-21
0.915820000E-09	-0.270160363E-21	-0.279969000000000E-21	-0.111122565E-21
0.919600000E-09	-0.264799211E-21	-0.246539000000000E-21	-0.100441181E-21
0.923370000E-09	-0.254410652E-21	-0.203459000000000E-21	-0.952527651E-22
0.927150000E-09	-0.239469506E-21	-0.156309000000000E-21	-0.930674980E-22
0.930900000E-09	-0.232706138E-21	-0.110369000000000E-21	-0.913461316E-22
0.934650000E-09	-0.227892768E-21	-0.673460000000000E-22	-0.909847648E-22
0.938430000E-09	-0.235016182E-21	-0.214750000000000E-22	-0.932811110E-22
0.942200000E-09	-0.236303058E-21	0.252570000000000E-22	-0.101731672E-21
0.945980000E-09	-0.238541908E-21	0.673970000000000E-22	-0.110816908E-21
0.949750000E-09	-0.237923234E-21	0.103312000000000E-21	-0.118373348E-21
0.953520000E-09	-0.234154784E-21	0.137351000000000E-21	-0.119174784E-21
0.957300000E-09	-0.239983636E-21	0.176621000000000E-21	-0.115529636E-21
0.961080000E-09	-0.247892486E-21	0.211861000000000E-21	-0.114869486E-21
0.964850000E-09	-0.253703926E-21	0.243041000000000E-21	-0.113172926E-21
0.968600000E-09	-0.259580656E-21	0.270641000000000E-21	-0.120848856E-21
0.972350000E-09	-0.260277186E-21	0.298741000000000E-21	-0.132897186E-21
0.976120000E-09	-0.265636863E-21	0.323581000000000E-21	-0.162113863E-21
0.979900000E-09	-0.273997478E-21	0.346641000000000E-21	-0.169875478E-21

Distance [m]	rr [J]	nn [J]	nr [J]
0.983680000E-09	-0.279356632E-21	0.366791000000000E-21	-0.182063332E-21
0.987450000E-09	-0.291507768E-21	0.392841000000000E-21	-0.187857768E-21
0.991200000E-09	-0.298834390E-21	0.416131000000000E-21	-0.185330390E-21
0.994950000E-09	-0.311185103E-21	0.440741000000000E-21	-0.188625030E-21
0.998650000E-09	-0.315010640E-21	0.470381000000000E-21	-0.196058460E-21
0.100240000E-08	-0.321067270E-21	0.495301000000000E-21	-0.210001270E-21
0.100620000E-08	-0.315670930E-21	0.505761000000000E-21	-0.222374930E-21
0.101000000E-08	-0.316914580E-21	0.515521000000000E-21	-0.233538580E-21
0.101380000E-08	-0.316258280E-21	0.531021000000000E-21	-0.243452540E-21
0.101750000E-08	-0.322267880E-21	0.550871000000000E-21	-0.254451855E-21
0.102130000E-08	-0.317381500E-21	0.561481000000000E-21	-0.266365550E-21
0.102500000E-08	-0.303401120E-21	0.566381000000000E-21	-0.282155120E-21
0.102880000E-08	-0.292250477E-21	0.566442100000000E-21	-0.289308770E-21
0.103250000E-08	-0.286644380E-21	0.566371000000000E-21	-0.292208380E-21
0.103630000E-08	-0.276318040E-21	0.571701000000000E-21	-0.289872040E-21
0.104000000E-08	-0.264107650E-21	0.576663100000000E-21	-0.298581650E-21
0.104400000E-08	-0.256662930E-21	0.575786100000000E-21	-0.303733390E-21
0.104800000E-08	-0.256480113E-21	0.571011000000000E-21	-0.309685130E-21
0.105180000E-08	-0.260174790E-21	0.570051000000000E-21	-0.302609790E-21
0.105550000E-08	-0.260926440E-21	0.567791000000000E-21	-0.303788400E-21
0.105930000E-08	-0.253768050E-21	0.554491000000000E-21	-0.304852050E-21
0.106300000E-08	-0.243927670E-21	0.538731000000000E-21	-0.314882670E-21
0.106680000E-08	-0.227851320E-21	0.522921000000000E-21	-0.317245320E-21
0.107050000E-08	-0.226350930E-21	0.507341000000000E-21	-0.316544930E-21
0.107430000E-08	-0.230074590E-21	0.487091000000000E-21	-0.310128590E-21
0.107800000E-08	-0.239314200E-21	0.468611000000000E-21	-0.301028200E-21
0.108180000E-08	-0.243377850E-21	0.454561000000000E-21	-0.295881850E-21
0.108550000E-08	-0.238477470E-21	0.443951000000000E-21	-0.291694470E-21
0.108930000E-08	-0.226301120E-21	0.427771000000000E-21	-0.286525120E-21

Distance [m]	Fr [J]	mm [J]	mr [J]
0.109300000E-08	-0.217910733E-21	0.405791010000000E-21	-0.280314733E-21
0.109680000E-08	-0.217337439E-21	0.382461010000000E-21	-0.275641899E-21
0.110050000E-08	-0.218324008E-21	0.362081010000000E-21	-0.275638008E-21
0.110430000E-08	-0.208977656E-21	0.339521010000000E-21	-0.275641658E-21
0.110800000E-08	-0.201047727E-21	0.306001010000000E-21	-0.277651277E-21
0.111180000E-08	-0.192380928E-21	0.269341010000000E-21	-0.277519288E-21
0.111550000E-08	-0.180000538E-21	0.239201010000000E-21	-0.274628538E-21
0.111930000E-08	-0.166391198E-21	0.218411010000000E-21	-0.268038198E-21
0.112300000E-08	-0.160328808E-21	0.200881010000000E-21	-0.264027808E-21
0.112680000E-08	-0.166841458E-21	0.179361010000000E-21	-0.266601458E-21
0.113050000E-08	-0.175677707E-21	0.150071010000000E-21	-0.271251077E-21
0.113430000E-08	-0.178852072E-21	0.121101010000000E-21	-0.274434728E-21
0.113800000E-08	-0.180920338E-21	0.101939800000000E-21	-0.272095438E-21
0.114180000E-08	-0.177183998E-21	0.913980000000000E-22	-0.262889798E-21
0.114550000E-08	-0.167880660E-21	0.783280000000000E-22	-0.260237608E-21
0.114930000E-08	-0.159440825E-21	0.613510000000000E-22	-0.259671258E-21
0.115300000E-08	-0.154077887E-21	0.399090900000000E-22	-0.258560878E-21
0.115700000E-08	-0.155090618E-21	0.236290000000000E-22	-0.249962618E-21
0.116100000E-08	-0.157245358E-21	0.110941010000000E-22	-0.243254358E-21
0.116480000E-08	-0.162868018E-21	-0.453000000000E-24	-0.246070018E-21
0.116850000E-08	-0.168583628E-21	-0.143740000000E-22	-0.249637628E-21
0.117230000E-08	-0.173997272E-21	-0.325250000000E-22	-0.251801277E-21
0.117600000E-08	-0.175548688E-21	-0.483350000000E-22	-0.248210888E-21
0.117980000E-08	-0.178700548E-21	-0.599930000000E-22	-0.244714548E-21
0.118350000E-08	-0.186690158E-21	-0.682110000000E-22	-0.240005158E-21
0.118730000E-08	-0.198053808E-21	-0.715270000000E-22	-0.241070808E-21
0.119110000E-08	-0.211103428E-21	-0.783480000000E-22	-0.246647428E-21
0.119480000E-08	-0.218967707E-21	-0.844400000000E-22	-0.245541078E-21
0.119850000E-08	-0.224806068E-21	-0.908190000000E-22	-0.240477068E-21

Distance [m]	Fr [J]	mm [J]	mr [J]
0.120230000E-08	-0.232890348E-21	-0.934790000000E-22	-0.249994348E-21
0.120600000E-08	-0.240389958E-21	-0.101249000000E-21	-0.252653958E-21
0.120980000E-08	-0.252493608E-21	-0.103779000000E-21	-0.254017608E-21
0.121350000E-08	-0.264533328E-21	-0.104059000000E-21	-0.250627228E-21
0.121730000E-08	-0.273516878E-21	-0.986890000000E-22	-0.254360878E-21
0.122100000E-08	-0.272946408E-21	-0.946590000000E-22	-0.264550488E-21
0.122480000E-08	-0.268790148E-21	-0.964190000000E-22	-0.274654148E-21
0.122850000E-08	-0.281599758E-21	-0.955290000000E-22	-0.282853758E-21
0.123230000E-08	-0.295953408E-21	-0.949890000000E-22	-0.284537408E-21
0.123600000E-08	-0.311383028E-21	-0.939190000000E-22	-0.290517028E-21
0.123980000E-08	-0.311806678E-21	-0.966190000000E-22	-0.299990678E-21
0.124350000E-08	-0.308858298E-21	-0.102779000000E-21	-0.310580288E-21
0.124730000E-08	-0.307479948E-21	-0.113069000000E-21	-0.318589348E-21
0.125100000E-08	-0.312029558E-21	-0.125219000000E-21	-0.320103558E-21
0.125500000E-08	-0.312571298E-21	-0.136739000000E-21	-0.324752598E-21
0.125900000E-08	-0.342903038E-21	-0.144179000000E-21	-0.331967038E-21
0.126280000E-08	-0.359946698E-21	-0.152209000000E-21	-0.339740698E-21
0.126650000E-08	-0.366926308E-21	-0.162139000000E-21	-0.346910308E-21
0.127030000E-08	-0.360289968E-21	-0.165319000000E-21	-0.349133968E-21
0.127400000E-08	-0.358909578E-21	-0.162599000000E-21	-0.353623578E-21
0.127780000E-08	-0.361943328E-21	-0.157369000000E-21	-0.355017228E-21
0.128150000E-08	-0.366323283E-21	-0.162929000000E-21	-0.358168238E-21
0.128530000E-08	-0.360966499E-21	-0.170149000000E-21	-0.358480499E-21
0.128900000E-08	-0.354644610E-21	-0.178609000000E-21	-0.358740108E-21
0.129280000E-08	-0.348549758E-21	-0.181059000000E-21	-0.356989758E-21
0.129650000E-08	-0.347579937E-21	-0.182882900000E-21	-0.355811337E-21
0.130030000E-08	-0.351569302E-21	-0.180239000000E-21	-0.355247028E-21
0.130400000E-08	-0.354192663E-21	-0.178039000000E-21	-0.351736683E-21
0.130780000E-08	-0.348986293E-21	-0.176490900000E-21	-0.348150298E-21

Distance [m]	rr [J]	mm [J]	mr [J]
0.1311500000E-08	-0.343345900E-21	-0.170469000000E-21	-0.341439900E-21
0.1315300000E-08	-0.341665950E-21	-0.161229000000E-21	-0.333589355E-21
0.1319000000E-08	-0.341889170E-21	-0.151709000000E-21	-0.326565517E-21
0.1322800000E-08	-0.337982820E-21	-0.149359000000E-21	-0.317556820E-21
0.1326500000E-08	-0.331117240E-21	-0.151189000000E-21	-0.310058643E-21
0.1330300000E-08	-0.324326090E-21	-0.151409000000E-21	-0.305669009E-21
0.1334000000E-08	-0.322785700E-21	-0.149449000000E-21	-0.302205970E-21
0.1337800000E-08	-0.313049350E-21	-0.148199000000E-21	-0.293023350E-21
0.1341500000E-08	-0.302458970E-21	-0.149879000000E-21	-0.283662970E-21
0.1345300000E-08	-0.299044620E-21	-0.149589000000E-21	-0.274606620E-21
0.1349000000E-08	-0.284462230E-21	-0.148919000000E-21	-0.267665230E-21
0.1353000000E-08	-0.274763970E-21	-0.147809000000E-21	-0.257847970E-21
0.1356500000E-08	-0.258935720E-21	-0.148619000000E-21	-0.250897220E-21
0.1360800000E-08	-0.245459370E-21	-0.153359000000E-21	-0.247603370E-21
0.1364500000E-08	-0.233928980E-21	-0.157199000000E-21	-0.242422980E-21
0.1368300000E-08	-0.223422640E-21	-0.162359000000E-21	-0.237576640E-21
0.1372000000E-08	-0.219088225E-21	-0.166589000000E-21	-0.226896225E-21
0.1375800000E-08	-0.203935910E-21	-0.170299000000E-21	-0.216649910E-21
0.1379500000E-08	-0.196605520E-21	-0.171809000000E-21	-0.205049520E-21
0.1383300000E-08	-0.169019170E-21	-0.172719000000E-21	-0.196223170E-21
0.1387000000E-08	-0.140787870E-21	-0.176829000000E-21	-0.189972278E-21
0.1390800000E-08	-0.129292440E-21	-0.183259000000E-21	-0.187436448E-21
0.1394500000E-08	-0.116020205E-21	-0.187199000000E-21	-0.183746058E-21
0.1398300000E-08	-0.120715700E-21	-0.189199000000E-21	-0.180689700E-21
0.1402000000E-08	-0.111555332E-21	-0.193129000000E-21	-0.177159332E-21
0.1405800000E-08	-0.990869720E-22	-0.191359000000E-21	-0.168752970E-21
0.1409500000E-08	-0.872676080E-22	-0.187599000000E-21	-0.154592580E-21
0.1413300000E-08	-0.846102380E-22	-0.181649000000E-21	-0.140382420E-21
0.1417000000E-08	-0.859985850E-22	-0.182579000000E-21	-0.135935585E-21
0.1420800000E-08	-0.842495050E-22	-0.183719000000E-21	-0.136809500E-21

Distance [m]	rr [J]	mm [J]	mr [J]
0.1424500000E-08	-0.771441116E-22	-0.183349000000E-21	-0.131889122E-21
0.1428300000E-08	-0.701137171E-22	-0.177679000000E-21	-0.120052778E-21
0.1432000000E-08	-0.169962900E-21	-0.169629000000E-21	-0.110372398E-21
0.1435800000E-08	-0.570980398E-22	-0.156239000000E-21	-0.107136048E-21
0.1439500000E-08	-0.156239000E-21	-0.143879000000E-21	-0.106889568E-21
0.1443300000E-08	-0.531636499E-22	-0.131759000000E-21	-0.991930058E-22
0.1447000000E-08	-0.560789160E-22	-0.121169000000E-21	-0.865189168E-22
0.1450800000E-08	-0.623976589E-22	-0.111989000000E-21	-0.741706588E-22
0.1454500000E-08	-0.657266400E-22	-0.994290000000E-22	-0.670374008E-22
0.1458300000E-08	-0.638040568E-22	-0.852350000000E-22	-0.623740568E-22
0.1462500000E-08	-0.594216678E-22	-0.712060000000E-22	-0.548306678E-22
0.1466300000E-08	-0.506573232E-22	-0.630660000000E-22	-0.464493228E-22
0.1470000000E-08	-0.423059348E-22	-0.575020000000E-22	-0.410499348E-22
0.1473800000E-08	-0.304405898E-22	-0.480600000000E-22	-0.352775898E-22
0.1477500000E-08	-0.234832008E-22	-0.371350000000E-22	-0.274702008E-22
0.1481300000E-08	-0.227138558E-22	-0.298520000000E-22	-0.197178558E-22
0.1485000000E-08	-0.229664678E-22	-0.233830000000E-22	-0.143674678E-22
0.1488800000E-08	-0.207901222E-22	-0.183320000000E-22	-0.995912198E-23
0.1492500000E-08	-0.143847338E-22	-0.102440000000E-22	-0.678473348E-23
0.1496300000E-08	-0.895388588E-23	-0.857600000000E-23	-0.607538858E-23
0.1500000000E-08	0.0000000	0.00000000000000E+00	0.00000000

Simulation tools

The molecular dynamics simulations reported in this PhD thesis were performed on the cluster of the Theoretical Physical Chemistry group of Prof. Florian Müller-Plathe at the Technische Universität Darmstadt. The cluster was supplied by the company TRANSTEC. Additional molecular dynamics calculations were carried out on IBM p575 machines of Hessisches Hochleistungrechner located at the Technische Universität Darmstadt.

For carrying out the viscosity calculations using the reverse nonequilibrium molecular dynamics (RNEMD) algorithm, the molecular dynamics package GMQ was used. This package was originally developed by Prof. David Brown and Dr. Sévérine Queyroy (Université de Savoie, France). The RNEMD algorithm was later embedded into this code by Dr. Welchy L. Cavalcanti and myself. For simulating atomistic polymers after backmapping, the molecular dynamics package GROMACS was used for both energy minimization run and molecular dynamics run (reference: Berendsen, H. J. C.; van der Spoel, D.; van Drunen, R. *Comput. Phys.Commun.* **1995**, *91*, 43-56.; Lindahl, E.; Hess, B.; van der Spoel, D. *J. Mol. Model*. **2001**, *7*, 306-317). Part of the atomistic molecular dynamics used the YASP package, which was originally developed by Prof. Florian Müller-Plathe and later parallelized by Dr. Konstantin B. Tarmyshov.

Publications

Publications based on the present dissertation

1. X. Chen; P. Carbone; G. Santangelo; A. D. Matteo; G. Milano and F. Müller-Plathe. *Backmapping coarse-grained polymer models under sheared nonequilibrium conditions* (submitted).

2. X. Chen; P. Carbone; W. L. Cavalcanti; G. Milano and F. Müller-Plathe. *Viscosity and Structural Alteration of a Coarse-grained model of Polystyrene under Steady Shear Flow Studied by Reverse Nonequilibrium Molecular Dynamics* Macromolecules, **2007**, *40*, 8087-8095

3. W. L. Cavalcanti; X. Chen and F. Müller-Plathe, *Shear viscosity calculations through a reverse nonequilibrium method*, Physica Status Solidi (a) **2007**, *204*, 935-939

4. P. Carbone; H. A. Karimi Varzaneh; X. Chen and F. Müller-Plathe. *Transferability of Boltzmann inverted coarse-grained force fields: the polymer case.* J. Chem. Phys. **2008**, *128*, 064904

Other publications

1. X. Chen; A. Galeski and G. H. Michler. *Morphological alteration and strength of polyamide 6 subjected to high plane–strain compression.* Polymer **2006**, *47*, 3171–3185.

2. A. Galeski; J. Morawiec; J. Mohanraj and X. Chen, *Deep plastic deformation of commodity crystalline polymers (PE, PP, PA6, POM)* Proceedings of the World Polymer Congress – Macro 2006, 41st International Symposium on Macromolecules

Acknowledgements

I take this opportunity with joy and fulfillment to thank the people who have contributed to the successful completion of my period of PhD thesis.

First, I give thanks to my research advisor, Prof. Dr. Florian Müller-Phathe, for believing in my ability to work hard and bring this PhD project to fruition. His supportive conversations have always provided me with new ideas and gave me the endurance and patience to continue with my research. I benefited immensely from his insight into the physics of the problems. He encouraged me to write publications. He has read my numerous revisions and helped make some sense of the confusion. Above all, he has been always willing to help me to understand any complicated scientific problems.

Many thanks to all my colleagues for fine and warm working atmosphere: Dr. Paola Carbone, who is taking her time and patience to help me with my research on an almost daily basis and giving me her extraordinary experiences throughout the work, as well as fruitful discussions of all research projects; Dr. Welchy L. Cavalcanti for tutoring and mentoring me during my initial months; Mr. Hossein Ali karimi Varzaneh for his valuable discussions and assistance in programming, especially parallelizing the code for reverse non-equilibrium molecular dynamics; Dr. Sudip Roy for guiding me in writing dissipative particle dynamics code; Dr. Frédéric Leroy in sharing his experience in GROMACS package and viscosity calculation; Dr. Hu-Jun Qian for his suggestions in modifying the backmapping procedure for nonequilibrium system.

I would like to express my gratitude to Mrs. Gabriele General, who is dealing with my formalities for the administrative issues in the Technical University of Darmstadt; Mr. Thomas Müller for finalizing this thesis; Dr. Volker Weiss for explaining me German documents and helping me in settling my German social issues.

I would like to thank my Italian colleagues: Dr. Giuseppe Milano for providing me his coarse-grained field parameters and settling an accommodation for my stay at

Xiaoyu Chen

Wiener Str. 79

D-64287 Darmstadt

Darmstadt, den 20. Mai 2008

Erklärung

Ich erkläre hiermit, noch keinen Promotionsversuch unternommen zu haben.

(Xiaoyu Chen)

Xiaoyu Chen   Darmstadt, den 20. Mai 2008

Wiener Str. 79

D-64287 Darmstadt

Eidesstattliche Erklärung

Ich erkläre hiermit an Eides Statt, dass ich meine Dissertation selbständig und nur mit

den angegebenen Hilfsmitteln angefertigt habe.

 (Xiaoyu Chen)